1991

The Photophysics Of Polycyclic Aromatic Hydrocarbons Adsorbed On Silica Gel Surfaces: A Lifetime Distribution Analysis Approach

Yuan-sheng Liu

THE PHOTOPHYSICS OF POLYCYCLIC AROMATIC HYDROCARBONS ADSORBED ON SILICA GEL SURFACES: A LIFETIME DISTRIBUTION ANALYSIS APPROACH

by

Yuan-Sheng Liu

Department of Chemistry

Submitted in partial fulfilment
of the requirements for the degree of
Doctor of Philosophy

Faculty of Graduate Studies
The University of Western Ontario
London, Ontario
June, 1991

ISBN 0-315-66308-1

ABSTRACT

The relaxation process of excited molecules, in homogeneous systems, is routinely studied through the measurements of fluorescence lifetimes and fluorescence quantum yields. From these data, the radiative decay rate, and hence the non-radiative decay rate, can be easily derived. Effort has been made, in the present work, to conduct such a fundamental study with molecules adsorbed on silica gel surfaces.

The photophysics of six polycyclic aromatic hydrocarbons(PAH), comprising phenanthrene, chrysene, pyrene, perylene, benzoperylene and coronene, adsorbed on variously dehydroxylated silica gel surfaces, has been investigated in this work. It has been observed that the fluorescence lifetimes of these adsorbed PAHs are dispersed into distributions, and that the recovery of these distributions is highly unstable, known as an "ill-conditioned" problem. In this thesis is discussed, in detail, the problem of the instability of lifetime distribution analysis. The regularization method of Phillips is used to obtain stable solutions. Based on these studies, a bimodal lifetime distribution, which represents the PAH molecules adsorbed on two types of surface sites, is suggested to describe the photophysical behaviour of the PAHs on the silica gel surfaces.

The fluorescence quantum yields of these PAHs have been measured by a diffuse reflectance method and also by an integrating sphere method. These results are then used, in conjunction with the measured lifetime distributions, to derive the radiative decay rates and the non-radiative decay rates for the PAH molecules adsorbed on each type of surface sites.

The so obtained lifetime distributions and quantum yields, as well as the derived radiative and non-radiative decay rates, seem to be physically plausible and self-consistent, which suggests that the techniques used are justifiable. The photophysics of the PAH adsorbed on silica gel surfaces is then discussed on the basis of these data.

Dedicated to the memory of my father

SHOU-CHU LIU (1905-1975)

ACKNOWLEDGEMENTS

I would like to express my deep appreciation to my supervisors, Professor William R. Ware and Professor Paul de Mayo, for their indispensable guidance, support and patience during the course of this research project.

I am grateful to my co-workers, especially Dr. Aleksander Siemiarczuk for his support throughout the duration of this work, and Dr. Douglas R. James and Prof. Mei-Gong Fan for their help at the early stage of this work. I am indebted to the graduate students, postdoctoral fellows and faculty members who have assisted and advised me. The assistance of many members of the technical staff in the University is also acknowledged.

I am greatly indebted to my mother Zhi-Qi Wang, my wife Zhi-Xian Lu and my son Qin Liu for their love, sacrifice and support.

TABLE OF CONTENTS PAGE

LIST OF TABLES

LIST OF FIGURES

CHAPTER 1 INTRODUCTION

The photophysical behaviour of molecules adsorbed on solid surfaces has been a subject of interest for over half a century. Perhaps the first serious study was conducted by J.H. de Boer and coworkers in the 1930s [1]. They observed the absorption spectra of halogens and some phenols adsorbed on sublimed fluoride films and found that the adsorption caused strong perturbations to the absorption maxima and molar absorption coefficients. It was soon found advantageous to use microporous materials with a highly developed internal surface (microporous glass, silica gel, alumina, etc.), because, not only were these materials important in many chemical processes, but also they allowed the adsorbed molecules of a high space density to be examined. Since then a number of alternative techniques have appeared. The application of infrared spectroscopy to surface studies was founded in the 1940s by Yaroslavskii, Terenin, and other Russian scientists [2]. Diffuse reflectance spectroscopy was introduced in the late 1950s by Kortum [3]. The study of the luminescence of adsorbed molecules, with which this work is mainly concerned, began to receive considerable attention in the late 1970s and flourished in the 1980s. Studies in this field have been recently reviewed by several authors [4-8].

There are many interesting questions concerning the

molecules adsorbed on solid surfaces [4-8]. On a surface, the molecules experience a very special environment. For example, these molecules are subject to an interaction where only a portion of a molecule interacts with the surface while the remainder is essentially in vacuum. Furthermore, the surface functional groups, such as hydroxyl groups, are bonded on a rigid framework of the adsorbent; their mutual interaction and their translational movement are, therefore, highly restricted, in comparison with any solvent environment. This provides the possibility that a large molecule may suffer multiple bonding and perhaps some strains. A major question then arises as to how the photophysical behaviour of the adsorbed molecules reflects such an environment. The significance of these studies, therefore, is twofold. On one hand, the observation of the adsorbed molecules, in comparison with these molecules in the gas phase or in solution, may reveal information about the nature of the surface of the adsorbents. On the other hand, such observations may bring deeper insight into the chemical or photophysical properties of the adsorbed molecules themselves. A better understanding of these two factors is essential for the interpretation and prediction of many important chemical and physical processes undergone on surfaces, such as heterogeneous catalysis, separation processes, solar energy storage, etc.

Historically, progress in this field of study has been

frequently made by extending the study of an observed phenomenon in solution to that on a surface. The majority of surface luminescence studies have involved the use of polycyclic aromatic hydrocarbons (PAH) as probes to examine the properties of the surfaces. These studies are usually analogues to their solution counterparts, and they are based on the known properties of the probe molecules in solution. Use has been made of the Ham effect to indicate the surface polarity [9-14], of the formation of excimers and the dynamic quenching of luminescence to evaluate the surface diffusion or "viscosity" [15-18], of intermolecular energy transfer to measure the fractal properties of silica gel [19-22], etc. On the other hand, a number of interesting surface effects has been reported. For example, multiple lifetimes have been frequently observed on surfaces [23-26]. Also, ground state dimers of some PAHs have been found on silica gel surfaces [27,28].

These successes encouraged the author to consider whether it is possible to probe the surface in a more quantitative manner. Attempts were made, in the early stage of this work, to associate the number of exponentials with the number of local environments. Two communications by Ware and co-workers demonstrated, however, that the double (or higher) exponential fluorescence decays often reported for adsorbed molecules might equally well fit a broad distribution of lifetimes and, in fact, may fit many such distributions

[24,29]. Questions then arose. If on a surface the adsorbed molecules were assumed to have lifetime distributions, then, how could one recover them? And further, could one derive, based on the recovered lifetime distribution, some quantitative information about the distribution of the fluorescent molecules on the surface, particularly, on different kinds of surface sites?

In recent years, efforts have been made by several groups, to develop the techniques to recover lifetime distributions from fluorescence decay data [30-34]. These intended techniques are different from the conventional lifetime distribution studies, in which one recovers the parameters for an a priori assumed model, such as a Gaussian distribution, in that it does not use any a priori model. The techniques which have been developed and used for this purpose are mainly of two types [30-34]: ESM (Exponential Series Method) and MEM (Maximum Entropy Method). The former uses the Marquardt approach, and the later uses the Conjugate Gradient approach combined with a maximum entropy constraint, to search for the least-squares solution from the decay data.

Interest is growing in the use of lifetime distribution recovery techniques to perform appropriate types of lifetime studies [35-53]. Examples can be found in studies of biological systems such as proteins [35-38], vesicles or

membranes [39-46], micellar systems [47,48], cyclodextrin inclusion complexes [49, 50], fluorophors in rigid or viscous media [51,52], and on surfaces [53]. In most of these applications, an *a priori* model, such as a single or double Gaussian or Lorentzian distribution, has been used in the data analysis.

Difficulties arose, however, when the model-free techniques were employed in the study of molecules adsorbed on silica gel surfaces. The most frustratingly troublesome problem was that the recovered lifetime distributions were rarely reproducible. It has been realized, since an early stage of this work, that the lifetime distribution analysis problem is an inverse of the Laplace transform [54], that is well known an "ill-conditioned" problem. Nevertheless, to understand fully the so called ill-conditioned nature of the lifetime recovery problem takes years of exploration. In fact, such a painful process has been experienced by many physicists, as remarked by J.G.McWhirter and E.R.Pike, "**Many physicists have discovered, after much wasted effort, that it is essential to understand this feature before attempting to compute solutions**" [55]. Unfortunately, many photophysicists and photochemists seem to be still ignoring this problem.

Before one can apply the desired "quantitative probing technique" to the study of the silica gel surface, a number

of fundamental, and rather difficult, problems have to be addressed:

(A) The ill-conditioned nature of lifetime distribution analysis must be fully understood, and be treated without bias. Although similar problems have been intensively investigated by applied mathematicians and physicists in some fields, they are not well known subjects yet to most photochemists and photophysicists.

(B) The determination of quantum yields on silica gel surfaces is difficult, because of the light scattering property of the silica gel powders. There are very few data available in the literature for reference. If one attempts, however, to derive some kind of molecular population distribution on a surface from the measurable lifetime distribution, it is first necessary to determine the fluorescence quantum yield on the surface, and then to derive the radiative decay rates, or, if possible, their distribution.

(C) When the lifetimes are treated as distributions, the derivation of the radiative decay rates becomes more complicated. Such a problem has not been addressed before.

The present work represents an effort to deal with these three fundamental problems. The author attempted to develop,

in surface work, the basic techniques for the lifetime distribution analysis, and for quantum yield measurements. The combination of these two techniques was used to obtain, in a first approximation, the radiative and non-radiative decay rates of PAHs adsorbed on the silica gel surface. To what extent these problems can be eventually fully resolved, is still not quite clear. The present work, perhaps, has raised more questions than that it has solved.

This thesis comprises three parts. In the first part, which includes chapters 2-7, the nature of lifetime distribution analysis is discussed in detail, on the basis of the theory of Fredholm integral equations and the theory of inverse problems. A regularization technique is introduced into the lifetime distribution analysis to improve the stability of the solutions. This technique is compared with a previously developed program available in this laboratory, using extensive simulated and real data. Some experimental details are described in Chapter 5. The second part, which includes Chapter 8 and 9, is devoted to fluorescence spectroscopic studies and quantum yield measurements; both primary and secondary methods are tested and discussed. The results of quantum yield measurements, and the absorption and emission spectra on surfaces are reported in this part. In the third part, Chapters 10 and 11, the method for deducing radiative and non-radiative decay rate constants, based on the measured lifetime distributions, is discussed. The

calculated decay rate constants are compared with the corresponding literature data of the same PAHs in solution. Chapter 10 also serves as a comprehensive assessment of the validity of the techniques employed. Then follow conclusions drawn from the present study, and a brief discussion of photophysics of these PAHs absorbed on silica gel surfaces.

CHAPTER 2 LIFETIME DISTRIBUTION ANALYSIS: THE CONCEPT, THE THEORY, AND THE METHODS

2.1 DISCRETE LIFETIME

The fluorescence lifetime of a fluorophor is normally considered as a discrete value, which describes the duration of fluorescence emission after the termination of the excitation light. Because an unimolecular relaxation process of an excited state species follows first order kinetics, we have equation

$$(2.1) \qquad -\frac{d[m^*]}{dt} = k[m^*]$$

where $[m^*]$ is the concentration of the excited molecules, and k is the decay rate constant. Integration of equation (2.1) leads to equation

$$(2.2) \qquad [m^*]_t = [m^*]_0 e^{-kt}$$

where $[m^*]_0$ is the initial concentration of the excited molecules. The lifetime, τ, is defined by $\tau = 1/k$, which is the time required for the initial concentration of the excited molecules to be reduced by a factor of 1/e.

Lifetimes or decay rates are most frequently determined by

monitoring the fluorescence intensity, I, as a function of time, t, elapsed after an impulse excitation. Assuming I(t) to be proportional to $[m^*]_t$, we then get equation

$$I(t) = I(0)e^{-kt} \qquad (2.3)$$

where I(t) is called a decay curve (for impulse excitation). Once the decay curve is available, I(0) and k, or τ (= 1/k), can be found by fitting the decay curve with the non-linear least-squares technique [56].

2.2 THE CONCEPT OF LIFETIME DISTRIBUTION ANALYSIS

Ideally, a pure fluorophor possesses only a discrete, single lifetime, as discussed in the previous section. In recent photophysical studies, however, the decays of many such pure single fluorophor systems have been found requiring two, or more than two, exponential terms to fit [23-26,57-59]. The decay kinetics of this type is termed, in general, "dispersed first order kinetics" [60-62]. A dispersed first order decay is distinguished from a classical first order decay by the following features. In contrast to a classical first order system, the semilogarithmic plot of such a decay curve is not linear. When the intensity of excitation light is varied, however, each decay curve, when normalized by its initial intensity, falls on a common curve. Such a normalization procedure will not work for systems where the

kinetics are higher than first order.

It has been found, as briefly reviewed in Chapter 1, that when a decay curve needs two or more than two exponential terms to fit, it can also be fitted equally well by a great variety of combinations of exponential terms. This suggests an alternative approach to the analysis of decay curves: the lifetimes may be assumed, in suitable cases, to have a continuous (or "piece-wise" continuous) distribution, which may be recovered from the decay curve as a distribution function. Thereafter, this approach will be referred to as "lifetime distribution analysis".

It should be noted that some other approaches are also being studied. For example, in some cases the dispersion is assumed, a priori, to be a Gaussian distribution, and the parameters of this Gaussian model are then recovered from the decay curves [60-62]. This approach will be referred to as the "a priori model approach". This approach is valid only when enough evidence is available to justify the model. The classical method, using one, two, three or four exponential terms to fit the decay, may be considered as a special type of the "a priori model" approach. Here the "a priori model" is a few discrete lifetimes. This approach will be called as "discrete lifetime approach". The "lifetime distribution analysis" approach studied in this work is different from the "a priori model approach" in that

it does not assume any such model.

Assuming a fluorescence system is excited by impulse excitation and this results in a decay curve I(t), we define a decay rate distribution function i(k) by an integral transform:

$$(2.4) \qquad I(t) = \int_a^b i(k)\ e^{-kt}\ dk$$

where $a > 0$, $b < \infty$ and e^{-kt} is the kernel deduced from the first order kinetics. This definition is, in fact, generalization of the classical approach of a sum of discrete decay rates. Under this generalized definition, the discrete decay rate components can be represented by a sum of delta functions:

$$(2.5) \qquad i(k) = \sum_i A_i\ \delta(k - k_i)$$

By substituting (2.5) into (2.4), the classical expression is obtained:

$$I(t) = \sum A_i \int_a^b \delta(k - k_i)\ e^{-kt}\ dk$$

$$= \sum_i A_i\ \exp(-k_i t)$$

By changing variable, the corresponding distributions in $\tau = 1/k$, $x = \ln k$, and $y = \ln\tau$ domain may be similarly defined. They read

$$(2.6) \qquad I(t) = \int_{a_\tau}^{b_\tau} i_\tau(\tau)\ e^{-t/\tau}\ d\tau$$

where $a_\tau > 0$, $b_\tau < \infty$,

$$(2.7) \qquad I(t) = \int_{a_x}^{b_x} i_x(x)\ e^{-\exp(x)t}\ dx$$

where $a_x > -\infty$, $b_x < +\infty$, and

$$(2.8) \qquad I(t) = \int_{a_y}^{b_y} i_y(y)\ e^{-\exp(-y)t} dy$$

where $a_y > -\infty$, $b_y < +\infty$. Hereafter, the four distribution functions will be named as k, τ, lnk or lnτ distribution respectively. For convenience, we will generally describe the recovery of all these distributions as "lifetime distribution analysis", unless it is necessary to specify the particular type of distribution.

From equations (2.4), (2.6), (2.7) and (2.8), the relationships between $i(k)$ and $i_\tau(\tau)$, $i_x(x)$, and $i_y(y)$ can be readily derived. They are equations

$$(2.9) \qquad i(k) = -\frac{i_\tau(1/k)}{k^2}$$

$$(2.10) \qquad i(k) = \frac{i_x(\ln k)}{k}$$

$$(2.11) \qquad i(k) = \frac{i_y(-\ln k)}{k}$$

It is evident that equations (2.4), (2.6), (2.7) and (2.8) all are of the form

$$(2.12) \qquad y(t) = \int_{a_s}^{b_s} X(s)\ K(t,s)\ ds$$

which is known as the Fredholm integral equation of the first kind [63]. This kind of equation appears frequently in many branches of physical science. If y(t) is experimentally determined, the problem of determining X(s) is referred to as an "inverse problem" [64,65].

The above discussion demonstrates that the problem of lifetime recovery from decay data may be treated from a functional approach. If a decay curve is given, we can solve equations (2.4), (2.6), (2.7), or (2.8) instead of (2.3), to get a corresponding distribution function. Conceptually, this represents a general approach to deal with any type of

lifetime recovery problem.

The significance of generalizing the classical lifetime recovery problem to a distribution analysis is profound. Since Fredholm integral equations of the first kind and the related inverse problems have been studied in depth by applied mathematicians and physicists in a number of branches of physical science, the nature and the mathematical properties of these problems are already well known. Furthermore, many methods have been well developed to solve these kinds of equations, and some of them are directly applicable to lifetime distribution analysis. Thus the generalization has opened a door for photochemists and photophysicists to get access to a huge body of literature, from which the theory and method for lifetime distribution analysis may be readily established.

2.3 INVERSE THEORY

Extensive experience obtained in this work, in dealing with the lifetime distribution recovery problems, has shown that they are indeed difficult ones. Although there is no lack of favourable examples that show that a complicated distribution may be precisely recovered, there are, however, also many counter-examples that show that a simple distribution may be distorted by the same method. Under these circumstances, a theoretical interpretation for these

properties, and a theoretical prediction about the potential and limitation in solving this kind of problem, are highly desirable.

During the course of this work, it became clear that three questions are of major theoretical concern in lifetime distribution analysis: (a) Is the instability an inherent property of lifetime distribution analysis? (b) If (a) is true, how unstable is the result expected to be, for a given decay curve? (c) How may one handle this situation so as to recover the maximum amount of reliable information from a given data set?

A rigorous discussion about the theories that deal with these problems is beyond the scope of this thesis. In the following, we attempt to describe some of the most important properties of the Fredholm integral equation of the first kind, particularly, the inverse Laplace transform, in relatively simple terms. These results, however, hold generally for any Fredholm integral equation of the first kind, and they can be strictly proved with singular value and singular function analysis.

The most salient feature of this problem is the instability of the solution. In other words, the problem is an "ill-conditioned problem". By ill-conditioned problem, we mean that a very small perturbation in I(t), the measured decay,

can cause an arbitrarily large perturbation in i(k), the desired underlying distribution. If the errors of the decay measurement are taken into account, equation (2.4) should be rewritten as

$$\bar{I}(t) = \int_a^b i(k)\ e^{-kt}\ dk + \bar{\epsilon}(t) \tag{2.13}$$

where $\bar{\epsilon}(t)$ is a stochastic function that represents th random error of the decay measurement. The presence of the uncertainty $\bar{\epsilon}(t)$ aggravates the normal problems of instability of the solution, because any function g(k) that satisfies

$$\left| \int_a^b g(k)\ e^{-kt}\ dk \right| < |\bar{\epsilon}(t)| \tag{2.14}$$

may be added onto the solution, and the sum i(k) + g(k) may still satisfy the integral equation within the limits of the experimental uncertainty. In the following, we will omit the $\bar{}$ sign for simplicity.

A very popular example, which is frequently cited by textbooks [66-68], is g(k) = sin(nk). It can be shown that

$$\int_a^b \sin(nk)\ e^{-kt}\ dk \longrightarrow 0 \quad \text{as } n \longrightarrow \infty. \tag{2.15}$$

Therefore by choosing n large enough we can ensure that, given $\epsilon(t)$ however small, equation (2.14) can be satisfied. This example shows that an arbitrarily large number of high frequency oscillatory components may be added to any solution, and the result may still be consistent with the measured decay curves when the experimental errors are taken into account. In fact, as will be seen in the following chapters, this kind of oscillatory distortion is indeed most frequently seen in the practice of lifetime distribution analysis.

We now illustrate some other important features of this problem, by using a Fourier series expansion of the desired solution i(k). For simplicity, we assume the underlying distribution spans the range [0, b]. Equation (2.4) is rewritten as

$$I(t) = \int_0^b i(k)\ e^{-kt}\ dk \qquad (2.16)$$

Assuming i(0) = 0 and i(b) = 0, and i(k) is piece-wise continuous, we can expand i(k) in [0, b] as a Fourier sine series [69]

$$i(k) = \sum_{n=1}^{\infty} c_n \sin\left(\frac{n\pi}{b} k\right) \qquad (2.17)$$

where the coefficient

$$c_n = \frac{2}{b} \int_0^b i(k) \sin(\frac{n\pi}{b} k) \, dk \quad < \quad \frac{2}{b} \int_0^b i(k) \, dk$$

is a finite number. Substituting (2.17) into (2.16) yields

$$(2.18) \qquad I(t) = \sum_{n=1}^{\infty} c_n I_n(t)$$

where

$$I_n(t) = \frac{1 - (-1)^n e^{-bt}}{(b/n\pi) t^2 + n\pi/b}$$

It can be proved that

$$(2.19) \qquad I_n(t) \longrightarrow 0, \quad \text{as } n \longrightarrow \infty,$$

and

$$(2.20) \qquad c_n \longrightarrow 0, \quad \text{as } n \longrightarrow \infty.$$

The latter is guaranteed by the Dirichlet theorem. Equations (2.17), (2.18), (2.19) and (2.20) together can be used to predict some most important properties of lifetime distribution analysis.

(A) Instability

Since $I_n(t)$ and c_n both decrease with an increase of n, for any given $\epsilon(t)$, there must be an n_e, for $n > n_e$, $c_n I_n(t) < \epsilon(t)$. This implies that the contribution of the high frequency components, corresponding to $n > n_e$, will be "submerged" in the random noise. Therefore, these high frequency components in the Fourier series cannot be effectively recovered, unless an "a priori model" is available. Furthermore, instead of the "true" high frequency components, many false high frequency oscillations may join into the solution without being detected through the fitting criterion. The recovered distribution, therefore, can be guaranteed correct by the goodness of fitting only with respect to a certain number of low frequency terms, depending on the $\epsilon(t)$.

(B) The "trade-off" between stability and resolution

If, in order to suppress the instability of the solution, the high frequency components are filtered out by some means (such as a truncation of the high frequency terms) in the data reduction process, then, in the meantime, the "true" high frequency components will be removed altogether with the false oscillation. Therefore, the improvement in the stability of the solution is bound to be accompanied by a sacrifice in resolution. This rule holds for all Fredholm

integral equations of the first kind, and it was proved by Backus and Gilbert [65,70] in the 1960s.

(C) The "favourable" and "unfavourable" shape

Since the high frequency components are not easily recovered by any method, a distribution function that does not contain high frequency components in its Fourier series expansion possesses inherently a favourable shape. On the contrary, a distribution function that contains a broad "spectrum" of components possesses an unfavourable shape. This property of a Fourier expansion of a function is characterized by the "rate of convergence", or the rate of the decrease of the Fourier coefficient c_n with the increase of n. According to the theory of Fourier series, the rapidity of convergence is closely related to the differential property of the function [69]. In simple words, the more smooth the function is, the more rapid its Fourier series converges. The worst convergence occurs at the point of discontinuity. Thus, we can predict that a smooth distribution, such as a Gaussian distribution, is more likely to be correctly reconstructed than a sharp cornered distribution, such as a rectangle. Also we can predict that at the position of a sharp corner, which is the point of discontinuity, an oscillation is more likely to occur in the reconstructed distribution. This property is called the "Gibbs phenomenon" [69].

The above qualitative discussion has shown that the problem of instability of the lifetime distribution analysis is related to two major factors. The first factor involves the errors $\epsilon(t)$, in the measured decay curve. The second factor is the shape of the distribution to be reconstructed, which is characterized by the rate of convergence of the Fourier expansion of the distribution function. The former is determined by the instrumentation and the conditions of data collection, such as the counts in the peak channel (CPC), the time base, and the interferences from electronic or optical sources, etc. The interaction of these factors makes the problem of instability in lifetime distribution analysis a very complicated matter to discuss.

Efforts have been made, in recent years, to describe quantitatively the resolution limit in solving the Fredholm integral equation of the first kind. For example, Pike and coworkers have studied in detail the recovery and resolution of exponential relaxation rates from experimental data [55,71-73]. They, based on some generalized concepts of information theory and singular function expansion, have described quantitatively how the resolution is affected by the level of noise in the data, by the <u>a priori</u> information about the range of the distribution, and by the limited number of data points and their distribution. They have found that the resolution limits are not evenly, but instead geometrically distributed along the k axis. This property

must be taken into account when the inversion is to be attempted (see Chapter 3). Further work is certainly desirable to introduce these ideas and methods into the study of lifetime distribution analysis.

2.4 PRINCIPLE OF INVERSION TECHNIQUES

Regarding the method of solving Fredholm integral equations of the first kind, or particularly the method of the inversion of Laplace transforms, there are two aspects to be considered. The first aspect is the trivial part of the problem, that is the general method for solving an integral equation. The commonly used method is to convert the original problem into a linear system of equations in some way, then to solve the system with a classical method, or to solve it as an under-determined, or over-determined problem [67]. In the case of lifetime distribution analysis, the technique for the decay measurement can provide, for example, 256 data points or more for the decay curve. On the other hand, the mesh points for the distribution to be recovered can hardly reach this number. Therefore, lifetime distribution analysis is considered more appropriate to be solved as an over-determined problem; in other words, a problem to be solved by some kind of least-squares technique.

The second aspect, and this is in fact the central part, is

how to deal with the problem of instability [66]. The key to handle this is, using some supplementary information if possible, to narrow the class of solutions to be searched. In case the supplementary information is quantitative in nature, the problem may be converted into a well-conditioned one in some sense. This kind of method is called the "selection method", and as the name implies, is such that an *a priori* model is selected in advance. The previously discussed "*a priori* model approach", and the "discrete lifetime approach" belong to this category. When this type of technique is used, some *a priori* assumptions have been made before the onset of the solution-searching process. In the case of fitting two discrete lifetimes, for instance, we assume that the underlying distribution is a double delta function, then search for a solution in this class only. With the employment of such an assumption, the problem of instability is hidden by the narrowed scope of the solution searching. Lifetime recovery problems have been dealt with in this way with fair success, and, in most cases, without the experimenter being aware of the inherent difficulties! In special cases, owing to the errors present in the decay curve, even when the model does not fit the decay adequately in a normal sense, the best possible fit has still to be considered theoretically acceptable. Such a solution is termed as a "quasisolution" [66].

In cases where no supplementary information is available, or

the information is only qualitative in nature, another type of method, collectively called the "regularization method", may be employed. This method has been proposed independently by Phillips [74] and Tikhonov [75], and subsequently developed by Twomey [76] and others. The idea is to filter out or to suppress the high frequency components, and to have only the adequately low frequency components, which are truly required by the data, recovered. Alternatively, this idea can also be stated in the following way. Since the details (the high frequency components) in the solution are not reliable (they might be "contaminated" by false information, and might mislead the investigator), we extract only the reliable part of the solution, and draw our conclusion, from just this part.

Some most popular regularization techniques, which have been previously developed in other fields of study and are presumably applicable to lifetime distribution analysis, are briefly described below.

(A) Method of Expansion [77]

We choose some basic system of functions, say $\{ p_j(k) \}$, and approximate $i(k)$ in the form

$$i^*(k) = \sum_{j=1}^{m} c_j^* \, p_j(k) \qquad (2.21)$$

where the c_j^m are undetermined coefficients. We then substitute (2.21) into (2.4) and get

$$(2.22) \qquad I(t) = \sum_{j=1}^{m} c_j^m \, I_j(k)$$

where

$$(2.23) \qquad I_j(k) = \int_a^b p_j(k) \, e^{-kt} \, dk$$

We seek a proper m and a set of c_j^m to satisfy the equation as closely as possible, e.g. in a least-squares sense, using an appropriate quadrature formula to approximate the integrals in (2.23).

In this method, the instability problem is controlled by using as small an m as possible. For a particular problem, the condition for this method to be successful is that the $\{p_j(k)\}$ must be properly selected to ensure that the expansion converges rapidly to the underlying i(k), so that m can be small. Failing this, the instability problem would show up. Another disadvantage is that the approximate solution may depend strongly on m and on the choice of the system $\{p_j(k)\}$.

(B) Method of Imposing Constraint [78]

The core of this method is to replace the original ill-conditioned problem by a stable minimization problem involving a parameter α: instead of attempting to solve the equation (2.4) directly we seek to minimize the quadratic functional

$$(2.24) \qquad ||(\mathbf{A}i)(t)-I(t)||^2 + \alpha ||\, \mathbf{L}i\, ||^2$$

where $\mathbf{A}i$ is the right hand side of equation (2.4), written in operator form, $\mathbf{L}$ is some other linear operator, and $\mathbf{L}i$ represents i(k) operated on by the operator. If $\mathbf{L}$ is properly chosen, the second term will have a smoothing or stabilizing effect on the solution. We may take $\mathbf{L}i = i$, i' or i'', etc. This method will be discussed in more detail in the next chapter.

It can be proved that the above two methods are essentially equivalent [63]. In the expansion method, the instability is eliminated by truncating the series at a selected term. The method of imposing constraint is equivalent to inserting a "filter factor" which suppresses the high frequency terms gradually to zero.

The methods of imposing constraint are to date the most popular ones in dealing with inverse problems [78]. They

have several attractive features as described by Miller [63]. (a) They proceed by converting an ill-conditioned problem into a well-conditioned one. (b) They allow more flexibility than the expansion methods in that the quality criterion is independent of the mode of representation of the solution. (c) They are comparatively easy to apply.

The above methods are designed to find a "definite" solution for an ill-conditioned problem. Another completely different approach is to treat this problem from a probabilistic or statistical standpoint [77,79,80]. The problem of solving the integral equation of the first kind is thus considered as determining the statistical information about the solution, from the similar information about the measurement. This method is also of great interest in the lifetime distribution analysis.

CHAPTER 3 SMOOTHED MARQUARDT METHOD (SMM)

3.1 THE MARQUARDT METHOD AND THE SMOOTHING TECHNIQUE OF PHILLIPS

The method used in this work for lifetime distribution analysis is based on a combination of the Marquardt method [81] and the smoothing technique of Phillips [74]. These two techniques are both widely employed for solving inverse problems in physical science [78,82]. In photophysical studies, the Marquardt method has long been a classic algorithm for the recovery of one, two or three discrete lifetimes [56]. In addition, James and Ware have previously applied the Marquardt method in their early work on lifetime distribution analysis [30,31].

The Marquardt method, also called the Marquardt-Levenberg method, is a modified version of the Gauss-Newton least-squares approach. It is sometimes known as the method of "damped least-squares" [78,82]. The modification, or the "damping" technique, introduces some degree of stabilization or regularization into the solution searching process, as compared with the simplest least-squares approach. It is, therefore, presumably appropriate for ill-conditioned problems. As will be seen in the following chapters, however, this method is not satisfactory for the purpose of this work, probably because of the complexity of the silica

gel system studied. This method, and some related problems in lifetime distribution analysis, as well as the techniques used in this work to handle these problems, are discussed below.

We start with the definition of the decay rate distribution introduced as equation (2.4) in Chapter 2. It is rewritten here as follows

$$(3.1) \qquad I(t) = \int_a^b f(k)\ e^{-kt}\ dk$$

This integral may be replaced, through a number of different approaches which will be discussed later, by a linear function of model parameters f_i, i = 1, 2, ... p, in the form of

$$(3.2) \qquad I(t) = \sum_{i=1}^{p} f_i I_i(t).$$

where f_i is a point-wise approximation to the unknown function f(k). For example, the integral may be replaced by the sum of p integrals over sub-intervals, so that we have

$$(3.3) \qquad I(t) = \sum_{i=1}^{p} \int_{k_i}^{k_{i+1}} f(k)\ e^{-kt}\ dk$$

where k_is are the mesh points in [a,b] and $k_1 = a$, $k_{p+1} = b$. P can be chosen to be large enough, so that in these small intervals the integrals may be approximated by some simple quadrature formula. Then we can manage to have

$$f_i I_i(t) = \int_{k_i}^{k_{i+1}} f(k)\ e^{-kt}\ dk. \tag{3.4}$$

In the technique of lifetime measurements, the impulse response I(t) in (3.2) has to be convoluted with the lamp profile (excitation pulse profile), E(t), to generate the calculated decay curve g(t), that is

$$g(t) = \int_0^t I(t')E(t-t')dt' \tag{3.5}$$

Substitution of (3.2) into (3.5) yields

$$g(t) = \sum_i f_i Z_i(t) \tag{3.6}$$

where

$$Z_i(t) = \int_0^t I_i(t')E(t-t')dt' \tag{3.7}$$

In equation (3.6), the calculated decay curve has been approximated by a linear function in the model parameter f_i.

Because in lifetime measurements, the decay curve is not a continuous function but is composed of n measured data points in n channels, we further rewrite (3.6) into

$$(3.8) \qquad g_j = \sum_{i=1}^{p} f_i Z_{ij} \qquad j = 1, 2, \ldots n.$$

We have now converted the lifetime distribution recovery into a problem of solving a linear system of equations. For simplicity, thereafter we use matrix and vector notations to continue the discussion.

In matrix algebra form, the system of equation (3.8) is

$$(3.9) \qquad \mathbf{g} = \mathbf{Z}\,\mathbf{f}$$

where $\mathbf{f} = (f_1, f_2, \ldots f_p)^T$ is the model parameter vector, $\mathbf{g} = (g_1, g_2, \ldots g_n)^T$ is the model response decay vector, and $\mathbf{Z}$ is the n x p matrix with elements Z_{ji}. We now give $\mathbf{f}$ an initial estimate $\mathbf{f}^0$, and assume a correction vector $\boldsymbol{\delta} = (\delta_1, \delta_2, \ldots \delta_p)^T$ to be added to the initial estimate $\mathbf{f}^0$, so that

$$(3.10) \qquad \mathbf{f} = \mathbf{f}^0 + \boldsymbol{\delta}$$

can better satisfy the equation (3.9).
Substituting (3.10) into (3.9) yields

(3.11) $\mathbf{g} = \mathbf{g}^0 + \mathbf{Z}\,\boldsymbol{\delta}$

where $\mathbf{g}^0 = \mathbf{Z}\,\mathbf{f}^0$. Let the observed decay be represented by the vector $\mathbf{d} = (d_1, d_2, \ldots d_n)^T$, and the difference between the model response $\mathbf{g}$ and the observed $\mathbf{d}$ be represented by residual vector $\mathbf{r}$, so that we have

(3.12) $\mathbf{r} = \mathbf{d} - \mathbf{g}.$

Combining (3.11) and (3.12) yields

(3.13) $\mathbf{r} = \mathbf{r}^0 - \mathbf{Z}\,\boldsymbol{\delta}$

where $\mathbf{r}^0 = \mathbf{d} - \mathbf{g}^0$.

In the simplest least-squares or "Gauss-Newton" approach, we seek to minimize the sum of squared errors $x = \mathbf{r}^T\mathbf{r}$ (chi-squared) with respect to the correction vector $\boldsymbol{\delta}$. From equation (3.13) we have

(3.14) $x = (\mathbf{r}^0 - \mathbf{Z}\boldsymbol{\delta})^T(\mathbf{r}^0 - \mathbf{Z}\boldsymbol{\delta})$

Minimization of x with respect to $\boldsymbol{\delta}$ requires that

(3.15) $$\frac{dx}{d\boldsymbol{\delta}} = 0$$

Substituting (3.14) into (3.15) and carrying out the differentiation with respect to δ, we obtain the so called "normal equations"

$$(3.16) \qquad \mathbf{Z}^T\mathbf{Z}\,\delta = \mathbf{Z}^T\mathbf{r}^0.$$

where matrix $\mathbf{Z}$ and vector $\mathbf{r}^0$ are known if $\mathbf{f}^0$ has been given. The solution of this equation for the correction vector δ is known as the Gauss-Newton solution. In principle, the original problem can now be solved in an iterative manner. We solve (3.16) to get a δ, then use (3.10) to calculate a new $\mathbf{f}$. This new $\mathbf{f}$ is then used as $\mathbf{f}^0$ to start a new iteration. This process is repeated until x is minimized in some sense.

This equation, however, has some undesirable properties. It is sensitive to the initial estimate, $\mathbf{f}^0$. When the initial estimate is poor, a diverging solution may result, or the convergence may be too slow. When the matrix $\mathbf{Z}^T\mathbf{Z}$ becomes nearly singular, the elements of δ tend to grow, without a bound, with the progress of iteration.

In order to reduce the above problem, the Marquardt-Levenberg approach imposes a constraint such that the sum of the squares of the elements of the correction vector δ be minimized in some sense. Thus, instead of minimizing x, the Marquardt approach searches a δ to minimize $x(\beta)$,

(3.17) $$x(\beta) = \mathbf{r}^T\mathbf{r} + \beta(\delta^T\delta)$$

Where β is a Lagrange multiplier. Differentiation of (3.17) with respect to the vector δ yields a modified form of the normal equations

(3.18) $$(\mathbf{Z}^T\mathbf{Z} + \beta\mathbf{I})\delta = \mathbf{Z}^T\mathbf{r}^0$$

In practice, the Marquardt algorithm leaves the off-diagonal elements of $\mathbf{Z}^T\mathbf{Z}$ unchanged but multiplies the diagonal elements by a factor of $(1+\beta)$ [83]. When $\beta = 0$, we search for the solution by the normal equation (3.16). If β is large, the off-diagonal elements become insignificant compared to the diagonal elements. The search direction is then along the path of "steepest descent" or the "gradient" method. Because of this modification, the initial estimate of $\mathbf{f}^0$ becomes relatively unimportant, and convergence can usually be guaranteed.

The smoothing technique of Phillips serves to minimize the sum of squares of the second derivative of f(k). In the present problem, the second derivative is approximated by the second difference of the elements of f. When the smoothing constraint of Phillips is also imposed, we seek to minimize $x(\beta,\alpha)$,

(3.19) $$x(\beta,\alpha) = \mathbf{r}^T\mathbf{r} + \beta(\delta^T\delta) + \alpha(\mathbf{s}^T\mathbf{s})$$

where $\mathbf{s}$ is the second difference vector. Differentiation of (3.19) with respect to δ yields equation

$$(3.20) \qquad (\mathbf{Z}^T\mathbf{Z} + \beta\mathbf{I} + \alpha\mathbf{C})\delta = \mathbf{Z}^T\mathbf{r}^0 + \alpha\mathbf{C}\,\mathbf{f}^0$$

where the n x n matrix C is defined by

$$(3.21) \qquad \mathbf{C} = \begin{bmatrix} 1 & -2 & 1 & 0 & 0 & 0 & \ldots & 0 \\ -2 & 5 & -4 & 1 & 0 & 0 & \ldots & 0 \\ 1 & -4 & 6 & -4 & 1 & 0 & \ldots & 0 \\ 0 & 1 & -4 & 6 & -4 & 1 & \ldots & 0 \\ \multicolumn{8}{c}{\ldots\ldots\ldots\ldots\ldots\ldots} \\ \multicolumn{8}{c}{\ldots\ldots\ldots\ldots\ldots\ldots} \\ 0 & \ldots & 0 & 1 & -4 & 6 & -4 & 1 \\ 0 & \ldots & 0 & 0 & 1 & -4 & 5 & -2 \\ 0 & \ldots & 0 & 0 & 0 & 1 & -2 & 1 \end{bmatrix}$$

When α is given, solving equation (3.20) will produce the correction vector δ toward a smoothed solution. In this work, we give α different values, to search for solutions under different levels of regularization or smoothing.

The above derivation is for un-weighted decay data. If a weighting factor of w_j for each channel is taken into account, then equation (3.20) becomes

$$(3.22) \qquad (\mathbf{Z}^T\mathbf{W}\mathbf{Z} + \beta\mathbf{I} + \alpha\mathbf{C})\ \delta = \mathbf{Z}^T\mathbf{W}\mathbf{r}^0 + \alpha\mathbf{C}\mathbf{f}^0$$

where $\mathbf{W} = \mathrm{diag}(w_1, w_2, \ldots w_n)$.

The working program uses standard procedures to carry out

the Marquardt minimization [83]. They are as follows:

(A) Make an initial guess for the $\mathbf{f}^0$. Calculate an initial x^0 for these values to yield the normal equation (3.16).

(B) Set $\beta = 0.01$ initially.

(C) Solve for the δ by the modified normal equation.

(D) Correct the initial values by the δ then evaluate the new x.

(E) If $x < x^0$ then accept the corrected f, reduce β to 0.1β, replace the initial $\mathbf{f}^0$ by the corrected ones then go to step (C).

(F) If $x > x^0$ then the corrected solutions are unacceptable. Increase β to 10β and return to (C).

3.2 SOME DETAILS IN THE WORKING PROGRAM

The solutions derived from the working programs are presented in one of the two styles, the vertical bar style or the profile line style, for convenience. The solutions are presented in either log τ or k space. When the vertical bar style is used, these vertical bars represent the number and distribution of the fitting components. Throughout this thesis, all the decays are fitted with 81 components, evenly spaced in log τ domain, or in other words, geometrically spaced in k domain. The goodness-of-fitting of a result is indicated by the residual profile shown below the result. Throughout this thesis, unless indicated otherwise, all the

decay curves have been collected or simulated to 200000 CPC in 256 channels, and they have been fitted from the first channel after the peak to the last channel available (the 256th channel).

For our particular problem, some additional techniques have been used to improve the performance of the program. These techniques are described in the following.

(A) The Non-negative Constraint

In the present work, a negative component in the lifetime distribution is assumed to have no physical significance, hence it should be suppressed. A constraint which directs the program to search for a non-negative solution is named a "non-negative constraint" in this thesis. In most of the cases, the non-negative constraint can be imposed in the following way. Whenever a corrected element of f becomes negative, this element is replaced by zero. This method has been described [84], and has been used earlier by James and Ware [30,31]. In the present work, this method works efficiently for broad distributions, such as those derived from PAHs adsorbed on silica gel surfaces. But when the method is used to fit narrow distributions or discrete lifetimes, and when highest resolution for these narrow distributions is the major concern, sometimes the convergence is slow or hard to achieve. In such cases, the

following measure has been taken to improve the performance. Instead of setting a negative component to zero, we multiply this negative component with an adjustable factor Γ, $0 \leq \Gamma < 0.8$, to suppress, more gently, such a negative component. Experience has shown that this weakened non-negative constraint is already strong enough to lead to a non-negative, or a nearly non-negative solution, and satisfactory convergence can be achieved in the meantime. With this technique the resolution of SMM can be even slightly better than MEM (Maximum Entropy Method) but, as might be expected, at the cost of more CPU time. Fig. 3.1 shows some examples of the reconstruction of two discrete lifetimes, using the normal "zero-return" non-negative constraint and the weakened "fraction-return" constraint respectively.

(B) The Readjustment of β

Since each time β is adjusted the matrix $\mathbf{Z}^T\mathbf{Z}$ has to be recalculated, this is the most time-consuming aspect of the calculation. Experience has shown that as the chi-squared decreases, the same β, therefore the same $\mathbf{Z}^T\mathbf{Z}$ matrix, may be used repeatedly as the chi-squared will keep decreasing. To decrease β, in most cases, will fail to decrease the chi-squared. In this work, therefore, the β is kept unchanged for ten consecutive successful iterations; then it is decreased by a factor of 0.1 for a trial. Considerable CPU

time can be saved in this way. This method has also been described in the literature [85].

(C) The Termination Criterion.

Normally the termination criterion is defined by a certain small change of chi-squared in one iteration. In this work, in some cases the non-negative constraint is imposed by a factor Γ. When $\Gamma>0.5$, the chi-squared cut-off criterion may be achieved before all negative components are sufficiently suppressed. Therefore in this work, when the chi-squared cut-off criterion is satisfied, the program checks if all the remaining negative components are smaller than 3% of the largest positive component. If this criterion is also fulfilled, the program will terminate the searching process, otherwise it will assign these negative components to zero then return to procedure (C) (see the end of section 3.1).

(D) The Elimination of Scattered Light Interference.

Because the decay data from the surface work are normally noisy, it is highly desirable to remove the scattered light and stray light interference whenever possible. The program has used two additional components, one corresponding to $\tau = 0$, another one corresponding to $\tau = \infty$, to fit the decay curves. This technique has been described [56]. Because these two components are not generated from fluorescence

light, they are physically not of interest and have been removed from the recovered distribution.

(E) Quadrature Formulas.

Two formulas have been used to approximate the integral in each interval (k_i, k_{i+1}). The first one assumes the f(k) is a constant, f_i, in this interval, then the integral is evaluated analytically (Laplace transform). This gives

$$I_i(t) = f_i \frac{\exp(-k_i t) - \exp(-k_{i+1} t)}{t} \tag{3.23}$$

The second formula assumes that the trapezoid rule is valid in this interval, therefore we have

(3.24)

$$I_i(t) = f_i \frac{k_{i+1}-k_i}{2} \exp(-k_i t) + f_{i+1} \frac{k_{i+1}-k_i}{2} \exp(-k_{i+1} t)$$

It has turned out that these two approximations give the same results. Figs. 3.2 and 3.3 show a set of results from a simulated experiment. A simulated decay curve is constructed from 150 lifetime components which form a distribution. This decay curve is analyzed with two programs using the two different quadrature formulas. The reconstructed distributions are very similar.

This indicates that the lifetime distribution analysis is insensitive to the approximation of f(k). It can be easily shown that when the intervals are equally spaced, formula (3.24) will be reduced to the exponential series approximation.

(F) The Selection of the Mesh Points

The selection of mesh points, k_is, in equation (3.3) is essential in the proper recovery of the underlying distribution. According to Pike and coworkers (see Chapter 2), the resolution limits of exponential relaxation rates are not evenly but geometrically distributed along the k axis. The distribution of the k_is should match the variation of resolution, therefore the k_is should also be geometrically spaced in the range [a,b]. Otherwise in the region where the inherent resolution is much higher than the mesh point density, serious distortions may occur. This way of setting the mesh point density has been suggested and used by Livesey and coworkers from a different point of view [32].

(G) Convolution Formulas

When the formula (3.24) is used, the fast iterative convolution formula is applicable. In this work, because usually the convolution calculation is just a small portion

of the whole calculation, we have used the more accurate Demas and Crosby method [56].

When formula (3.23) is used, no iterative convolution formula is available. We have used, therefore, the definition directly to carry out the convolution, that is

$$Z_i(t) = \sum_{t'=0}^{t} I_i(t')\, E(t-t'). \tag{3.25}$$

As might be expected, in this case the convolution calculation is much slower. The convergence, however, seems faster.

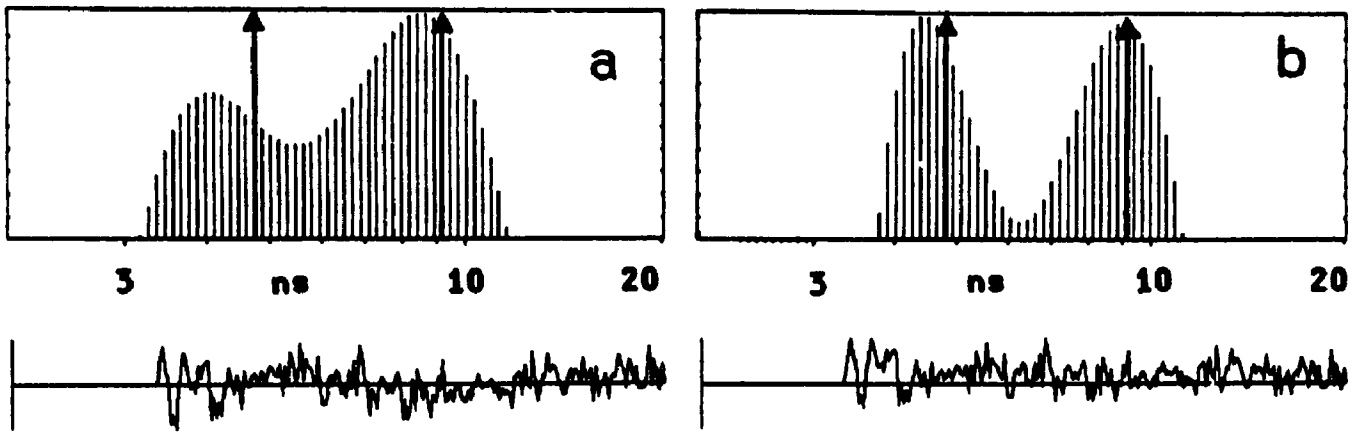

Fig. 3.1 The effect of the "weakened" non-negative constraint [see also Fig.4.1(c)]: a recovery of a real double exponential decay, (a) with the "zero-return" non-negative constraint, and (b) with the "fraction-return" non-negative constraint(Γ=0.8). The two bold arrows represent the underlying double lifetimes to be recovered. It can be seen that the weakened, "fraction-return" constraint leads to a better reconstruction, although there are a few very small negative components remained in the short lifetime region of the solution. To suppress completely these negative components, under the weakened constraint, takes too much computing time, but is not likely to affect the solution significantly.

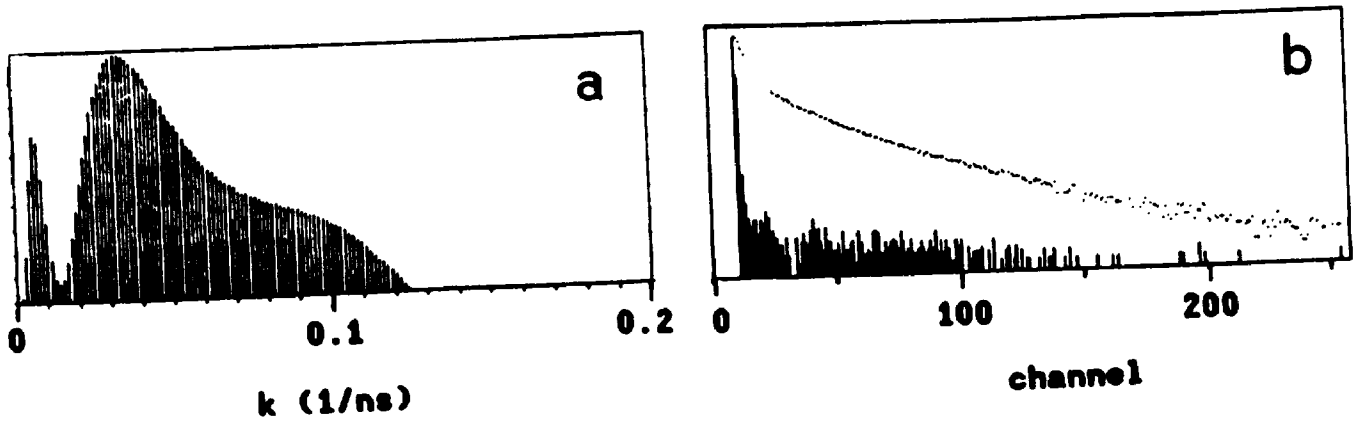

Fig. 3.2 An example of the generation of a simulated decay curve: (a) 150 lifetime components with proper amplitudes, used to simulate a distribution (in this example the distribution is made in k space); (b) the decay curve generated from the lifetime components in (a).

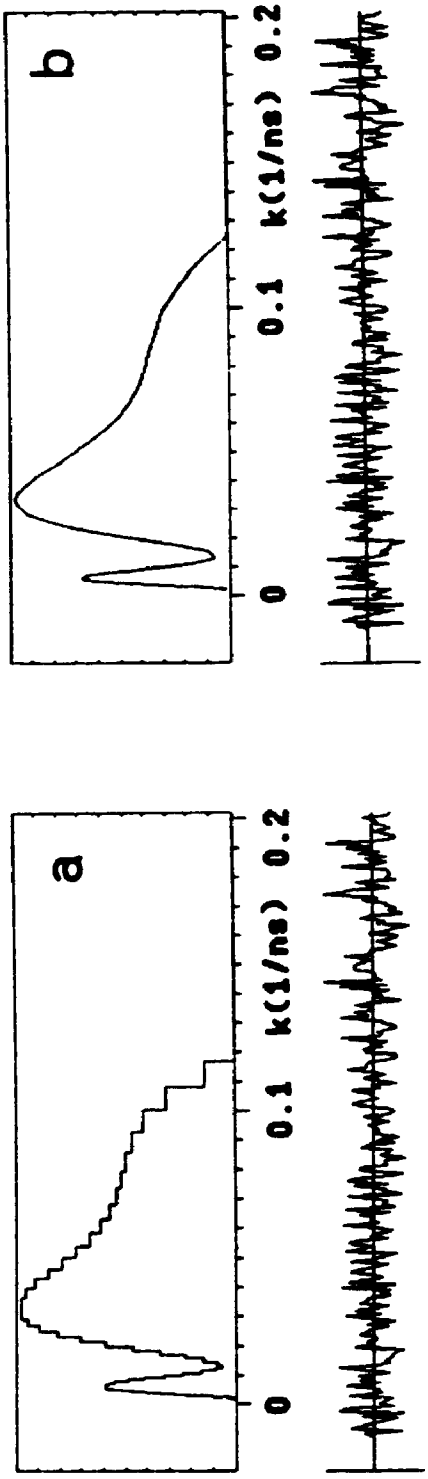

Fig. 3.3 The results of distribution analysis for the simulated decay in Fig. 3.2(b): (a) the distribution recovered with quadrature formula (3.21); (b) The distribution recovered with quadrature formula (3.22).

CHAPTER 4 TEST OF THE SMM PROGRAM WITH SIMULATED DATA

4.1 WHAT IS MEANT BY A "TEST"

When an inverse technique is suggested, it is a common practice that a series of tests is used to show the utility of the technique. However, in the study of inverse problems, the so called "test" is a very ambiguous issue. As discussed in the previous chapters, an inverse technique seeks the solution according to some criterion, for instance least-squares; thus every solution is tested by the goodness of its fit to the data in the searching process. From this viewpoint, no additional test seems necessary. On the other hand, because of the ill-conditioned nature of the problem, there are always many solutions equally compatible with the same set of data. An inverse technique, no matter how it is designed, can give only one particular solution. From this viewpoint, it is vain to try to prove, by these tests, that a technique or a program can always give the "true" solution. The latter statement will become more clear in the following discussions. Under such a circumstances, what is the purpose of a "test"?

In the previous chapters, the mathematical properties of lifetime distribution analysis have been generally described. These discussions cannot answer, however, specifically for data obtained by the single photon counting

(SPC) technique, how "ill-conditioned" the problem is, and whether or not any useful information can be derived from these data. In this regard, the tests examine the sensitivity of the solution to the quality of the SPC data. This is an important aspect of the tests.

In a lifetime distribution analysis, a particular program, depending on the algorithm used and the constraint applied, will tend to find a particular type of solution, out of the whole family of feasible solutions. We therefore need to know what type of solution a particular program is appropriate to seek. The test, therefore, should also be understood as a demonstration of the properties and the performance of the working program.

The SMM program contains an adjustable parameter, α, which controls the relative weight of the smoothing constraint. This parameter is intentionally made adjustable because we want to know what variety of solutions may fit the same set of data. When the α is set to 0, the smoothing constraint is completely removed, the program uses the ordinary Marquardt method. We will denote particularly by MM the SMM program running in this smooth-constraint-free mode. On the other hand, SMM program refers to, unless indicated otherwise, the case that the smoothing constraint, α, takes the largest possible value under the condition that the chi-squared and the residual profile are statistically acceptable.

4.2 "RESOLUTION" TESTS

By this title, we mean to demonstrate what is the finest structure which the program can possibly resolve, and in what cases the program fails to reconstruct the correct underlying distribution. This kind of test is significant only in the sense that it demonstrates the maximum power of the program in resolving the details given by the data, but it by no means guarantees that the resolved details are always real. That is, the success in a resolution test is a necessary, but not a sufficient, condition, for the recovered details to be the "true" one. If the complexity of this problem is not fully understood, the resolution tests may create a false sense of confidence in the reality of recovered distributions obtained by a previously tested program.

In all these tests, unless indicated otherwise, a simulated decay curve was generated from a combination of a number of Gaussian distributions, constructed from 120 exponential terms. The impulse decay was calculated from the 120 exponential terms, based on equation (3) in Chapter 2, and was then convoluted with a suitable experimental lamp profile. The decay curves were generated to a moderately high precision (200000 CPC and 256 channels) with a Gaussian noise added. In fact, most of the real data in the present work were collected under such or similar conditions (≈

200000 CPC and 256 channels). The artificial distributions were designed mostly in shapes similar to those discovered in the real samples. In Chapter 3 Fig. 3.2, the procedure used to generate a simulated decay curve has been illustrated.

The results of these simulated experiments are presented in Figs. 4.1-10. In most of these figures, the results derived from the MM and the SMM program with different levels of smoothing are presented. In some cases the corresponding results derived from the MEM program [33,34,47,48], previously developed in this laboratory, are also shown for comparison. The details of the simulations and the fitting conditions are given in the corresponding figure captions.

Figs. 4.1-2 demonstrate the recovery of two discrete lifetimes as a function of CPC counts and the separation of the two lifetimes. The MM program with a weakened non-negative constraint and the MEM program are used in these tests. These results show that, as far as resolution is concerned, the MM program is as good as MEM program. Figs. 4.3-5 demonstrate the possibility of recovering multiple, narrow distributions. In the first two cases, both the MM and MEM programs give reasonably good results, the MM program seems to be slightly better. Fig. 4.5, however, is a counter-example which demonstrates that both programs may lead to a qualitatively wrong solution. Figs. 4.6-9 show the

possibility of recovering broad and flat distributions. The results suggest that the SMM program can best reconstruct these distributions. The MM program, although the best in analyzing narrow distributions, distorts these broad distributions to some degree. Fig. 10 is a mixed case. The distribution to be analyzed is a combination of a broad and a narrow distribution. SMM recovers the broad peak better, but MM recovers the narrow peak better. The results given by the MEM program, which does not adjust a parameter of smoothing constraint, are mostly in between of those given by SMM and MM.

These examples indicate the following. (a) If the input distribution has two broad peaks of different relative heights, as will be seen in Chapter 6 and 7 for the real PAH-silica gel samples, they can be "accurately" reconstructed by the SMM. This is, of course, a necessary condition to justify these models. (b) Every program tested has its favourable cases and its unfavourable cases. A particular program can be "good" only in a certain type of problem. (c) Even for the simplest situation it is still quite possible to obtain a "wrong" solution.

A question then arises as to whether or not we can clearly define, and distinguish in practice, the so-called "favourable case" and "unfavourable case" for a program tested. If we can do so, then, at least, we will have

confidence in the recovered distribution when the "favourable condition" is well recognized. Unfortunately, as discussed in Chapter 2, this is a very complicated matter. The distinction between favourable and unfavourable cases for a decay curve and a program depends on CPC, the number of channels, time base (time per channel), and, most frustratingly, the type (widths and shape) of the unknown distribution. The major difficulty lies in that whenever an inverse technique is needed, there is no information available about the type of the underlying distribution. On the other hand, because every program tends, due to the ill-conditioning of the problem, to cast the solution into its preferred style, the real type of the underlying distribution cannot be recognized by the solution itself. In this regard, some examples will be further discussed in the following.

The simplest type of task is to examine under what conditions two single exponentials can be resolved by a program employed, and to derive a "resolution limit" for this program [32-34,47,48,86]. There is no doubt that this is an important parameter to characterize a property of a program. The question is that, in the practice of dealing with unknown distributions, if we find two peaks justifiable by the "resolution limit", can we be certain that they represent reality? The answer to this question, generally speaking, is "no".

Examples can be found in the Figures. Although from the tests we have evidence that two, three, even four peaks can be resolved in favourable cases (such as Fig. 4.1 through Fig. 4.4); in Fig. 4.5 and Fig. 4.6 the two or three peaks recovered with the same program, well qualified as favourable cases by the distances between these peaks (the peak lifetime ratio is about 2 or 3), are not true! It is well known that to establish a scientific law by the inductive method requires thousands of thousands of tests, but to disprove this law needs only one valid, reproducible counter-example.

In fact, the result of the above resolution limit tests is applicable only when we know a priori that the decay curve to be analyzed is indeed composed of two single exponentials or two narrow distributions. If, however, we know a priori such information, we do not need, in practice, to use any lifetime distribution analysis technique, because in such a case there is no reason to refuse the use of the classical, "well-conditioned", two exponential fitting technique. We come, therefore, to the surprising conclusion that the resolution tests cannot really help us, in some sense, to deal with unknown distributions!

The embarrassing situation discussed above is a direct consequence of the ill-conditioned nature of lifetime distribution analysis. Because there are always many

solutions which fit a decay curve equally well, and because a particular program or algorithm gives only one solution for a given set of data, the "reality" of a recovered solution can never be guaranteed, on mathematical grounds alone.

Having arrived at the nature of lifetime distribution analysis, one might want to ask: "what is the use of the lifetime distribution analysis, if the result is not guaranteed to be true?" A brief answer is the following: there must be something true and something untrue in a result of such analysis, the ultimate criterion for a distinction between the true and the untrue must be based on physical grounds, rather than a mathematical basis. We now turn attention to the physical aspect of this problem.

4.3 ROBUSTNESS TESTS

The purpose of undertaking the lifetime distribution analysis is to seek the parameters which describe a real, physical process. The physical determinacy of such a process requires that the solution must be reasonably stable against random errors. Otherwise, the solution cannot be used as a model to describe the physical process. This requirement has led to a desire for inversion techniques to be "rob· t".

The word "robust" has been used by a number of authors

[86,87] to describe the property that an inverse technique can give similar results, when analyzing data sets that are derived from the same underlying distribution, but have different samples of random noise added to them. Robustness is thus the ability of a program to compute a "stable solution" against random noise. If a program is not "robust" enough, then the results acquired by it will be noise-dependent. Consequently, these results are not reproducible, and thus, from a physical standpoint, not acceptable as a true model. Robustness can therefore be considered as another necessary condition for a program to be useful in lifetime distribution analysis.

Figs. 4.11 and 4.12 show the results of robustness tests of the MM and the SMM program, using two distributions. The two input distributions are shown as (a) in each Figure. The seven simulated decays have been generated from each of these two distributions, with different samples of random Gaussian noise added. All decay curves have been made to about 200000 CPC, at 4 ns/channel and in 256 channels. The results obtained from the MM are shown as (c). The fact that these remarkably different distributions in each graph are all derived from the same input distribution clearly illustrates the inherent instability of lifetime distribution analysis at the given level of data precision. In comparison, the results from the SMM, shown as (b), are very similar, which demonstrate the desired robustness

property of the SMM.

The SMM is robust also in the sense that it gives stable results under varied "data collection" conditions. In Figs. 4.11 and 4.12, (d) and (e) are the recovered distributions derived from the decay curves that have been generated, using the same two distributions as (a), at a much decreased time base, 0.5 ns/channel, with other conditions remained unchanged. The SMM still gives similar results, (d), as those in (b), But the MM severely distorts its results as shown in (e).

Another point of interest in these results is the comparison between the chi-squared achieved by the SMM and the MM program. Table 4.1 shows the final chi-squared for those results shown in (b) and (c) of Figs. 4.11 and 4.12.

Table 4.1 The final chi-squared achieved by the SMM and the MM program.

#	χ^2 (chi-squared)			
	(b) SMM	(b) MM	(c) SMM	(c) MM
1	1.1145	1.0628	1.0439	1.0077
2	0.9788	0.9727	0.9052	0.8964
3	0.7212	0.7213	1.0878	1.0618
4	1.0254	1.0275	0.8815	0.8632
5	1.0292	1.0176	1.0986	1.0787
6	0.9330	0.9241	1.0651	1.0436
7	0.9179	0.9136	1.1127	1.1050
average	0.9600 ±0.12	0.9485 ±0.11	1.0278 ±0.095	1.0081 ±0.093

It can be seen that, although the smoothed results are closer to the true distribution, their corresponding chi-squared is mostly higher than that of the unsmoothed results. This indicates that, as already noticed by some authors [86], the lower chi-squared obtained by the unconstrained program, compared with those obtained by the constrained program, is a consequence of "fitting" noise, therefore this further decreased chi-squared is indeed insignificant.

In this context, it is important to note that the robustness of a program is still not a sufficient condition for a recovered solution to be true. Robustness is achieved, to some degree, by the sacrifice of resolution. This is the reason why in cases that when the highest resolution is the major concern, the smoothing constraint (and in some cases even the positive constraint also) have to be weakened to get the best results. In this regard, to analyze an unknown distribution is a subtle balance between the two requirements, resolution and stability, of the solution. This is just where the additional information, other than the decay curve itself, is required to solve this type of problem.

It should also be emphasized, again, that the instability of the results given by the MM program is not a problem of the program algorithm, but a problem inherent in the nature of

lifetime distribution analysis. The tests of the unconstrained program shown in (c) of Figs. 4.11 and 4.12, resulting in a variety of compatible solutions to the same decay curve, may be employed for the purpose of error estimation. We may generate as many such compatible solutions as desired. These solutions together, then, can serve as a rough but simple demonstration of the inherent uncertainty of the data obtained from the given shape of the distribution, under the given conditions of data collection (CPC, number of channels, time base, etc). As a rigorously theoretical error estimate for inverse problems is rather difficult, the above tests may be considered as a kind of Monte Carlo experiment devoted to the same purpose. Some examples of such "Monte Carlo experiments" are given in Fig. 4.13 and Fig. 4.14. Fig. 4.13 shows a group of experiments, which demonstrate the uncertainty of the reconstructed distribution as a function of CPC of the decay curve. It is evident that with the increase of the CPC of the simulated decay curve, the stability of the result is greatly improved. Fig. 4.14 demonstrates the "Gibbs phenomenon": the oscillations caused by a sharp corner in the underlying distribution.

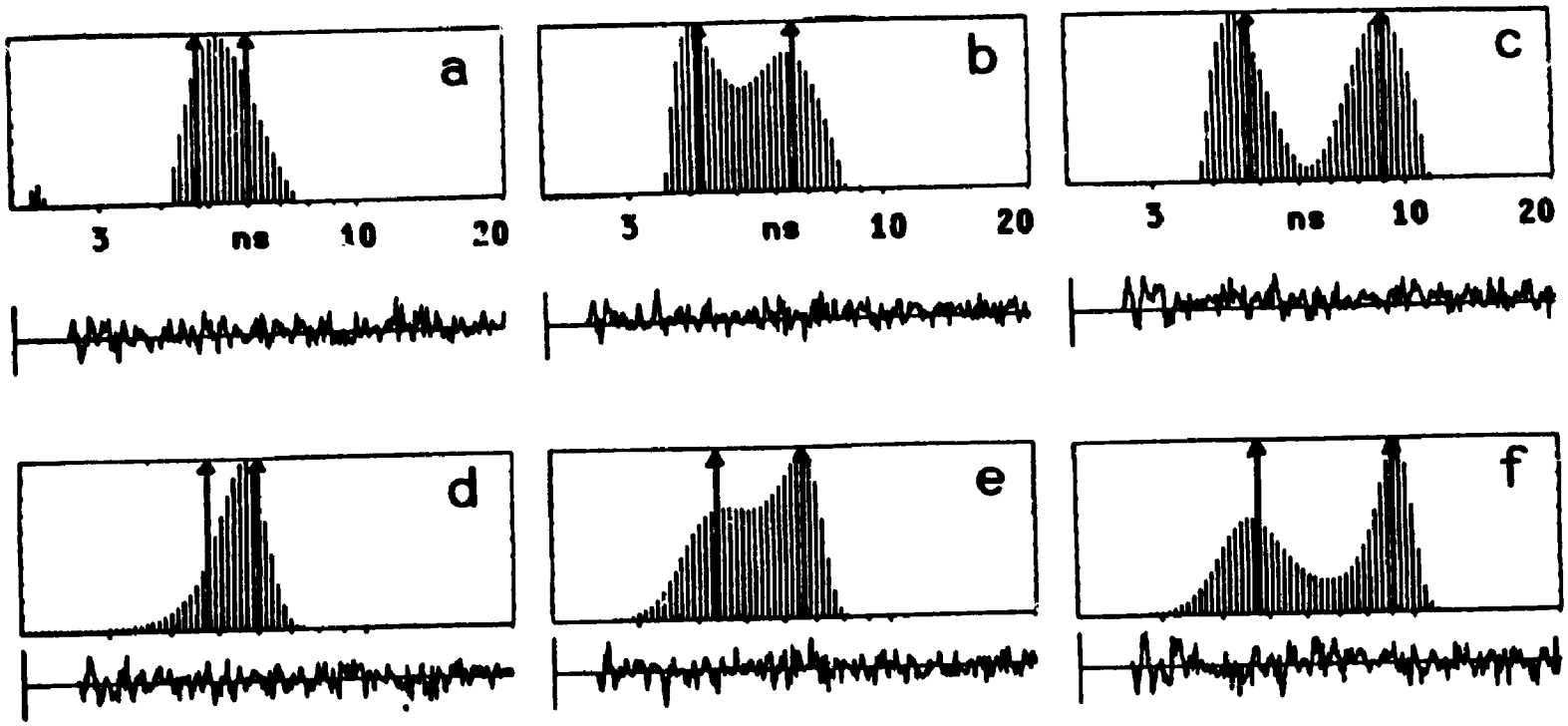

Fig. 4.1 The analysis of some real double-exponential decays of equal amplitude, separated by a variety of lifetime ratios. The decays are all 500000 CPC, 256 channels, and 0.297 ns/channel. (a), (b) and (c) are results derived from MM program, (d), (e) and (f) are from MEM program. The lifetime ratios, $r=\tau_2/\tau_1$, are: (a) and (d), 1.27; (b) and (e), 1.53; (c) and (f), 1.89.

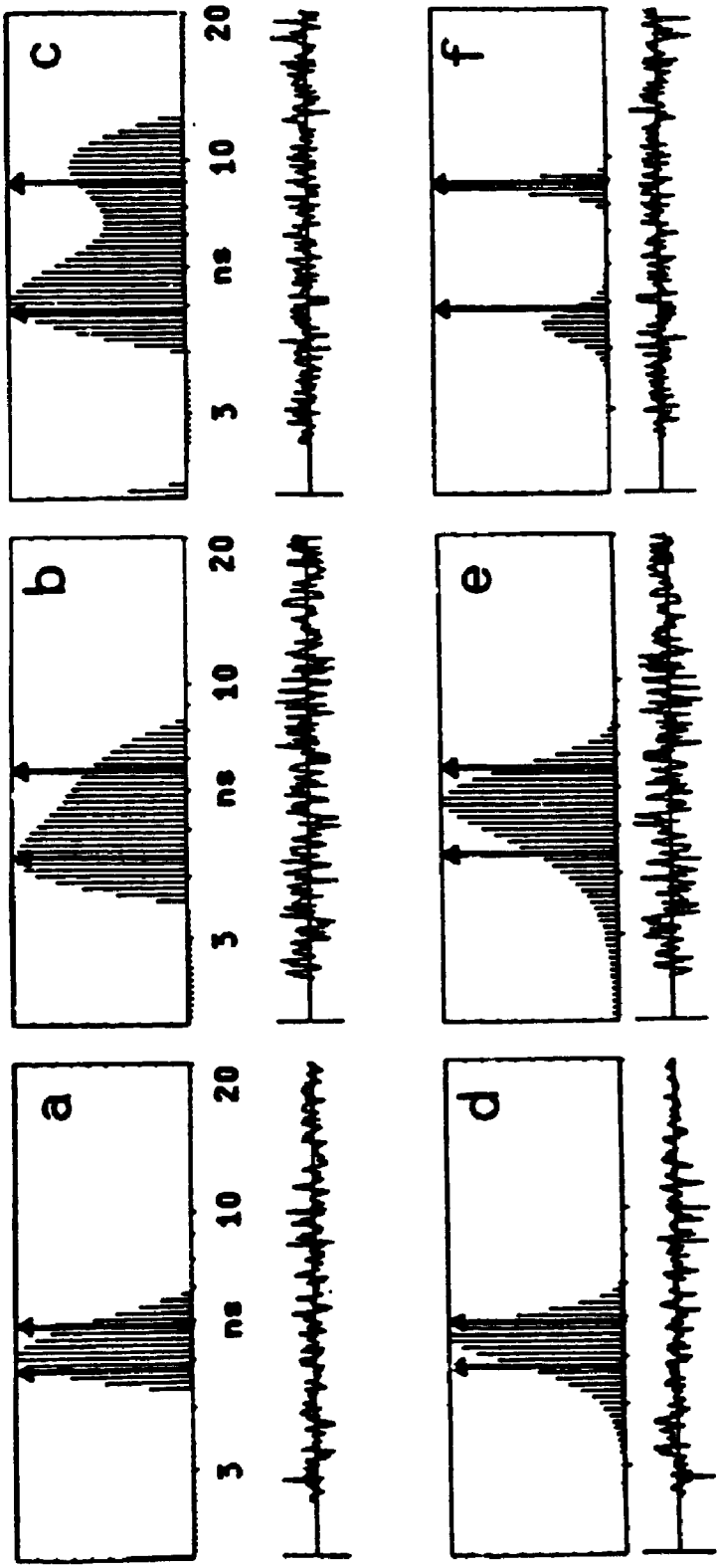

Fig. 4.2 The analysis of some real double-exponential decays of equal amplitude, separated by a variety of lifetime ratios. All the conditions are the same as those for Fig. 4.1, except the decays all have 20000 CPC.

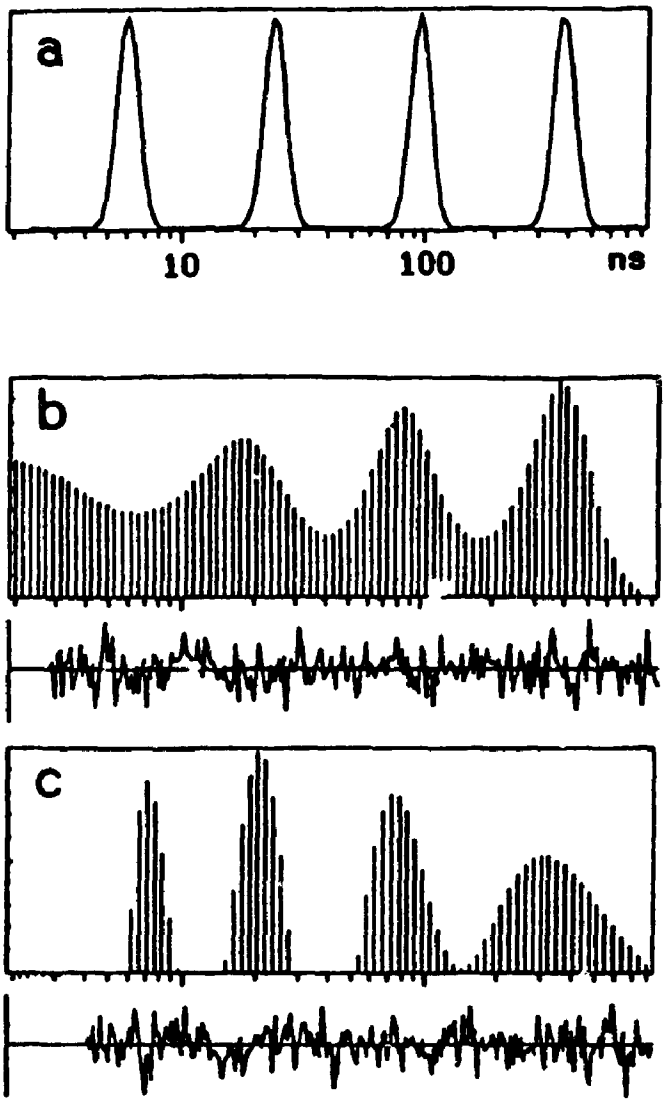

Fig. 4.3 The possibility of recovering four narrow distributions: (a) the input distribution from which the simulated decay was constructed; the reconstructed distribution for the input, using (b) MEM; (c) MM program.

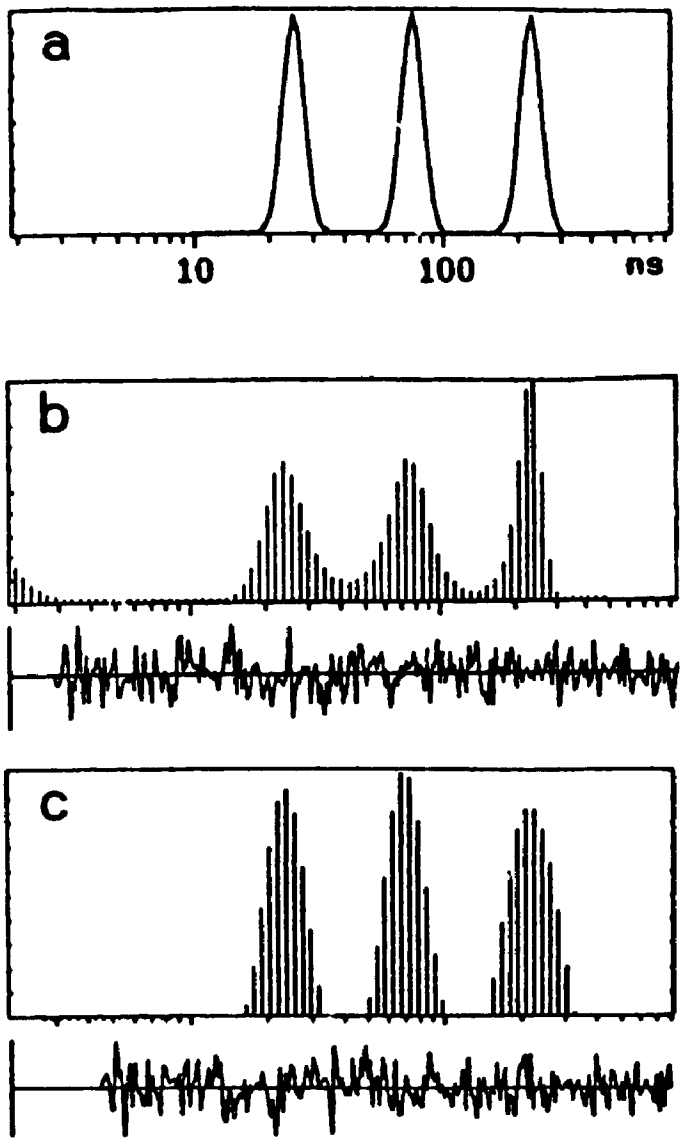

Fig. 4.4 The possibility of recovering three narrow distributions: (a) the input distribution; the reconstructed distribution for the input, using (b) MEM; (c) MM program.

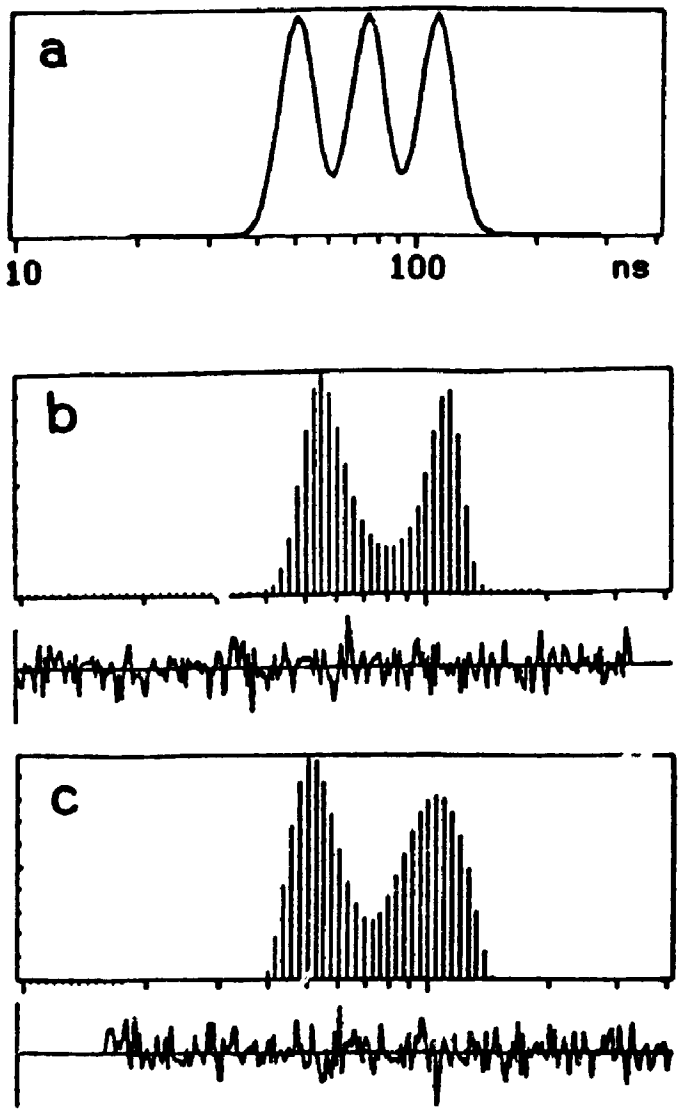

Fig. 4.5 An example of misreconstruction: (a) the input distribution; the reconstructed distribution for the input, using (b) MEM; (c) MM program.

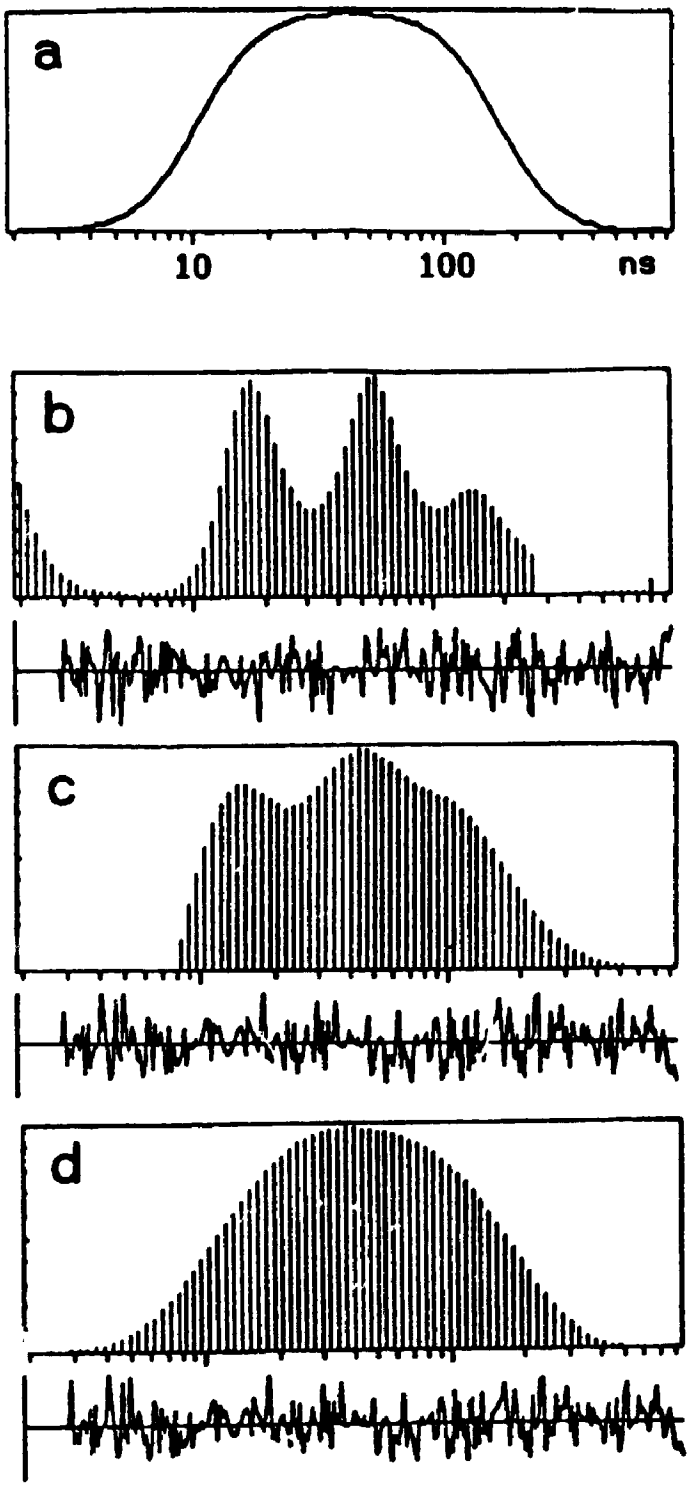

Fig. 4.6 The recovery of a broad, monomodal distribution: (a) the input distribution; the reconstructed distribution for the input, using (b) MEM; (c) MM; (d) SMM program.

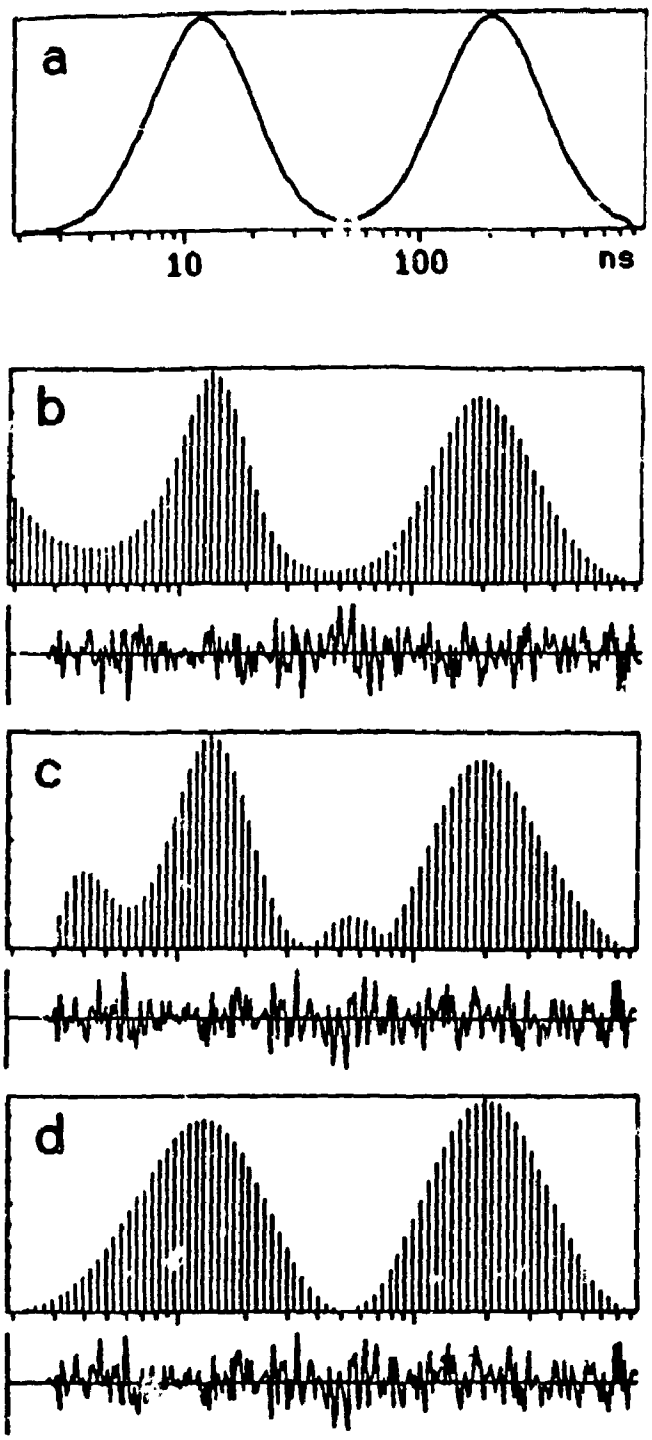

Fig. 4.7 The recovery of a bimodal distribution: (a) the input distribution; the reconstructed distribution using (b) MEM; (c) MM; (d) SMM.

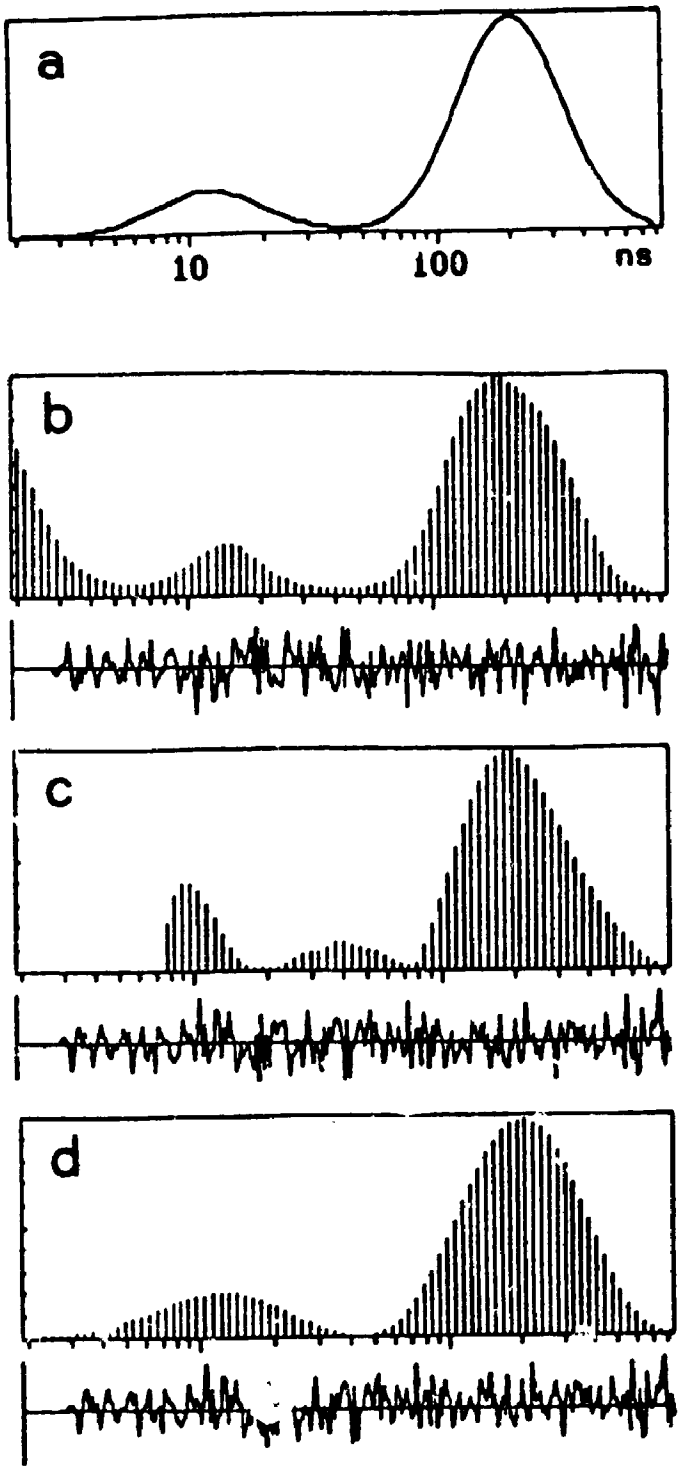

Fig. 4.8 The recovery of a bimodal distribution: (a) the input distribution; the reconstructed distribution using (b) MEM; (c) MM; (d) SMM.

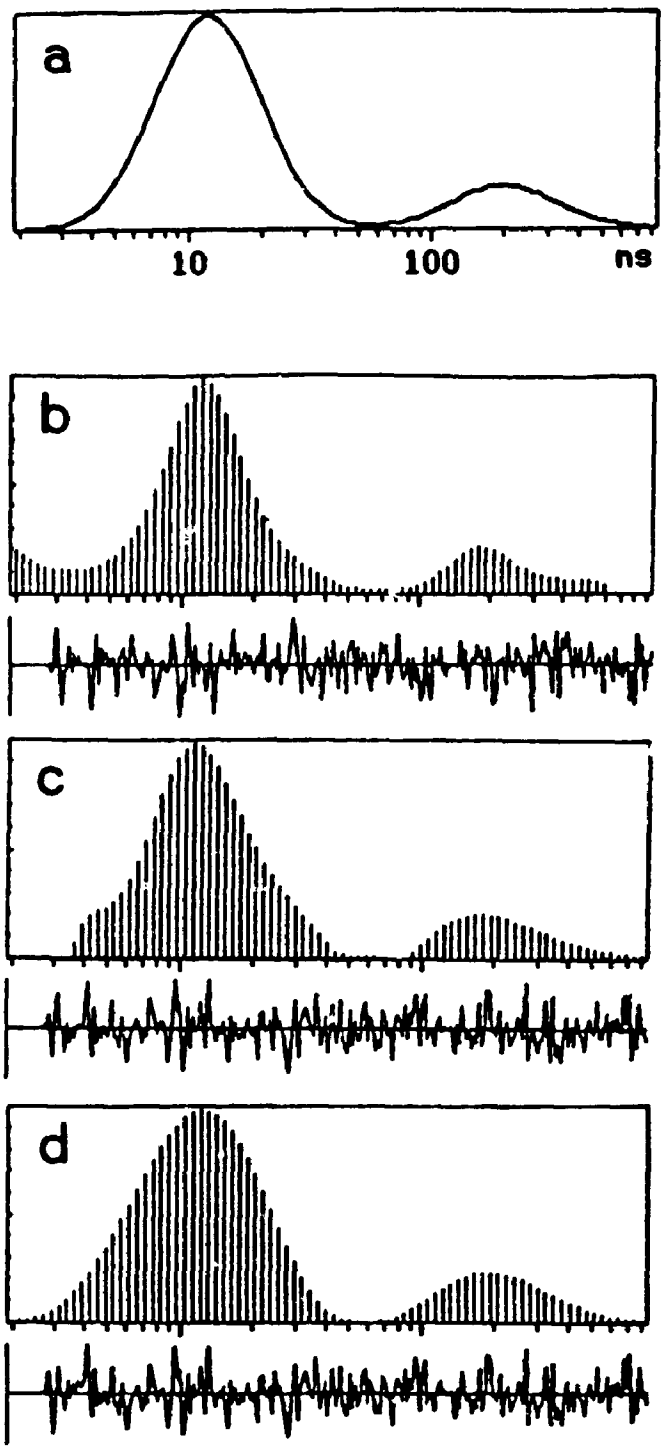

Fig. 4.9 The recovery of a bimodal distribution: (a) the input distribution; the reconstructed distribution using (b) MEM; (c) MM; (d) SMM.

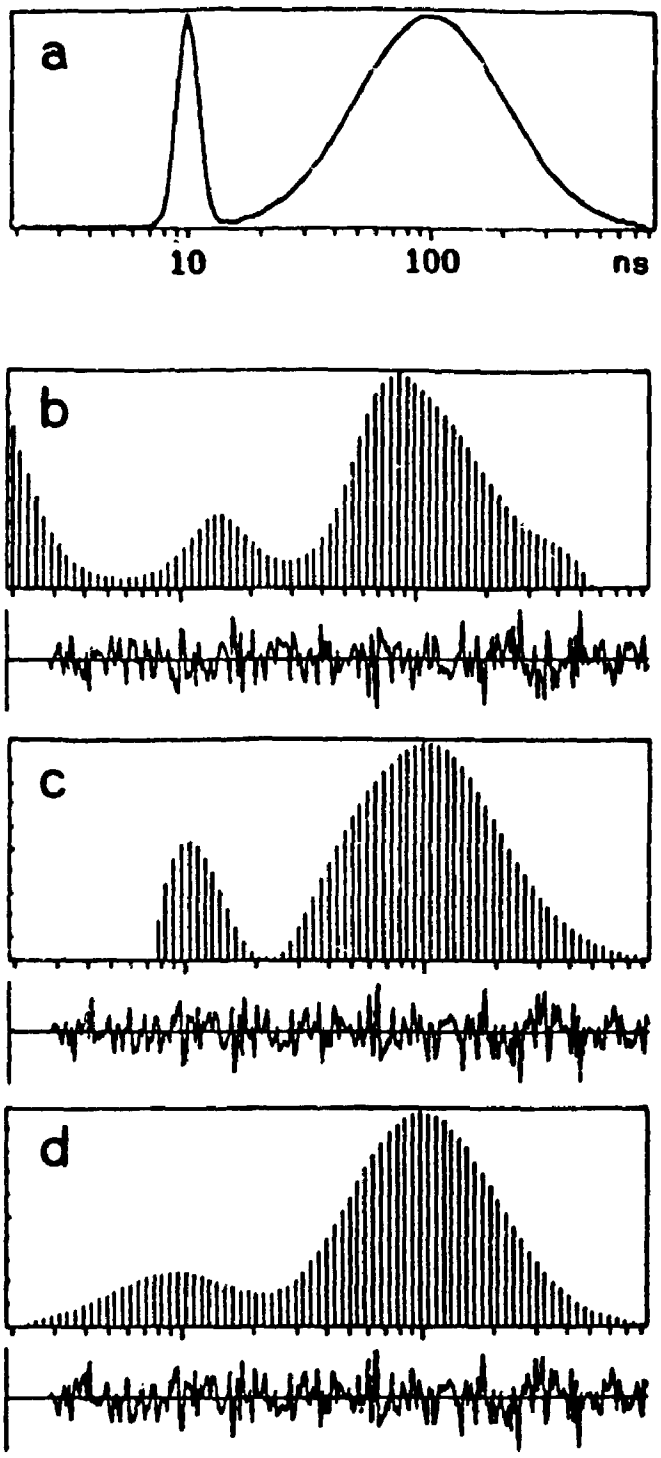

Fig. 4.10 The recovery of a bimodal distribution: (a) the input distribution; the reconstructed distribution using (b) MEM; (c) MM; (d) SMM.

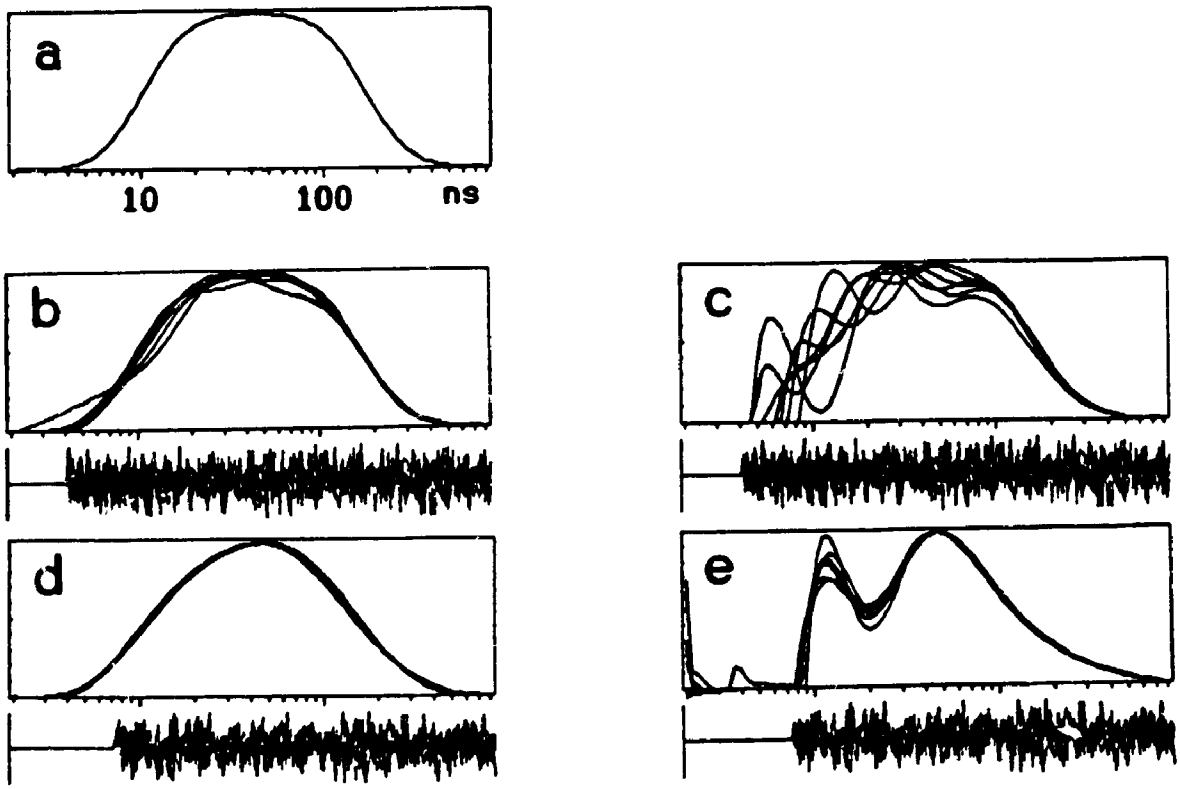

Fig. 4.11 A robustness test using a monomodal distribution shown in (a): Seven simulated decay curves were generated, and added with different samples of Gaussian noise. (b) - (e) are the reconstructed distributions. There are seven results overlapped in each graph. (b) & (d) using SMM; (c) & (e) using MM. The time bases of the decay curves are 4 ns/channel for (b) & (c); 0.5 ns/channel for (d) & (e).

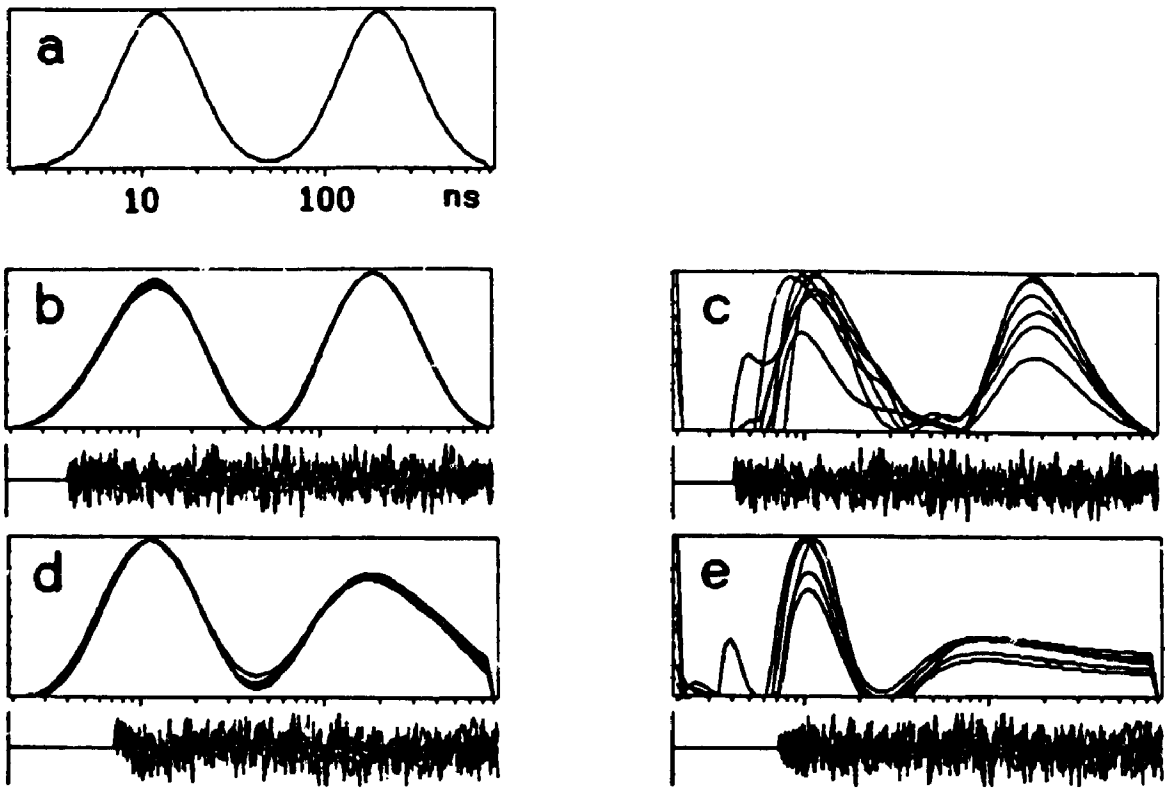

Fig. 4.12 A robustness test using a bimodal distribution shown in (a): Seven simulated decay curves were generated, and added with different samples of Gaussian noise. (b) - (e) are the reconstructed distributions. Seven results are overlapped in each graph. (b) & (d) using SMM; (c) & (e) using MM. The time bases of the decay curves are 4 ns/channel for (b) & (c); 0.5 ns/channel for (d) & (e).

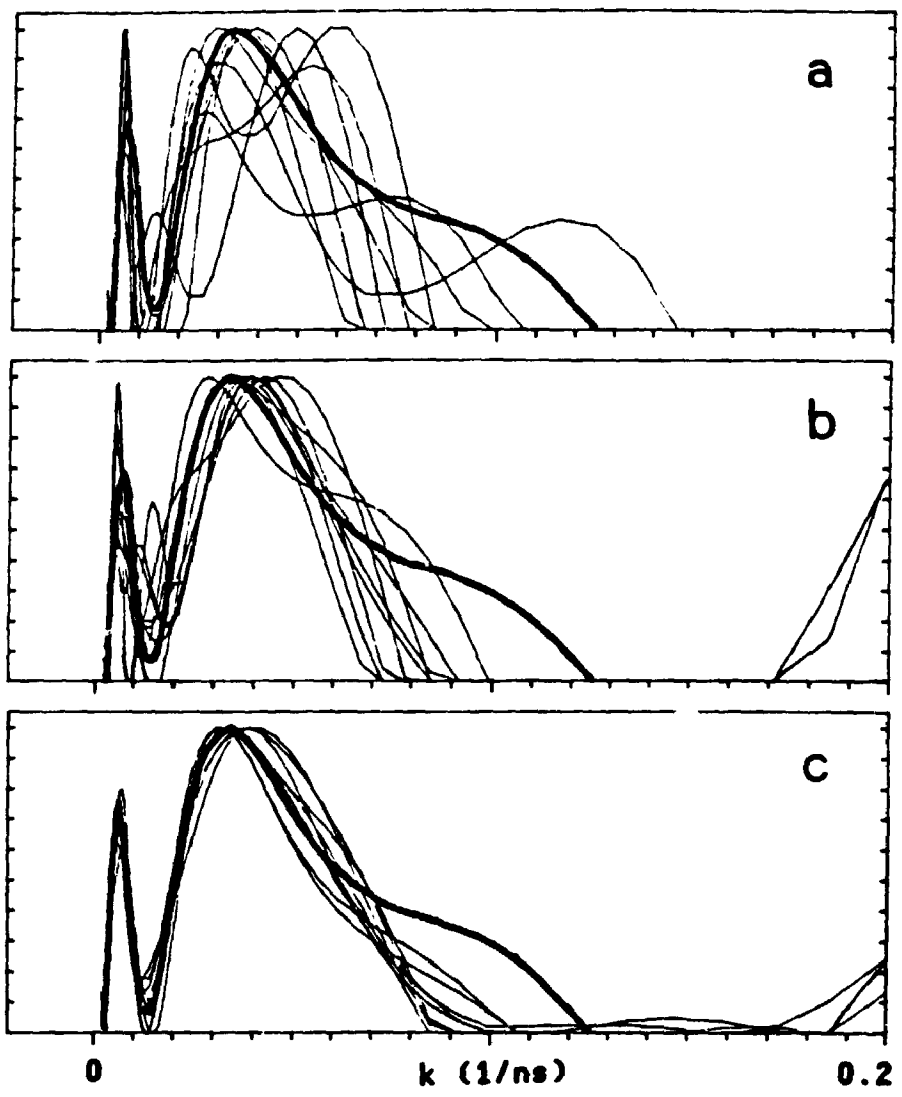

Fig. 4.13 An uncertainty test showing the effect of CPC, the decay datum precision, on the stability of the solution: (a) 5000 CPC, (b) 20000 CPC, (c) 500000 CPC. In each figure, the bold line represents the true underlying distribution being recovered. The thin lines represent the distributions recovered from 9 simulated decay curves, with different samples of Gaussian noise added.

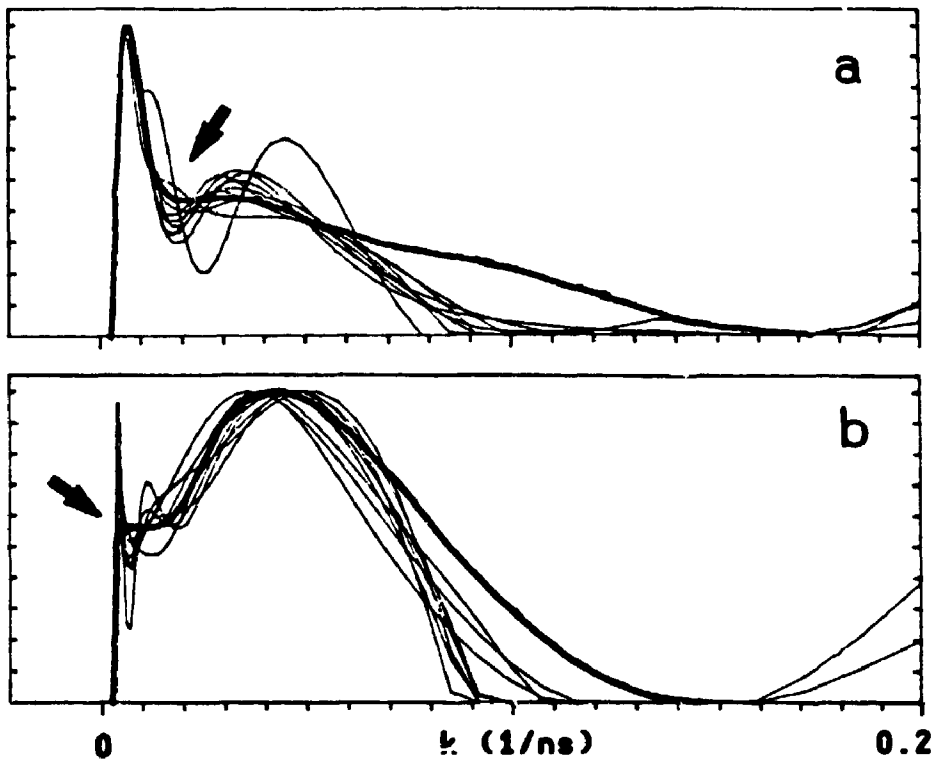

Fig. 4.14 An uncertainty test showing the influence of the form of the distribution on the stability of the solutions. The bold line and the thin lines mean the same as those in Fig. 4.13. A sharp corner, as indicated by the arrows, in an underlying distribution tends to cause overshooting and oscillations, therefore, is an unfavourable case. (a) and (b) are two examples of such cases, derived both from simulated decays of 100000 CPC.

CHAPTER 5 SURFACE SAMPLE PREPARATION AND FLUORESCENCE DECAY MEASUREMENT

Before the validity of the lifetime distribution analysis technique is examined on real data from surface samples, a description of the experimental details is necessary. Since the process of dehydroxylation of the silica gel reflects the basic underlying change of the organization of hydroxyl sites on the surface, observations of this process have traditionally played a central role in the investigation of the silica gel surface.

5.1 THE SILICA GEL SURFACE AND ITS DEHYDROXYLATION

The density of hydroxyl groups on a fully hydroxylated silica gel surface, and the decrease of this density upon dehydroxylation treatment have been extensively studied [88]. By "fully hydroxylated surface", it is meant that the physically adsorbed water on the surface has been removed (normally by heating the silica gel at 180°C), but the surface silanol or geminal groups remain to the greatest extent. In a recent study by Zhuravlev [89], it has been shown that the surface density of OH groups is a physicochemical constant for a fully hydroxylated surface and that the density as a function of the temperature of vacuum treatment does not depend, in a significant way, on the type of silica. His results agree well with previous

studies and are listed in Table 5.1.

Table 5.1 Average concentrations of OH groups on the surface of amorphous silica after vacuum treatments at various temperatures.

°C	OH/nm^2 [89]	OH/nm^2 [92]	isolated/total[92]
200	4.9	4.7	0.06
400	2.3	2.2	0.23
600	1.5	1.6	0.87
800	0.7	1.0	1.00

Numerous infrared spectroscopy studies have shown that the infrared absorption, attributed mainly to the OH stretching vibration of the surface hydroxyls, consists of a sharp band (a) at 3750 cm^{-1} and a broad one (b) between 3100 and 3750 cm^{-1}. The relative area of the broad (b) band decreases with the increase of the preheating temperature, and vanishes after a prolonged dehydroxylation at about 800°C. The sharp (a) band and the broad (b) band have been assigned to isolated hydroxyls and hydrogen bonded hydroxyls, respectively [90]. The broadness of the (b) band has been traditionally attributed to the fact that the distances of O—H·····O, between the interacting hydroxyl groups, are distributed over a certain value range as a consequence of the disordered nature of the surface [90]. Although later investigations have revealed some further details, for

example, that the isolated and hydrogen bonded OH groups can be classified further into subgroups [91], the original interpretation, as a first approximation, is still valid.

There have been a number of experimental and theoretical studies [92-94] about how the relative populations of isolated and hydrogen bonded OH groups vary during the dehydroxylation process. The surface density of total OH groups, and the ratio of the isolated to the total OH groups, as a function of preheating temperature, obtained by P.V.D.Voort and coworkers [92], are also listed in Table 5.1.

It has long been commonly accepted that the adsorption of PAHs on silica gel surface is caused by the surface hydroxyl groups [95-99]. The nature of this interaction is most popularly referred to as a "hydrogen bonding", though, in some sense, "dipole induced dipole interaction" is a name conceptually more precise. Whatever the nature of the interaction is, it should be reflected by the photophysical behaviour of the adsorbed PAH molecules. The basic idea in the experimental design of the present work is to observe the photophysical behaviours of PAH molecules adsorbed on variously dehydroxylated silica gel surfaces in order to seek information about the photophysical properties of PAH molecules and about the surface.

5.2 MATERIALS

Six PAHs have been studied in this work. Pyrene (Aldrich) was purified by recrystallization from alcohol solution and then by vacuum sublimation. Phenanthrene was zone-refined, chrysene (Princetone Organics), perylene (Litton Chemicals), benzoperylene and coronene (Aldrich) were used as received. The solvent used for quantitatively loading hydrocarbons onto surfaces was cyclohexane (Fisher Scientific, spectroanalized). It was passed through a silica gel column to remove residual water. The silica gel used were Kieselgel-60 (35-70 mesh) and Fractosil-500 (120-230 mesh) from Merck; hereafter they will be referred to as K-60 and F-500 respectively. The surface areas, as specified by the manufacturer, were 640 m^2/g and 50 m^2/g respectively.

5.3 SAMPLE PREPARATION

The pretreatment of the silica gel and the loading procedure of the PAHs are very critical factors in the photophysical behaviour of the adsorbate. Special attention must be given to highly dehydroxylated silica gel samples, because the surface of such silica gel is covered with isolated hydroxyl groups and strained Si-O-Si bonds, and is extremely active to moisture. Although a complete rehydration takes a very long time, to destroy completely the "dry surface effect" can be just a matter of seconds or minutes. It has been

repeatedly observed in this work, that simply dumping the high temperature heated silica gel from one apparatus to another may partly or even completely eliminate the dry surface effect. This is probably because the remaining isolated hydroxyl groups on a heated silica gel surface, whenever exposed to the atmosphere, tend to rapidly pick up water molecules and to become instantly hydrogen bonded (with water). Consequently, all the effects caused by these isolated OH groups disappear, before the rehydration of Si-O-Si bonds actually takes place.

The manner of the adsorption of PAH molecules is also very important. In the early stage of this work, the aromatic molecules were adsorbed onto the silica gel surface directly from the cyclohexane solution. From the thermodynamic point of view, such an adsorption, i.e. adsorption under an equilibrium condition, was preferred. However, it was soon found that it was too difficult to prevent the solution from absorbing traces of water from the atmosphere, and surprisingly, such a small amount of dissolved water was already enough to considerably reduce the dry surface effect. To avoid this interference, for the dehydroxylated silica gel sample, the adsorption was undertaken from the gas phase under a high vacuum condition. Such "dry" loading techniques have been described by Oelkrug and coworkers [4].

The apparatus used for preparing dehydroxylated samples is

shown in Fig. 5.2. Part A is quartz tubing or a cuvette that contains the prepared sample, and is used for later measurement. Part B is a quartz bulb in which the silica gel is subject to preheating. C and D are vacuum valves and D is a joint used for connecting the apparatus to the vacuum line. In the dehydroxylation experiment, the first step was to introduce the desired amount of PAH solution into A. The solvent was then evaporated and removed through the vacuum line, so that the PAH deposited in A. Then valve C was closed, so that the inside of A was maintained in a high vacuum condition. The next step was to introduce silica gel, which had been previously weighed and kept in a 180°C oven, into B. Then, the system was rejoined to the vacuum line and was evacuated to $< 10^{-3}$ torr while B was placed in a sand bath, heated at the desired temperature. When the heating was finished, the sand bath was removed, the apparatus cooled, then C was opened when system was still on the vacuum line. D was closed and the silica gel moved from B to A. Finally the quartz tubing or cuvette was sealed off the system for further experimental measurements.

The sealed samples had to be warmed to a proper temperature (depending on the molecular mass of the PAH), and were kept at this temperature for a period of time, to move the deposited hydrocarbon molecules onto the silica gel surface [4]. Also the samples had to be sufficiently tumbled to reach an equilibrium state.

5.4 FLUORESCENCE DECAY MEASUREMENTS

The fluorescence decay curves were determined with the single-photon counting (SPC) technique [100-102] using a PRA Model 3000 nanosecond flashlamp, or occasionally a Coherent picosecond laser system consisting of a Model CR-80 argon ion laser pumping a Model 590 dye laser. A simplified block diagram of the SPC instrument used in this work is shown in Fig. 5.3. In the SPC technique, the sample is repeatedly excited with short pulses of light from the flashlamp or the laser, and the resulting fluorescence photons are detected by a high-gain fast photomultiplier. By adjusting the intensity of the excitation light, the number of fluorescence photons received by the photomultiplier is controlled to be less than 2% of the number of excitation pulses. Under this condition, the probability that the first photon is detected at a time t after the initiation of a excitation pulse is proportional to the fluorescence intensity at that time [103,104]. The time of arrival of each photon is measured with reference to a fixed zero-time, usually the time of the initial rise of the excitation pulse. The record of the number of the photons as a function of time, which is stored in a multi-channel analyzer, gives an approximation of the time-course of the fluorescence intensity. This record is the so-called decay curve.

Many factors contribute to the uncertainties in the SPC

measurements [102]. Among these factors, the counting error, which varies from channel to channel, is of fundamental importance. In a SPC experiment, the probability of observing any specific number of counts in a channel i is given by the Poisson probability function, with a mean μ_i and a variance $\sigma_i^2 = \mu_i$. The actually collected counts, N_i, in this channel can be considered as an estimate of the mean μ_i. Hence the uncertainty in the ith channel is estimated by

$$\sigma_i = \sqrt{N_i} \tag{5.1}$$

Under a normal operation condition with currently available instruments, the number of counts in the peak channel (CPC) rarely exceeds 10^6. Assuming it is 10^6 and in the last channel the number of counts drops to 1% of that number, we can thus estimate the data precision from the peak channel to the last channel as 0.1%-1%. This is probably the highest precision achievable with the present instrumentation.

In addition to the counting error, errors from the instability and nonlinearity of the electronic devices, from optical origins, and from the unavoidable inconsistency in sample preparations, have to be considered also. The effect of the combination of all these factors on the result of lifetime distribution analysis is not quite clear at present. An intensive study of this subject would be highly desirable, but is beyond the scope of this work. We do not

to discuss or to pursue the highest possible precision. Instead, we choose to learn whether useful information can be obtained under normal operation. The true information is distinguished from the errors by the reproducibility of the results in a large number of repeated experiments.

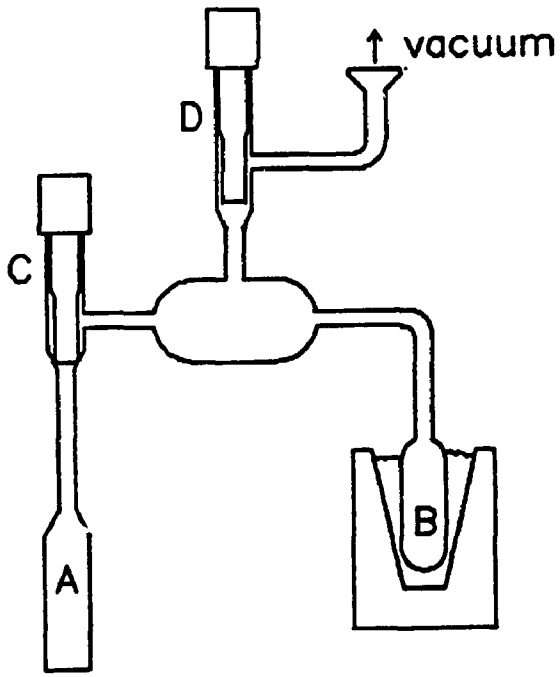

Fig. 5.1 The apparatus used for preparing dehydroxylated silica gel samples.

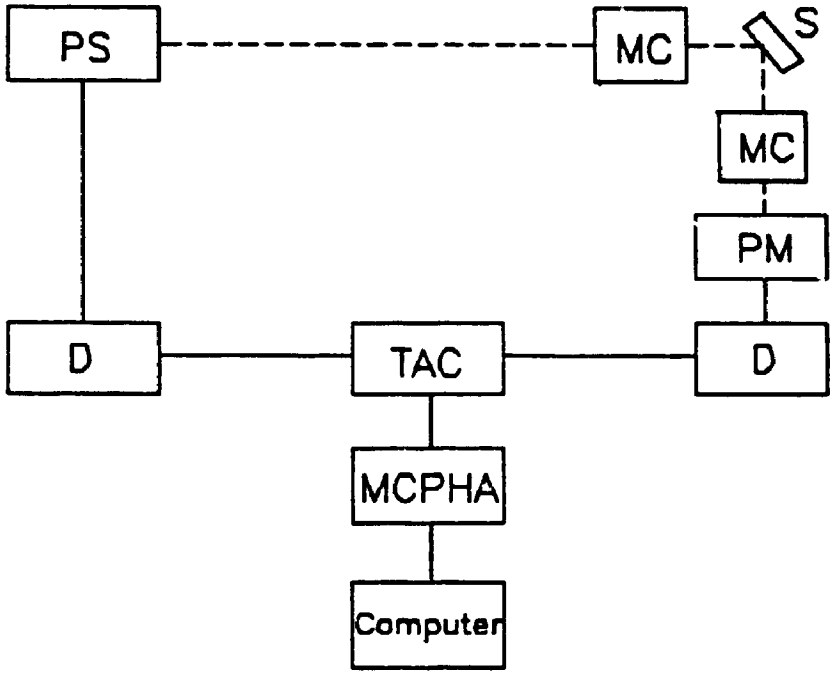

Fig. 5.2 A simplified block diagram showing the major components of the SPC instrument used in this work: **PS**, pulse source (laser or flash lamp); **MC**, monochromator; **S**, sample in a cuvette; **PM**, photomultiplier; **D**, discriminator; **TAC**, time-to-amplitude converter; **MCPHA**, multichannel pulse height analyzer.

CHAPTER 6 LIFETIME DISTRIBUTION ANALYSIS FOR PYRENE ADSORBED ON SILICA GEL SURFACES

6.1 INTRODUCTION

Pyrene is one of the most popular probes in photophysical studies. This is mainly because of its photostability, its relatively high fluorescence quantum yield, its long fluorescence lifetime, and its sensitivity to polarity. In the SPC measurement, a fluorescent compound with a long lifetime allows the time base to be set to cover a relatively long period, compared with the width of the excitation pulse, thus the error caused by the lamp profile and convolution can be minimized. Therefore, in a test of the validity of the lifetime distribution analysis techniques, pyrene becomes an excellent candidate.

The lifetimes of pyrene adsorbed on the surface of silica gel and some other adsorbents have been observed by several groups [9,10,24,105-109], using the classical discrete lifetime recovery technique. As mentioned earlier, these results are all non-exponential decays, and are reported normally as a sum of two or three lifetime components. This multiple-exponential feature has been mainly attributed to two reasons: the surface inhomogeneity, and the formation of an excimer (self-quenching) or ground state dimer.

De Mayo, Ware and coworkers extensively studied the lifetime of pyrene and some other PAHs adsorbed on variously modified silica gel surfaces [9,10,24,108]. They reported the results with two exponential terms, and pointed out that these two components did not necessarily represent two species, and that the existence of these two exponentials was an indication of surface inhomogeneity. They found that on highly dehydroxylated silica gel the lifetime of pyrene tended to decrease, and the micro-environment of the adsorbed molecules seemed more polar. These results were obtained from samples at a low surface coverage of 0.05% (area%), at which the formation of excimer or ground state dimer was very unlikely to occur in a significant extent.

At a higher surface coverage, say 1% or more, the situation is further complicated by the increasing possibility of forming excimer or ground state dimer. The results of lifetime analysis become more confusing. For example, Anpo and coworkers, in the study of pyrene adsorbed on porous glass, once used four exponentials to fit the decay. The four components were then assigned to monomer (349 ns), normal excimer (54 ns), ground state dimer (140 ns), and 1:n-type excimer (8 ns). In a paper [106] published later, they used three exponentials to fit the decay data, obtained under similar conditions. The three components were assigned to monomeric (305 ns), dimeric (105), and excimer-like (20 ns) pyrene species, and the 1:n-type excimer was dismissed.

These observations were done at a surface coverage of 0.14%-6%. It should also be mentioned that in an early study by de Mayo, Ware and coworkers [9,10,108], the decay of pyrene on a silica gel surface (16% coverage) was fitted with two exponentials. The two lifetimes were 200 ns and 70 ns, and were assigned to monomer and excimer-like pyrene respectively. A similar system of pyrene on a silica gel surface (1-88% coverage) was also studied by Francis and coworkers [109]. They used a kinetic model

$$I = I_0 \exp(n[\exp(-k_e t)-1]-k_1 t)$$

to fit the decay, and attributed the non-exponential decay to self-quenching only.

These examples show that the decay data of a complex system, such as pyrene adsorbed on silica gel surface, may be fitted, and then interpreted, in many alternative ways. It has been intensively discussed, in previous chapters, that lifetime recovery is a multiple solution problem. If a decay can be fitted by, for example, two exponentials, then it can be equally well fitted by many different combinations of lifetimes and distributions. Many photochemists and photophysicists have long ignored the complexity of this problem [29], because the classical method employed, which is the discrete lifetime analysis, has automatically ruled out a large number of alternative solutions. According to

the inverse theory, however, as stated by R.L.Parker [65], **"practical inverse problems never possess unique solutions and ... an honest attempt to interpret the data must appraise the variety of compatible solutions".**

In the following, as a typical example, we analyze a set of decay curves obtained in a series of dehydroxylation experiments, using a variety of different techniques. We intend to show how complicated this problem is, and to discuss how the selection of a reasonable solution can be made.

6.2 DEHYDROXYLATION PROCESS: DISCRETE LIFETIME ANALYSIS

In this group of dehydroxylation experiments, silica gel samples were pretreated at 25, 200, 400, 600, and 800°C in vacuum ($<10^{-3}$ torr) for 8 hours (hereafter, these five samples will be referred to as **a**, **b**, **c**, **d**, **e**, respectively). Pyrene was loaded to 0.01 mg/g. If the size of a pyrene molecule was estimated as 1.5 nm^2, then the monolayer coverage was 143 mg/g. Therefore, in these samples, the actual coverage of the surface by pyrene molecules was 0.007%. In comparison with those cited above, this was an extremely low coverage, and these experiments should be considered as the simplest cases, because the likelihood of forming excimer or excimer-like species might be ignored. All decay curves were obtained on the flash lamp system, to

a CPC of about 200000, at the excitation wavelength of 331 nm and the emission wavelength of 394 nm. Throughout this thesis, no matter what method was used, all the decay curves, unless indicated otherwise, were constantly fitted from the first channel after the peak to the last channel available (the 256th channel).

Let us assume first that the adsorbed pyrene molecules possess several discrete lifetimes; then the classical discrete lifetime analysis method should be valid. The standard procedure is to try to fit a decay sequentially with one, two, three and finally four exponentials until a satisfactory fit is obtained. Applying this procedure to this set of data, we have found that sample a needs at least 2 exponential terms to fit, sample b needs at least three exponentials to fit, and sample c, d, and e need four exponentials to fit. These results are presented in Tables 6.1 - 6.3.

Table 6.1 Two exponential analysis for the decay data a - e

sample	A_1	τ_1	A_2	τ_2	χ^2
a	0.443	142	0.557	237	1.546
b	0.540	51	0.460	223	11.953
c	0.746	44	0.254	238	23.150
d	0.840	39	0.160	237	30.356
e	0.920	28	0.080	177	11.050

Table 6.2 Three exponential analysis for the decay data a - e

sample	A_1	τ_1	A_2	τ_2	A_3	τ_3	χ^2
a	0.043	38	0.508	157	0.450	244	1.351
b	0.449	26	0.326	135	0.225	257	1.542
c	0.648	27	0.257	132	0.095	302	1.984
d	0.764	26	0.195	133	0.041	343	2.621
e	0.854	22	0.116	86	0.030	232	2.250

Table 6.3 Four exponential analysis for the decay data a-e

sample	A_1	τ_1	A_2	τ_2	A_3	τ_3	A_4	τ_4	χ^2
a	-0.136	78	0.235	79	0.628	179	0.304	257	1.396
b	0.366	18	0.206	62	0.319	179	0.109	284	1.118
c	0.503	18	0.257	56	0.191	176	0.048	338	1.033
d	0.571	17	0.278	48	0.130	170	0.021	386	1.179
e	0.609	16	0.322	36	0.060	144	0.009	294	1.112

Difficulties arise when we try to interpret these results. To accept these solutions and to describe the system in terms of these solutions, imply that we believe all the discovered exponential components are physical realities. Thus we have to assume a rather complicated model, including up to four states of pyrene molecules or four species made from pyrene molecules, to match these results. The low surface coverage and the observed fluorescence spectra, which will be shown in Chapter 3, do not allow us to assume the existence of excimer or excimer-like species in any of these sample. Perhaps we can interpret the four exponentials by the number of hydroxyl groups bonded on one pyrene molecule, thus we assign, for example, 16-18 ns to pyrene

molecules bonded by one OH, 36-62 ns to those bonded by two OHs, 144-179 ns to those bonded by three OHs, and 294-386 ns to those bonded by four OHs. But obviously, such a model can hardly be justified on the ground of the currently available knowledge. In addition, it has been commonly noted that four exponentials can actually fit almost any decay curve observed. The success of fitting data with four exponentials provides very little evidence for the existence of four species [110].

There are some "easy" ways to "avoid" these difficulties. One may decrease the number of channels to be fitted, say, fitting the decay from the fifth channel, instead of the first channel after the peak. Then a smaller number of exponential terms might be sufficient. Or alternatively, one might intentionally collect fewer counts in the decay curve, say 20000 CPC instead of 200000 CPC, so that by using a smaller number of terms, a "good fit" can still be achieved. In the practice of routine lifetime measurements, there is indeed no strict rule for the selection of these parameters. These are, perhaps, just the reasons that the lifetimes of pyrene on the surface of silica gel, and of many other compounds adsorbed on surfaces, have been reported, arbitrarily, as two, three, or four exponentials, and different interpretations have been attached to these exponentials without proper justification. Here by "arbitrary" we mean that one picks a solution without

appraising different types of compatible solutions.

The above discussion suggests that if a decay system is complex, or in other words the decay needs two or more exponentials to achieve a proper fit, the classical discrete lifetime analysis is not sufficient. A more complete analysis is demanded. The results listed in Table 6.3 are, though acceptable on statistical basis, not an attractive model to be used to describe the system under investigation. To seek some other possible solutions is, therefore, desirable. In the following, we examine the results given by the distribution analysis methods.

6.3 MEM ANALYSIS

The MEM refers to the "Maximum Entropy Method" [32]. This method have been successfully used in our lab for some relatively simple systems [47,111]. The MEM seeks a solution in the lifetime distribution analysis, which maximizes the entropy-like function

$$S = - \sum_i f_i \ln(f_i / \sum_i f_i)$$

subject to the condition of $x \approx 1$, where x is the chi-squared. According to Livesey [32], the MEM solution is "the best choice we can make for any given data set". Therefore the MEM solutions seem to deserve serious consideration.

Fig. 6.1 illustrates the results given by the MEM analysis. What these results show are the following. There is a major peak located in the range of 100 ns to 300 ns on unheated silica gel. With the increase of preheating temperature, the relative area under this peak decreases, and the peak splits into two at 400°C, then the two split into three at 800°C. There is a second major peak between 8 ns and 80 ns whose size increases with the increase of preheating temperature. This second peak splits into two at 800°C. There is a third peak between 2 to 8 ns. The relative size of this peak seems to increase with the preheating temperature until 600°C then decreases at 800°C.

All these complicated changes are interesting, but would be more so if we could relate them to a body of independently established knowledge about the system. Unfortunately, this seems also a very difficult, if not impossible, task. Suppose we try to interpret the splitting of the peaks with some unknown reason whereby the distributions are narrowed upon dehydroxylation. The locations of these splitting peaks, however, shift from sample to sample (preheated at different temperatures), which does not agree with this assumption. Another bothersome feature is the presence of a third peak in the short lifetime range. Peaks of this type can be seen in some simulation experiments in which broad distributions are involved. This indicates that these peaks are not always derived from the scattered light, as

straightforwardly assumed, but, most probably, are artifacts. If, as an alternative interpretation, we attribute these peaks to a lack of information because the time basé is larger than the lifetime of the components in this region, then we have to explain why these components should not be given zero amplitudes, for so called "lack of information". If we state that where there is a lack of information the program is expected to give such a huge, unwanted peak, then we are, in effect, saying that the program gives a false distribution in this particular case.

6.4 SMM ANALYSIS

The SMM analysis is different from the MEM in that it uses a smoothing constraint, instead of the "entropy" constraint, to stabilize the least-squares searching process, and it leads to a smoothed solution instead of a maximum entropy solution. There appears to be no statistical or pure mathematical reason which is in favour of any one of these approaches. The selection between these two types of solutions has to be based on physical grounds. If a problem to be solved has no physical background, probably, as Livesey has stated, the MEM solution is a good choice. If the problem has some physical background, then any presumably "true" solution must be at least physically reasonable. What we mean by "physically reasonable" is one or more than one of the following: (a) the solutions are

evidently interpretable on the basis of existing knowledge; (b) one solution is compatible, or consistent, with the other solutions within a group of experiments, (c) the solutions are reproducible.

The solutions given by the MM analysis, that is the SMM without smoothing constraints applied, are presented in Fig. 6.2. Similar physical considerations, as discussed for the MEM solutions, in what may be referred to as a "physical consistency test", suggest that the results given by MM are, also, not acceptable. For example, the results constantly show a single peak in the 100-300 ns region, which is physically plausible, but the distributions below 100 ns are not quite stable. In other words, the results are not self-consistent within the group of experiments.

In comparison, the smoothed SMM results, shown in Fig. 6.3, are stable over the whole range of the distributions. They show a clear trend throughout this group of experiments, namely that one peak in the range of 100-300 ns decreases with the increase of the preheating temperature, while a second peak in the range of 5-80 ns increases with the increase of the preheating temperature. The two peaks are well separated. On a fully hydroxylated surface (sample a), only the first peak can be seen. On a highly dehydroxylated surface (sample e), the second peak grows to its maximum size, while the first peak is almost eliminated, with only a

residual remaining. In this group of experiments, only the preheating temperature has been systematically altered; thus a corresponding change in the photophysical behaviour of pyrene should be expected. Obviously, this group of distributions shows such a comprehensible change, and it is, therefore, physically reasonable. The goodness of the fit to the decay curves well qualify them as feasible solutions. Of greatest significance is the fact that these results show that the bothersome features in Fig. 6.1 and Fig. 6.2, the plateaus and oscillations found in solutions given by MEM or MM, are all possibly caused by random error rather than by any aspect of physical reality. This is because they can be completely removed from these results without a significant sacrifice of chi-squared.

There are some other, more general, considerations that are in favour of the smoothest solutions. In any other set of solutions, say, those given by MEM, if we ignore the doubtful features and details, such as the plateaus on the short lifetime side and the splitting of peaks on the long lifetime side, then the information left in these solutions is just what is revealed by the smoothest solutions. That is, that with the increase of preheating temperature, one peak shown in the range of 100-300 ns decreases, while another peak, in the range of 8-80 ns, increases. This suggests that the smoothest solutions contain the features common to other solutions. The smoothest solutions are

simplified versions of the other solutions. Even if in the future, because of an improvement in instrumentation or because of the achievement of a deeper understanding of the system, some details in the other solutions are eventually established, the smoothest solution will still be acceptable as a first approximation. For the present, however, it seems more reasonable to accept as simple a model as possible which is compatible with our current knowledge, than to use a more complicated model without physical justification. Such an attitude toward simple solutions is well founded. In the early fourteenth century William of Occam wrote that " it is vain to do with more what can be done with fewer" [112,113]. This has been known as Occam's razor, and has become a fundamental tenet of modern science: hypotheses should be neither unnecessarily complicated nor unnecessarily numerous. The regularized lifetime distribution analysis technique is just such a useful tool, an Occam's razor, in seeking the simplest solution.

The SMM can be further tested by applying it to a variety of similar pyrene/silica-gel systems. If we change one parameter in the sample preparation, a similar solution, varied in some aspect, should be expected. If this is the case, then a consistent model may be proposed to describe all these similar system. Results from two more groups of dehydroxylation experiments are shown in Fig. 6.4 through Fig. 6.7. In one group of the experiments, the F-500 silica

gel was used, which is a larger pore size silica gel with a surface area of 50 m^2/g. Here pyrene was loaded to 0.01mg/g. The results are presented in Fig. 6.4, obtained from MM, and Fig. 6.5, obtained from SMM. We can see, again, that the SMM results show a clear trend, similar to Fig. 6.3. The major difference is that on the large pore size silica gel surface, the peak in the range of 5-80 ns appears at a higher temperature, but the whole dehydroxylation process is still completed at about 800°C. In another group of experiments, shown in Fig. 6.6 (MM results) and Fig. 6.7 (SMM results), the silica gel was of a small pore size, S-60, preheated for 2 hours, and pyrene was loaded to 0.1 mg/g. The SMM results are very similar to those of Fig. 6.3, except the relative size of the peaks in the 5-80 ns region is smaller than those in Fig. 6.3 for the 200°C and 400°C preheated samples, probably due to the shorter preheating period and the higher surface coverage.

Fig. 6.8 shows the results derived from fluorescence decays of a single sample, measured at various low temperatures. The sample was prepared under similar conditions as sample c in Fig. 6.3. The decays were measured at 293K, 200K and 100K respectively. In the SMM results, we can see a systematic shifting of both peaks towards the long lifetime side, and a broadening of both peaks at the lower temperatures. Fig. 6.9 shows how the solutions are remarkably changed with the increase of the smoothing constraint parameter α, without a

significant sacrifice of the chi-squared.

These results clearly show that the SMM solutions are consistent in all of these examined experiments. In comparison with the other solutions, the SMM solution is the simplest, and most easily comprehensible solution. This strongly suggests that the two ever present peaks, in the SMM solutions, are not artifacts, but most likely are features of the "true" model with which we may describe the photophysical behaviour of pyrene adsorbed on silica gel surfaces.

To summarize, we consider the smoothest solution to be a first choice in this study for the following reasons:

(A) The smoothed results are physically self-consistent within each group of experiments and between different groups of experiments. They are, therefore, physically more reasonable than other available results.

(B) The smoothed results provide a simple model for the observed photophysical behaviour. At present our knowledge about the system is not sufficient to support a more detailed model as implied by other results.

(C) The smoothed results appear to be the "average" of all the available solutions, in that they reveal the common features of all these solutions.

Fig. 6.1 The lifetime distributions of adsorbed pyrene, analyzed with MEM program, from a group of dehydroxylation experiments. The silica gel was K-60, preheated for 8 hours in vacuum at (a) 25°C; (b) 200°C; (c) 400°C; (d) 600°C; (e) 800°C. Pyrene was loaded to 0.01 mg/g, corresponding to a surface coverage of 0.007%.

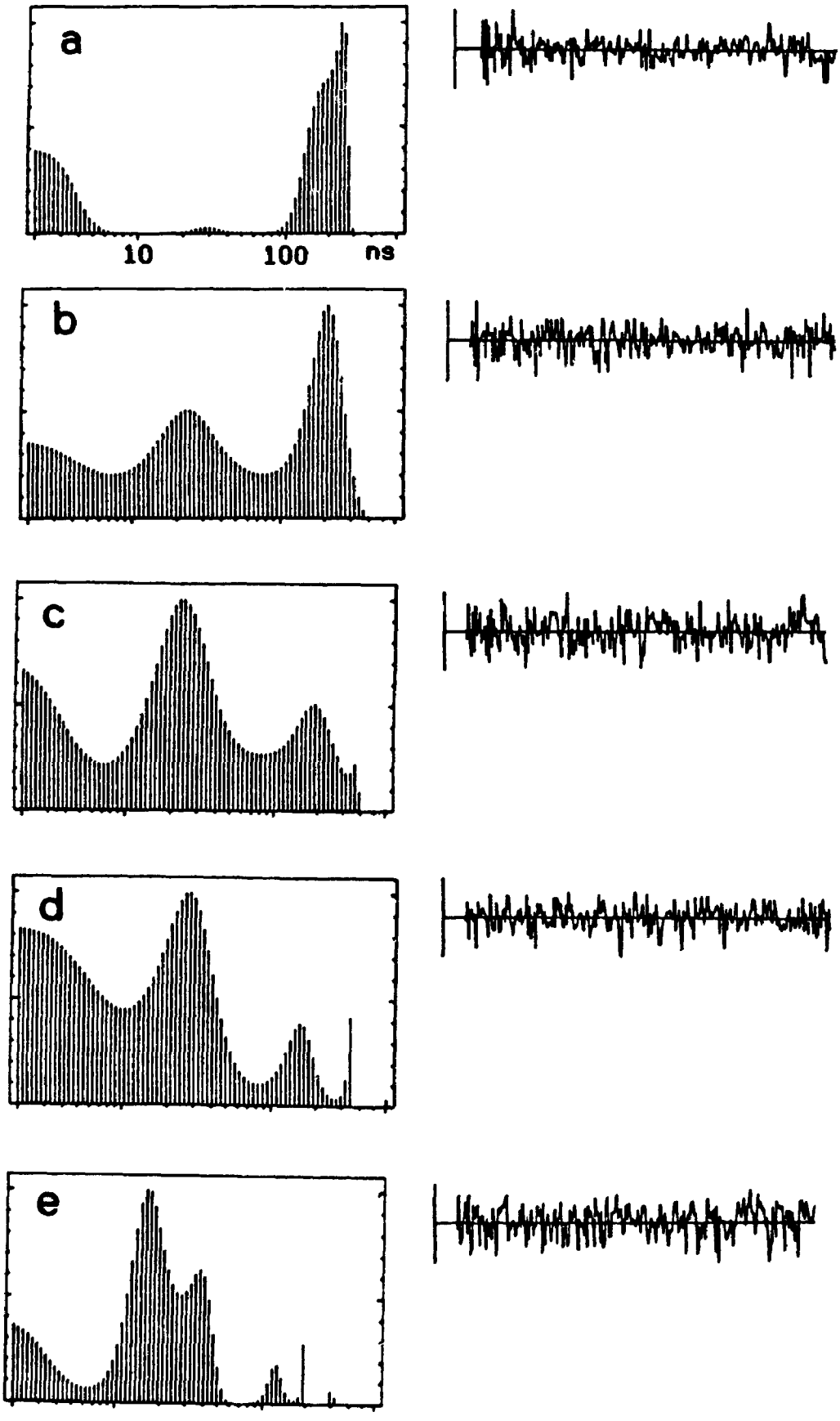
a
10
100
ns
b
c
d
e

Fig. 6.2 The lifetime distributions derived from the same group of decay curves as those in Fig.6.1, analyzed with MM program.

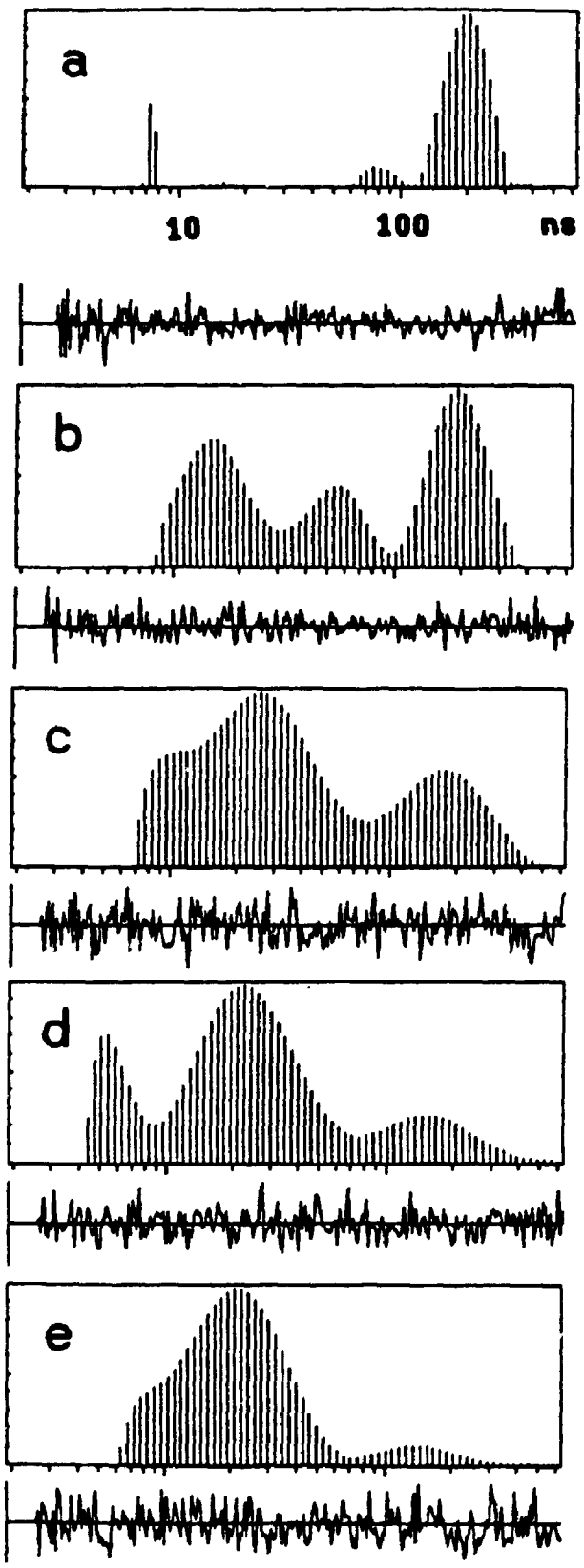
a
10
100
ns
b
c
d
e

Fig. 6.3 The lifetime distributions derived from the same group of decay curves as those in Fig. 6.1, analyzed with SMM program.

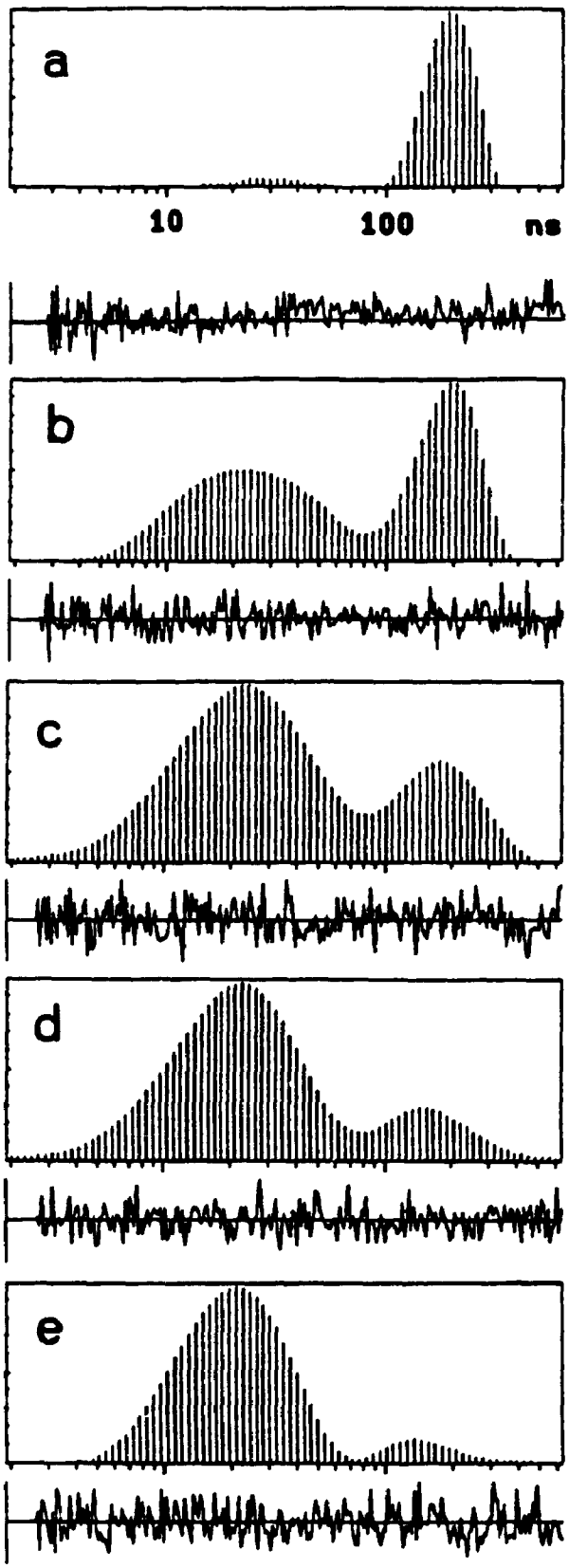
a
10
100
ns
b
c
d
e

Fig. 6.4 The lifetime distributions of pyrene adsorbed on F-500 silica gel, analyzed with MM program. The silica gel was preheated for 8 hours in vacuum at (a) 25°C; (b) 200°C; (c) 400°C; (d) 600°C; (e) 800°C. Pyrene was loaded to 0.01 mg/g, corresponding to a surface coverage of 0.09%.

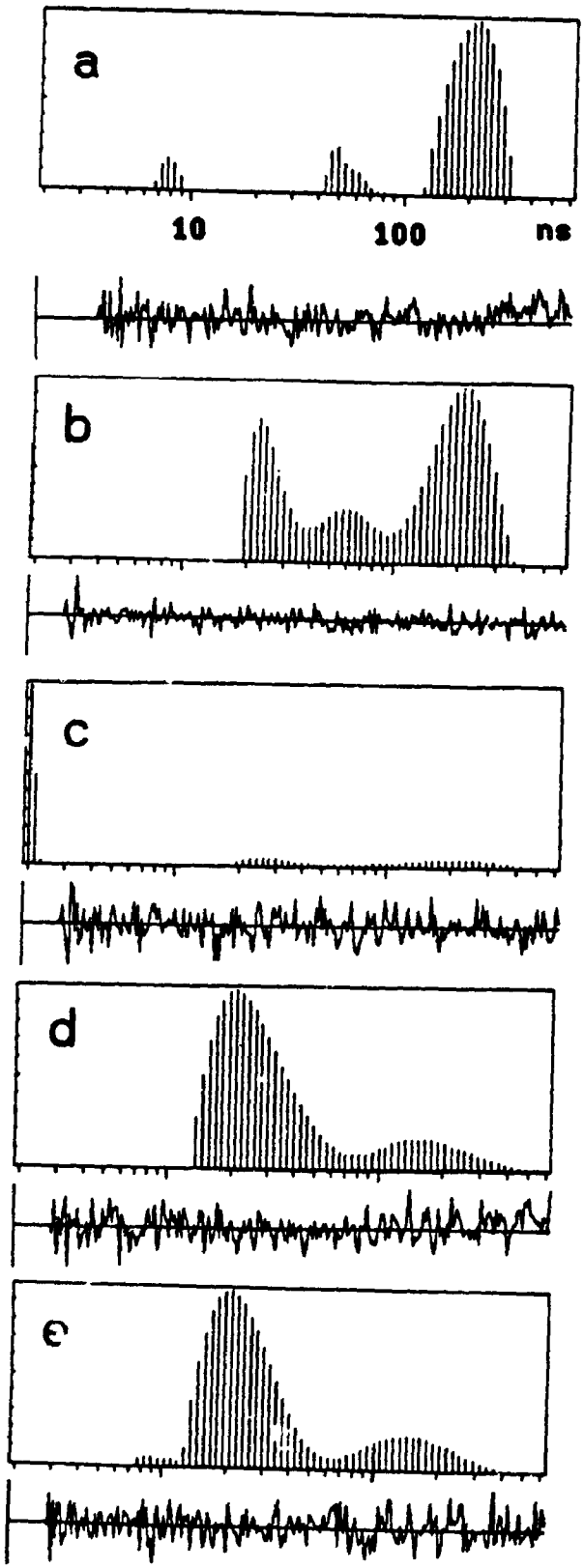
a
10
100
ns
b
c
d
e

Fig. 6.5 The lifetime distributions derived from the same group of decay curves as those in Fig. 6.4, analyzed with SMM program.

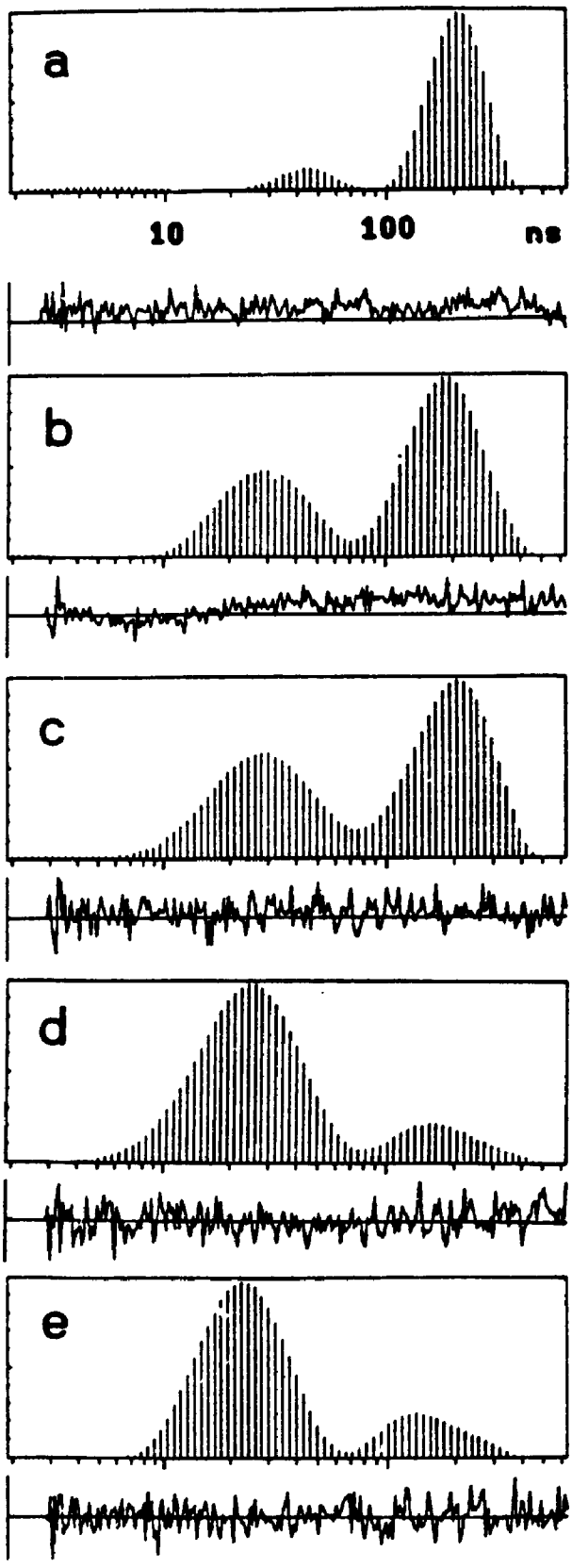
a
10
100
ns
b
c
d
e

Fig. 6.6 The lifetime distributions of pyrene adsorbed on K-60 silica gel, analyzed with MM program. The silica gel was preheated for 2 hours in vacuum at (a) 25°C; (b) 200°C; (c) 400°C; (d) 600°C; (e) 800°C. Pyrene was loaded to 0.01 mg/g, corresponding to a surface coverage of 0.007%.

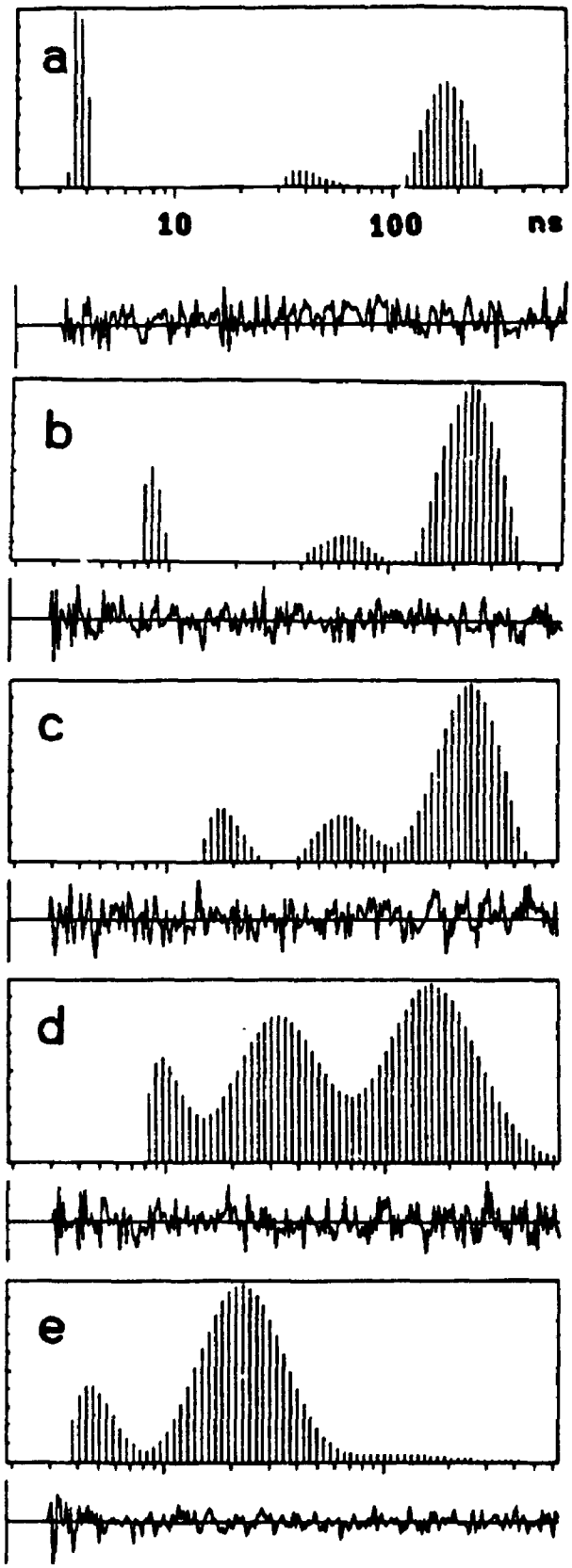
a
10
100
ns
b
c
d
e

Fig. 6.7 The lifetime distributions derived from the same group of decay curves as those in Fig. 6.6, analyzed with SMM program.

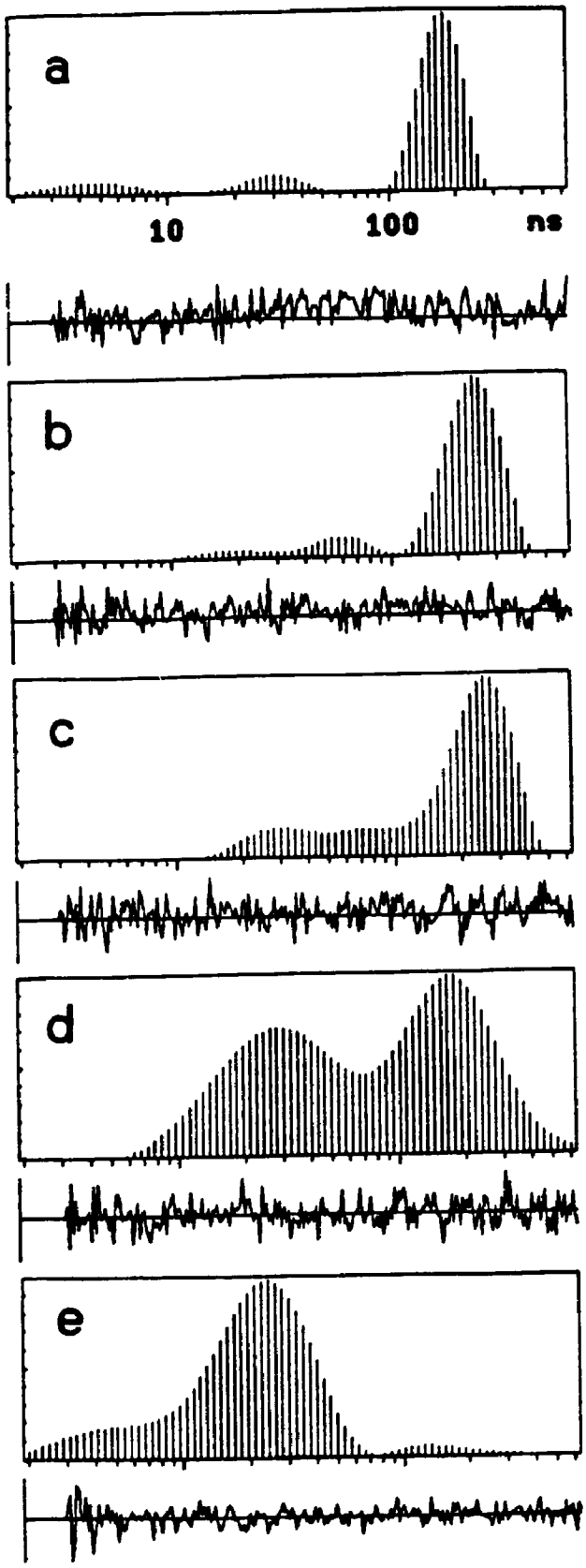
a
10
100
ns
b
c
d
e

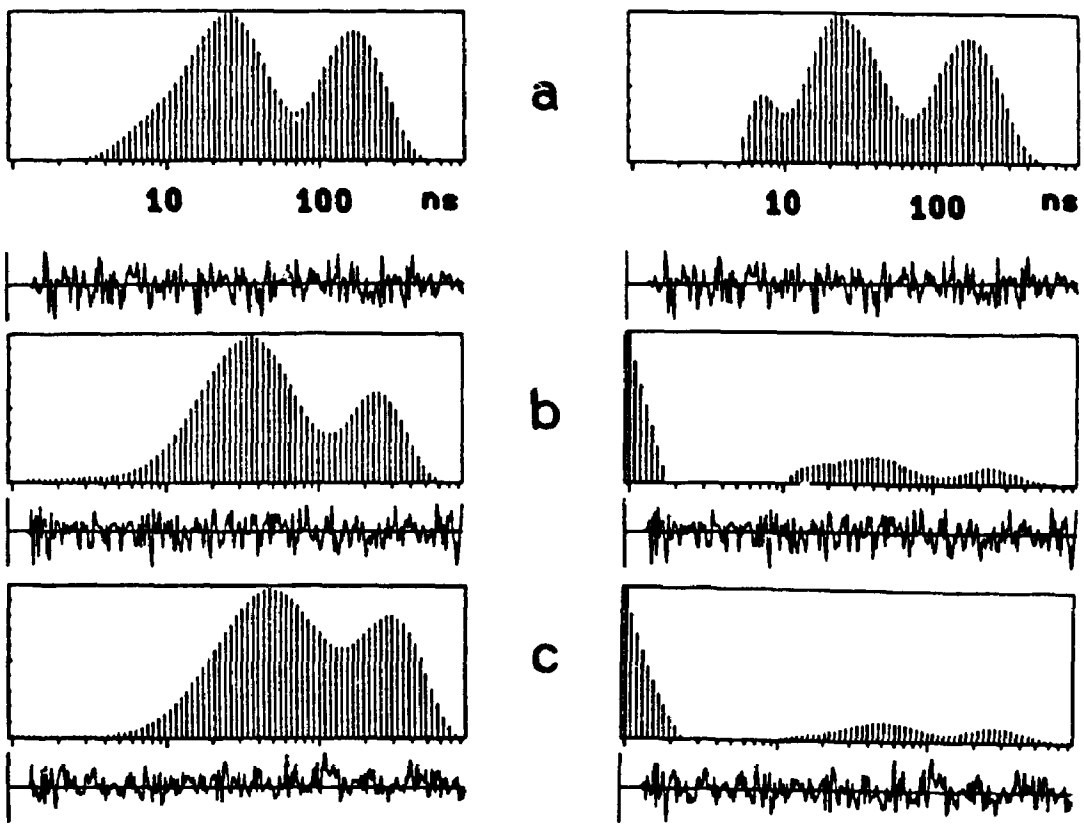

Fig.6.8 The lifetime distributions of pyrene adsorbed on a silica gel surface, measured at various low temperatures. The sample was made under the same conditions as in Fig. 6.1 (c), the silica gel was preheated for 8 hours in vacuum at 400°C, then loaded with pyrene to 0.01 mg/g. The measuring temperatures, at which the decay curves were collected were (a) 293K; (b) 200K; (c) 100K. The left column shows the results given by the SMM program, the right column shows the results given by the MM program.

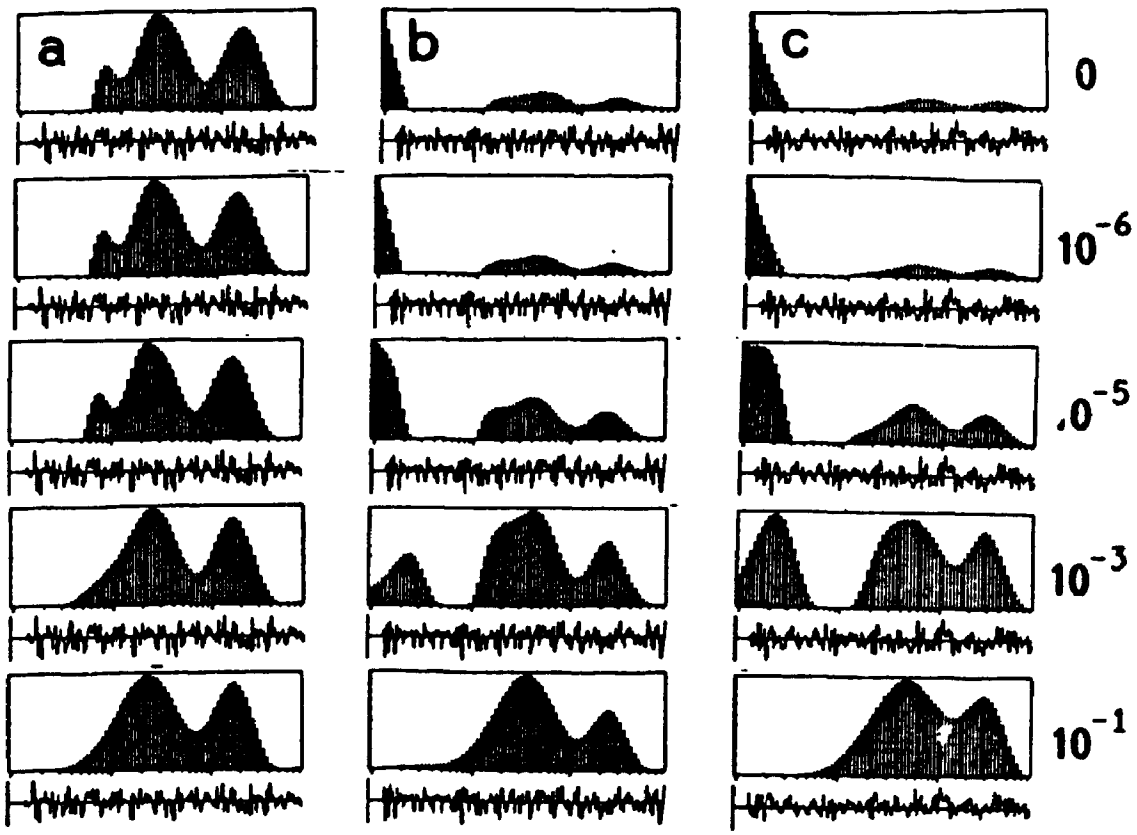

Fig. 6.9 The large variety of solutions which can fit the same set of decay curves. From left to right, the three columns are results derived from the same three decay curves as those used for Fig. 6.8, collected at 293K, 200K, 100K respectively. The top row shows the results given by the MM program. From top to bottom, the smoothing constraint was gradually enhanced as relatively indicated by the numbers shown on the right. The varying smoothing constraint led to a great variety of different solutions, all possessing satisfactory residual profile! However, only the smoothest solutions are self-consistent, in some sense, within the group of low temperature experiments.

CHAPTER 7 LIFETIME DISTRIBUTION ANALYSIS FOR FIVE OTHER PAHS ADSORBED ON SILICA GEL SURFACES

7.1 INTRODUCTION

In Chapter 6, the lifetime distributions of pyrene adsorbed on silica gel surfaces have been examined, using the variety of techniques available in this laboratory. These results suggest that a smoothing constraint is necessary in dealing with surface decay data. When the smoothing technique (the SMM program) is applied, a bimodal distribution is consistently obtained from several groups of data sets, and appears to be the most reasonable model representing the photophysical behaviour of pyrene adsorbed on the surface.

If the bimodal distribution is accepted, and is considered as a physical reality, then this implies that the surface sites available to pyrene molecules may be conceptually divided into two groups. For convenience, hereafter we will refer to the sites in the first group as "type 1 sites", and the sites in the second group as "type 2 sites", although such a distinct division is arbitrary in some sense. When adsorbed on the type 1 sites, pyrene shows a lifetime distribution in the range of 100-300 ns. When adsorbed on the type 2 sites, pyrene shows a lifetime distribution in the range of 5-80 ns. The natures of these two types of sites are not known at present. Whatever they are, if the

two types of surface sites are "real", then their association with other PAHs should be expected to produce similar observations. Such a demonstration would constitute a further test of the validity of the model.

The lifetime distribution analysis suggests that, on the hydroxylated silica gel surface (pretreated at 25°C), type 1 sites are dominant, while on the highly dehydroxylated surface (preheated at 800°C), type 2 sites are dominant. For simplicity, we will concentrate on these two typical types of silica gel, and denote them as "wet" and "dry" silica gel respectively.

7.2 COMPARISON OF LIFETIME DISTRIBUTIONS OF SIX PAHS ADSORBED ON WET AND DRY SILICA GEL SURFACES

The five PAHs, selected for the further tests, are phenanthrene, chrysene, perylene, benzoperylene and coronene. Their molecular structures are shown in Fig. 7.1. These compounds are all highly fluorescent substances sharing a common feature, a system of delocalized π-electrons, in their electronic structures.

In Fig. 7.2 through Fig. 7.6, the lifetime distributions of the five PAHs, adsorbed on the wet and the dry silica gel surface, obtained from SMM analysis, are presented. Some details of the experimental conditions are described in the

figure captions. These results accord well with the model describing two types of surface sites on silica gel surfaces, because two peaks can be seen in almost all cases. Also type 2 sites, that appear dominantly on the highly dehydroxylated silica gel surface, almost always shorten the lifetimes of the PAHs adsorbed on them.

The only exception that apparently does not fit the "bimodal description" about the surface is perylene. The lifetime distributions of perylene, on dry and wet surfaces, do not show any drastic change as do those of other PAHs. This suggests that perylene may be a special case, where the decay process of the excited state is not sensitive to the two types of surface sites. If we intend to persist in our model, a satisfactory interpretation of this exception has to be provided. A discussion about this problem will be given in next section. For the present, we shall review some lifetime data of these PAHs in solutions, collected from the literature.

The fluorescence lifetimes of pyrene and perylene in various solvents have been most extensively studied. Lifetime data of the other three PAHs are rarely available in the literature. These data [114-127] are listed in Tables 7.1 - 7.6. These data, and the lifetime distributions of these PAHs on the wet and the dry silica gel surfaces, show an interesting trend, which is common to pyrene, phenanthrene,

chrysene, benzoperylene and coronene. The lifetimes of these PAHs adsorbed on the wet surface are slightly shorter than, but still comparable to, those observed in solution. The lifetimes of these PAHs are drastically further shortened on the dry surface. On contrast, perylene shows a different trend. On proceeding from solution to the wet surface, then to the dry surface, perylene lifetimes become slightly longer. The special behaviour of perylene, compared with the other five PAHs, immediately suggests that this might be in some way related to a special electronic state, compared with the other five PAHs. This will be discussed in the next section.

Table 7.1 Fluorescence lifetime of phenanthrene in various solvents

Solvents	τ(ns)	ref.
cyclohexane	56	[124]
heptane	59.5	[125]
isobutanol	63	[125]
cyclohexanol	60.7	[125]

Table 7.2 Fluorescence lifetime of chrysene in various solvents

Solvents	τ(ns)	ref.
cyclohexane	44.7	[121]
ethanol	42.6	[121]

Table 7.3 Fluorescence lifetime of pyrene in various solvents

Solvents	τ(ns)	ref.
cyclohexane	450	[117]
	430	[115]
	408	[120]
ethyl ether	415	[115]
2-propanol	386	[115]
ethanol	373	[115]
ethyl acetate	367	[115]
acetonitrile	340	[115]
acetone	324	[115]
benzene	311	[115]
dioxane	309	[115]
	295	[117]
dimethylformamide	280	[115]
dimethyl sulfoxide	275	[120]
1,2-dichloroethane	202	[120]
water	200	[117]
water + 2-propanol (10% by volume)	225	[114]

Table 7.4 Fluorescence lifetime of 1:12-benzoperylene in various solvents

Solvents	τ(ns)	ref.
n-hexane	110	[126]
benzene	107	[121]

Table 7.5 Fluorescence lifetime of coronene in various solvents

Solvents	τ(ns)	ref.
n-hexane	282	[126]
ethanol	286	[127]

Table 7.6 Fluorescence lifetime of perylene in various solvents

Solvents	τ(ns)	ref.
cyclohexane	6.4	[121]
ethanol	6.0	[122]
acetone	6.1	[122]
benzene	4.9	[123]
dioxane	5.9	[122]
heptane	5.7	[122]
isobutanol	6.1	[122]
methanol	6.2	[122]
n-octanol	5.8	[122]
toluene	5.5	[122]
xylene	5.7	[122]

7.3 THE PERIMETER FREE ELECTRON ORBITAL (PFEO) MODEL AND THE LOWEST EXCITED SINGLET STATE OF THE PAHS

A useful quantum mechanical treatment of these PAHs is the perimeter free electron orbital (PFEO) model for the cata-condensed PAHs (in which every C atom is on the molecular periphery), introduced by J.R.Platt [128]. It can also be applied to the peri-condensed PAHs. In an unsubstituted PAH molecule, each C atom possesses one π-electron, and the π atomic orbitals interact to form the same number of delocalized π molecular orbitals. In the PFEO model the π orbitals are treated as orbitals of free electrons travelling in a one dimensional loop around the molecular perimeter. Based on this model, the one-electron energy levels, labelled by the orbital ring quantum number q, are calculated to be quadratically spaced, and all doubly

degenerate except for the lowest, since electrons that have a finite velocity may travel either clockwise or counterclockwise around the loop. In many electron systems, the q's of the different electrons may be added and subtracted algebraically to give a total ring quantum number Q for the system. Q may take on the values 0, 1, ... and also the values 2n, 2n+1, ..., where n is the ring quantum number of the highest filled orbital. These states are designated as A, B, ... and K, L, ... respectively.

Since the "Optical" electrons are those in the highest filled shells, Platt has introduced the nomenclature f, g, etc., to describe the highest filled shell, q = n, and lowest empty shell, q = n+1, as shown in Fig. 7.7. Thus the lowest excited state corresponds to a configuration of f^3g, that is one electron goes from an f to a g orbital. The total ring quantum number Q, obtained from f and g ring quantum numbers added or subtracted, will be 1 or 2n+1. These are B and L states. In real molecules, the periodic potential due to the C atoms removes the degeneracy, the two states split into B_a, B_b, L_a, L_b. The spins of the two unpaired electrons may be antiparallel or parallel, giving two sets of excited states, singlets and triplets. This gives totally eight states for the f^3g configuration.

Empirically, the energy order of states of a given configuration is determined by the Hund rule. Triplets lie

below singlets; and within the singlet group, or the triplet group, states of high Q lie below low Q states. Thus for these PAH molecules, the lowest excited singlet state, which is primarily concerned in this work, may be either L_a or L_b. The assignments for the lowest excited singlet state of the PAHs, together with the corresponding ϵ_{max}, are listed in Table 7.7.

Table 7.7 The S_0 - S_1 transitions of some PAHs

PAHs	state	ϵ_{max}	assignment
phenanthrene	S_1	250	^1L_b
pyrene	S_1	510	^1L_b
chrysene	S_1	200	^1L_b
benzoperylene	S_1	500	^1L_b
coronene	S_1	500	^1L_b
perylene	S_1	39500	^1L_a
naphthacene	S_1	14000	^1L_a
9,10-diphenyl -anthracene	S_1	12600	^1L_a

It is then immediately notable that among the six PAHs studied in this work, only perylene possesses an ^1L_a lowest excited singlet state. If this is the reason for the "strange" behaviour of perylene, then other PAHs with a ^1L_a as their lowest excited singlet state would be expected to show the same trend. Some preliminary experiments with 9,10-diphenylanthracene, which belongs to the ^1L_a type, appear to be in accord with this prediction. Recently, Bjarneson [129] observed the lifetime of naphthacene (^1L_a type) on silica gel surfaces. The behaviour of naphthacene he reported is

indeed like perylene.

7.4 Summary

When the SMM lifetime distribution analysis is extended to more PAHs, consistent results can still be obtained. This suggests that the bimodal distribution appears to be a reasonable description of the lifetime of the PAHs adsorbed on these surfaces.

The measured lifetime distributions of these PAHs are generally shortened, on going from solutions to the wet surface, then to the dry surface. The only exception is perylene. The special behaviour of perylene might be related to its characteristic electronic state. In this regard, more discussion will be given in the following chapters.

Phenanthrene	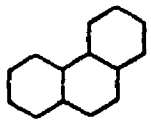	$C_{14}H_{10}$
Pyrene	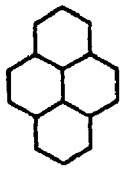	$C_{16}H_{10}$
Chrysene	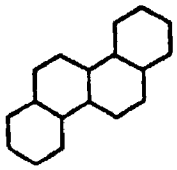	$C_{18}H_{12}$
Perylene	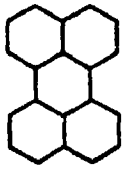	$C_{20}H_{12}$
1:12-Benzoperylene	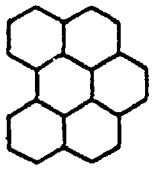	$C_{22}H_{12}$
Coronene	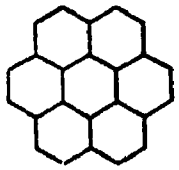	$C_{24}H_{12}$

Fig. 7.1 The molecular structures of the PAHs studied in this work.

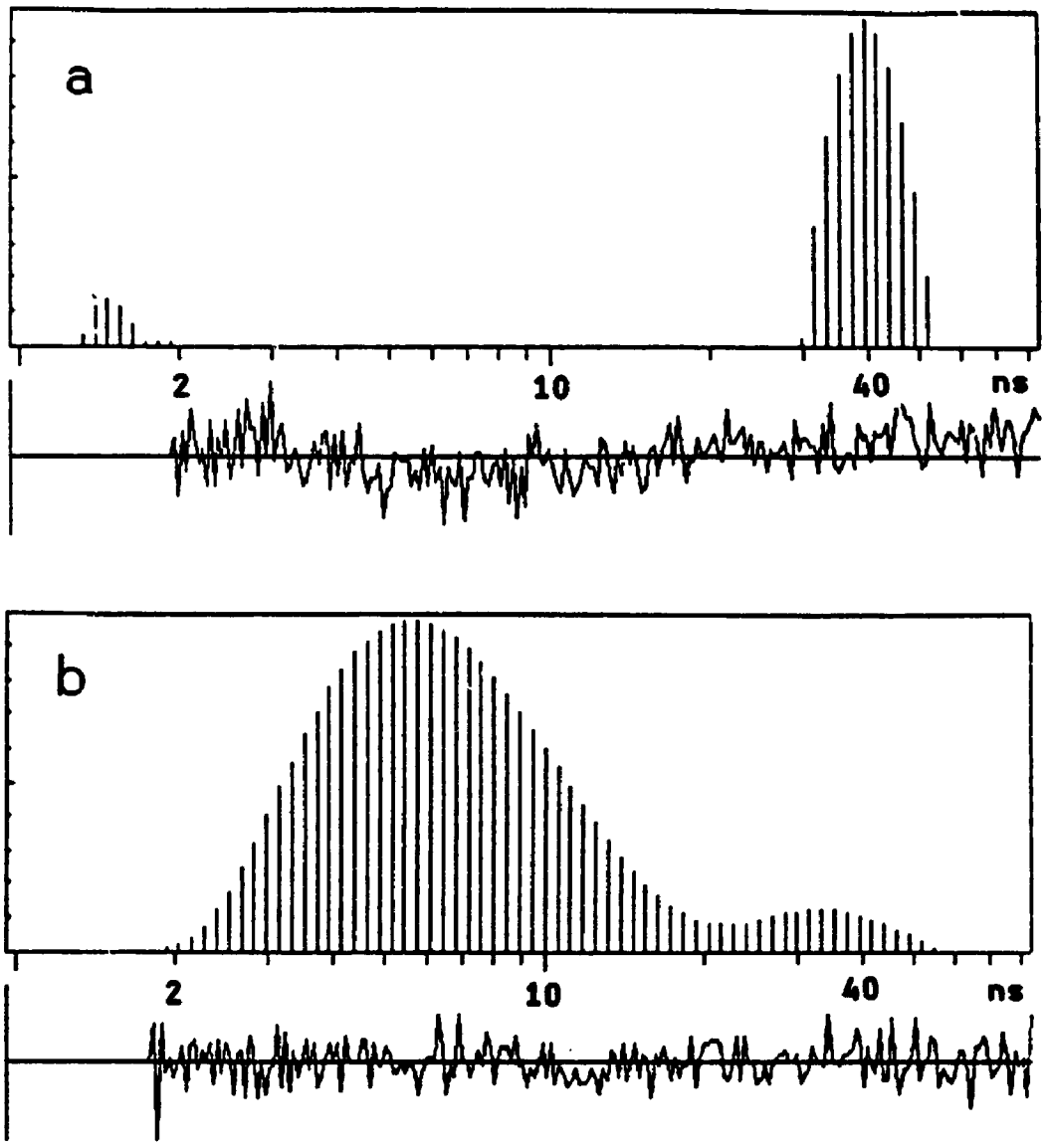

Fig. 7.2 The lifetime distributions of phenanthrene adsorbed on the wet and the dry silica gel surfaces, analyzed with SMM program. The silica gel was K-60, preheated for 8 hours in vacuum at (a) 25°C, the so called wet surface; (b) 800°C, the so called dry surface. Phenanthrene was loaded to 0.22 mg/g. The decay curves were collected at excitation wavelength 290 nm, emission wavelength 370 nm, 300000 CPC.

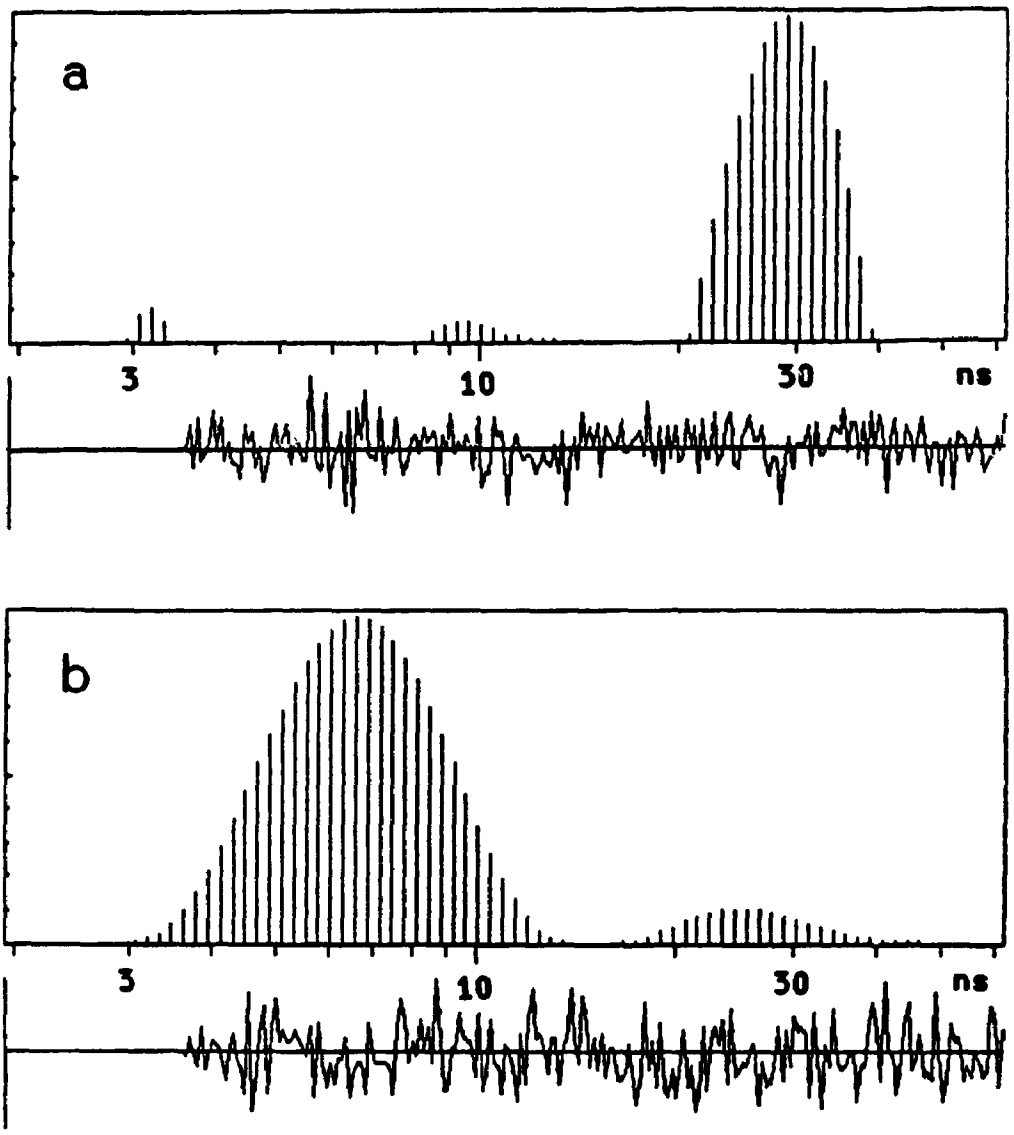

Fig. 7.3 The lifetime distributions of chrysene adsorbed on the wet and the dry silica gel surfaces, analyzed with SMM program. The silica gel was K-60, preheated for 8 hours in vacuum at (a) 25°C, the wet surface; (b) 800°C, the dry surface. Chrysene was loaded to 0.24 mg/g. The decay curves were collected at excitation wavelength 290 nm, emission wavelength 380 nm, 300000 CPC.

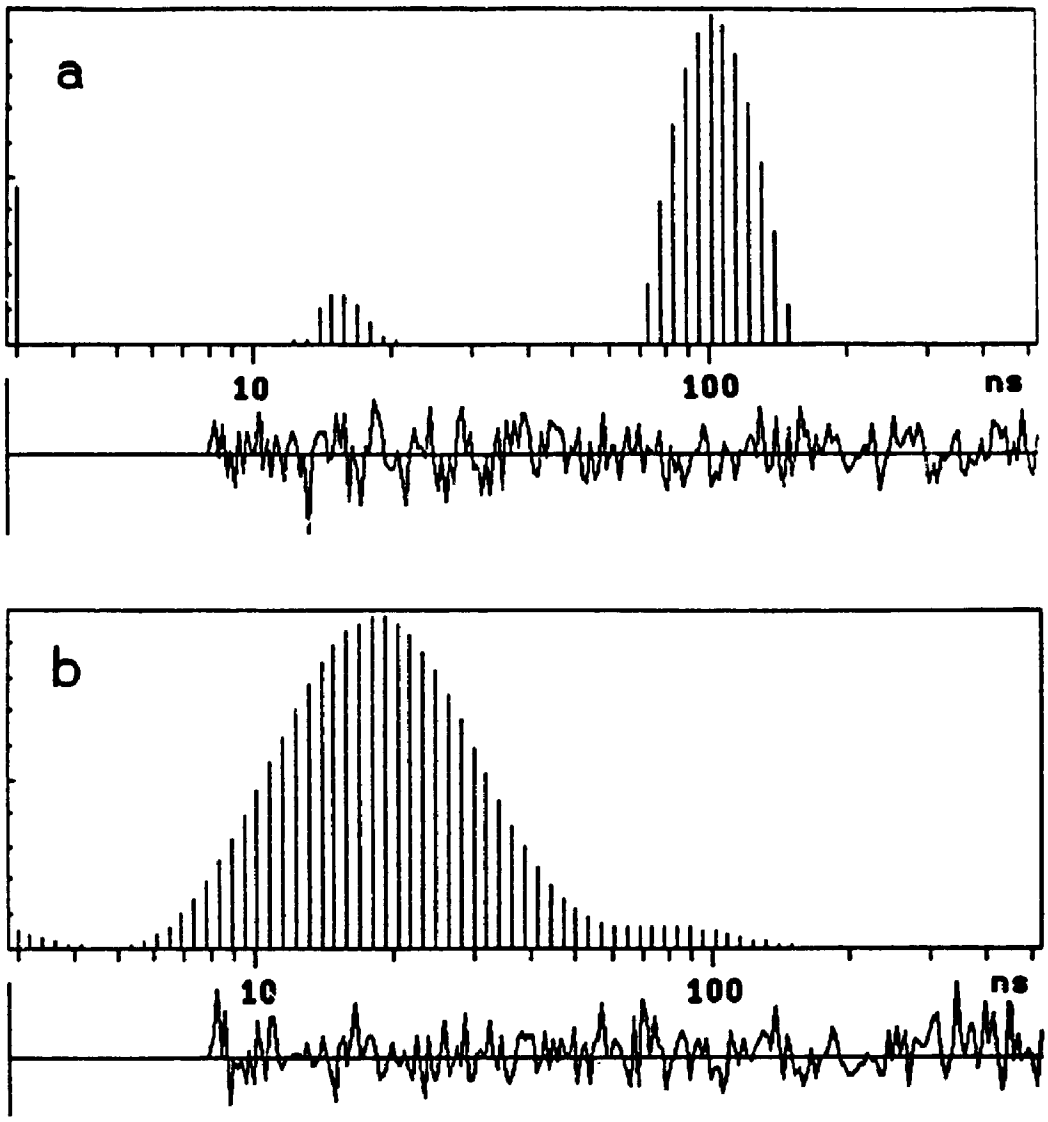

Fig. 7.4 The lifetime distributions of benzoperylene adsorbed on the wet and the dry silica gel surfaces, analyzed with SMM program. The silica gel was K-60, preheated for 8 hours in vacuum at (a) 25°C, the wet surface; (b) 800°C, the dry surface. Benzoperylene was loaded to 0.024 mg/g. The decay curves were collected at excitation wavelength 290 nm, emission wavelength 430 nm, 200000 CPC.

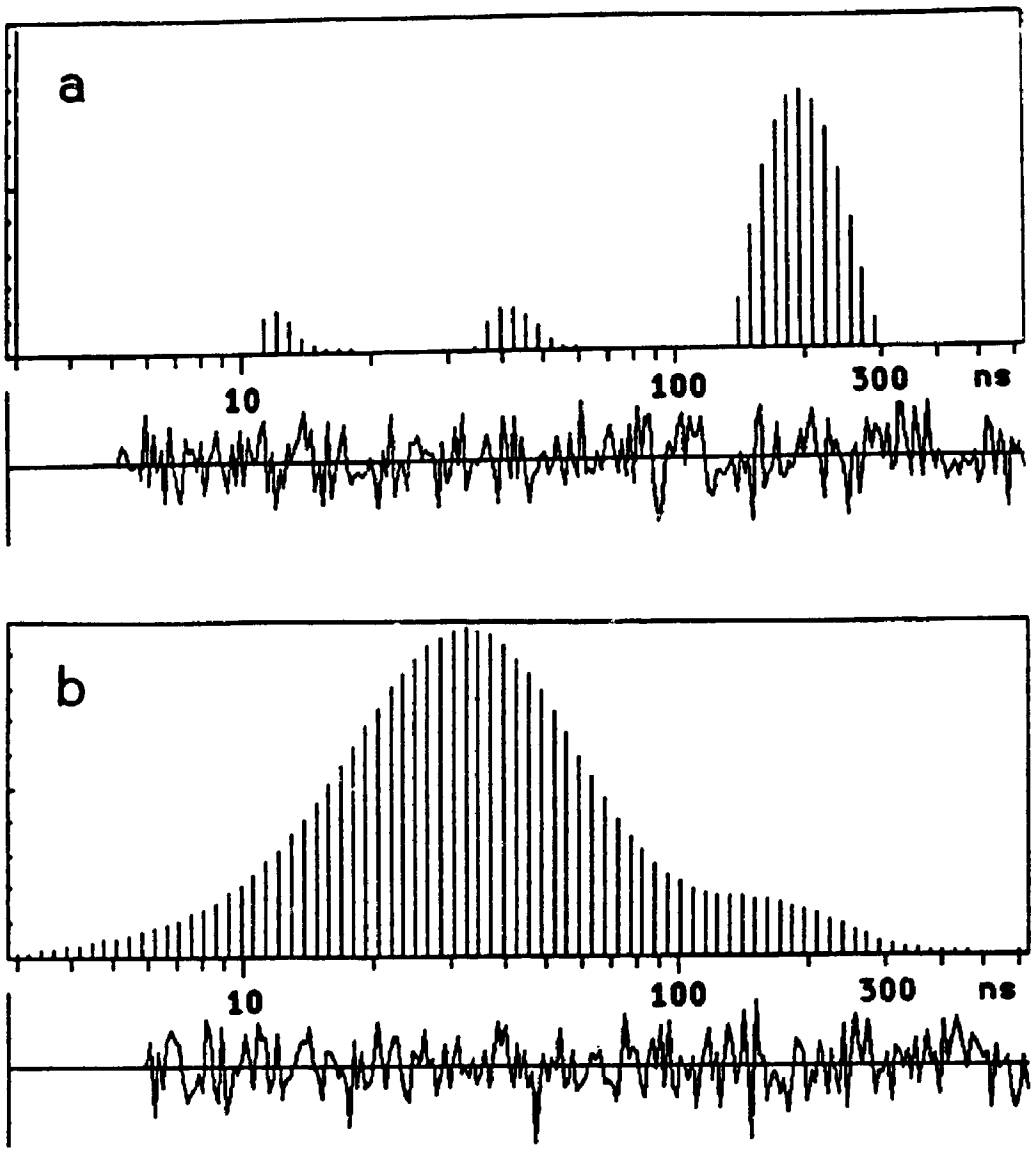

Fig. 7.5 The lifetime distributions of coronene adsorbed on the wet and the dry silica gel surfaces, analyzed with SMM program. The silica gel was K-60, preheated for 8 hours in vacuum at (a) 25°C, the wet surface; (b) 800°C, the dry surface. Coronene was loaded to 0.040 mg/g. The decay curves were collected at excitation wavelength 290 nm, emission wavelength 450 nm, 300000 CPC.

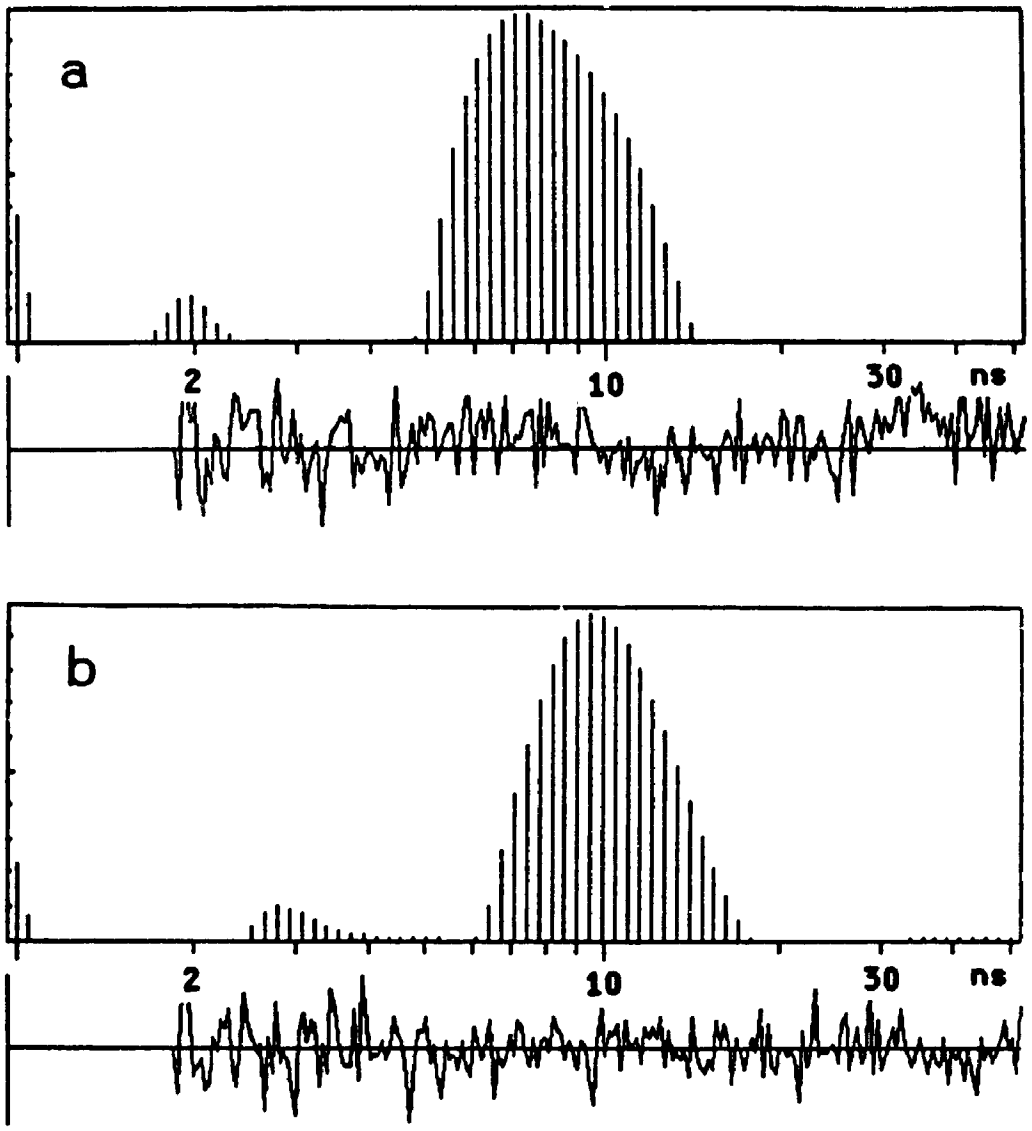

Fig. 7.6 The lifetime distributions of perylene adsorbed on the wet and the dry silica gel surfaces, analyzed with SMM program. The silica gel was K-60, preheated for 8 hours in vacuum at (a) 25°C, the wet surface; (b) 800°C, the dry surface. Perylene was loaded to 0.022 mg/g. The decay curves were collected at excitation wavelength 290 nm, emission wavelength 460 nm, 200000 CPC.

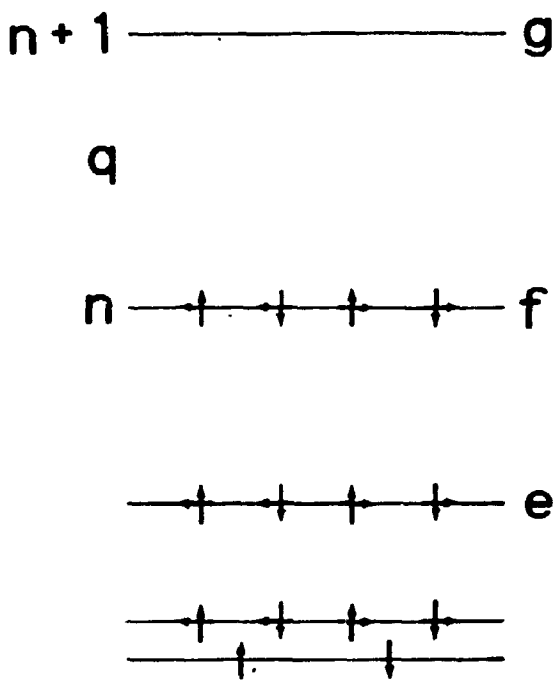

Fig. 7.7 The π-electron orbital energy levels in the perimeter free-electron orbital model. Vertical arrows represent spin, and horizontal arrows represent orbital momentum.

CHAPTER 8 EMISSION AND ABSORPTION SPECTRA OF PAHS ADSORBED ON SILICA GEL SURFACES

8.1 INTRODUCTION

The study of absorption and luminescence spectra can provide significant information about the properties of luminescent molecules and of their micro-environments. Three features of the spectra are most informative: the vibronic fine structure, the broadening of the structure, and the overall spectral shift. For many PAHs in solutions, these aspects have been intensively studied [130], and are well understood.

This chapter is devoted to the observation of the spectroscopic features of the PAHs, adsorbed on silica gel surfaces. We need additional information in this aspect in order to determine its compatibility with our model. Also these observations are a necessary preparation for the measurement of fluorescence quantum yields on silica gel surfaces.

8.2 EXPERIMENTAL

All the emission and absorption spectra were obtained using a Perkin-Elmer 650-40 fluorescence spectrophotometer. Luminescence spectra were measured in the front viewing

mode. A loaded silica gel sample was sealed in a 1 mm cuvette or a 5 mm diameter tube and held by a home-made attachment in the sample compartment. The incidence angle of the excitation light beam was set at 30° with respect to the normal of the cuvette surface to avoid specular reflection light being received by the detector. All spectra presented in this thesis are corrected. A schematic diagram of the experimental set-up is shown in Fig. 8.1.

The absorption spectra of aromatic molecules adsorbed on silica gel surfaces have rarely been reported in the literature, probably because the scattering property of silica gel powders makes it difficult to be measured on a conventional spectrophotometer. However, silica gel powders are translucent rather than opaque, and during the course of this work the fluorescence spectrophotometer was found suitable to detect the diffusely transmitted light passed through up to a 10 mm layer of silica gel powders. Advantage was taken of this to obtain conveniently the absorption spectra of adsorbed molecules. Both reflection and transmission modes were tested to obtain absorption spectra from silica gel samples contained in an 1 x 10 mm cuvette or even a 10 x 10 mm cuvette. The optical arrangements for measuring absorption spectra in the reflection mode are the same as given in Fig. 8.1, and those in the transmission mode are shown in Fig. 8.2 (a), (b).

The spectrophotometer scanned both emission and excitation monochromators synchronously, the diffusely reflected light or transmitted light was measured, corrected and recorded. For each absorption spectrum two measurements were conducted, one for a blank silica gel sample ($I_0(\lambda)$), another for a loaded silica gel sample ($I_s(\lambda)$). The absorption spectrum was calculated according to

$$A(\lambda) = \frac{I_0(\lambda) - I_s(\lambda)}{I_0(\lambda)} \qquad (8.1)$$

where λ is the wavelength of the incident light, I is the intensity of the diffusely reflected or transmitted light from the sample. Similar techniques have been described by a number of authors [3,131-133].

The sensitivity of this method in the transmission mode was impressive. With an 1 mm cuvette, the absorption spectrum of as low as 0.005 mg pyrene per gram of silica gel was easily measured. Fig. 8.3 shows absorption spectra of pyrene, measured at different surface concentrations on the transmission mode.

8.3 THE INFLUENCE OF SILICA GEL DEHYDROXYLATION ON THE ABSORPTION SPECTRA AND THE VIBRONIC FINE STRUCTURE OF FLUORESCENCE SPECTRA OF THE ADSORBED PAHS

In the cases where the electronic transition is forbidden or

weakly allowed, the vibronic structures of absorption and emission spectra may undergo great changes on dissolving in different media. This effect was first noticed in the absorption spectrum of benzene by J.S.Ham [134] in 1953, and is now generally termed the "Ham effect". It was soon generally recognized that the "Ham bands" were due to the symmetry forbidden "0-0 progression" in the first singlet-singlet band system. This phenomenon was further investigated by Durocher and Sandorfy [135] who predicted the general occurrence of this effect in certain types of aromatic hydrocarbons. Briefly speaking, for the first singlet-singlet transitions, pronounced Ham effects were expected in molecules whose first band was of the α-type (or $^1L_b - {}^1A$) while no such effects were expected for those molecules in whose spectra the first band was of the p-type ($^1L_a - {}^1A$). The α-type or p-type bands were initially distinguished by E.Clar [136], on the basis of the band intensity (and, therefore, the "allowableness"): the α-bands were weak, while the p-bands were moderately intense. In the PFEO model (Sec.7.3) these two types correspond to ($^1L_b - {}^1A$) and ($^1L_a - {}^1A$) transitions respectively.

In the 1970s Nakajima [137-139] extended the observation of the Ham effect to encompass fluorescence spectra. Following Nakajima's work, a great deal of effort was devoted to correlating the enhancement of the fluorescence fine structure of the fluorophor with some property of the

solvent, and to the potential applications of this effect for probing the properties of the environment. The fluorescence spectra of pyrene, naphthalene, benzoperylene, and coronene in a number of different solvents were extensively studied [117-119,140-144]. It was suggested that the enhancement of forbidden or weakly allowed bands of these aromatic hydrocarbons was roughly correlated with solvent polarity. In some cases specific interactions between the fluorophor and polar solvent and even the formation of complexes between them, were also found responsible for this enhancement. These interactions or complexations modify the symmetry of the fluorophor, hence the intensity of these weak bands were increased. The fluorescence spectra of pyrene, benzoperylene and coronene in typical non-polar and polar solvents are shown in Fig. 8.4, based on literature data. These results were immediately applied to the study of a number of heterogeneous systems, such as colloidal and biological systems, and solid surfaces, for which the aromatic hydrocarbons were used as indicators of the polarity of the micro-environment. Studies in this field have been extensively reviewed [7]. Thus, for instance, the Ham effects on the fluorescence spectra of pyrene and naphthalene on a "wet" surface were previously studied by de Mayo, Ware and coworkers [9,10]. They showed that the silica gel surface provided a polar environment for the adsorbed molecules.

The fluorescence spectra and absorption spectra of the six PAHs adsorbed on the wet and dry silica gel surfaces are presented in Fig. 8.5 - Fig. 8.10. In these results the following features are notable.

(A) The fluorescence spectra of pyrene, benzoperylene and coronene show very pronounced Ham effects on wet surfaces. The characteristic bands are named a, b, c, d, e, f following Nakajima [137-139]. On wet surfaces, the enhancements of bands a, e in the pyrene spectrum, bands b, d in the benzoperylene spectrum and bands a, d, f in the coronene spectrum approximately correspond to those observed for these compounds in dimethylsulfoxide (dielectric constant = 46.7) or water. On dry surfaces, these bands are further enhanced so that the originally more allowed bands can no longer be seen. In fact, in all spectra involving dry surfaces, the original fine structure, if any, has been completely lost, being replaced a set of equally spaced bands. It is interesting to note that a similar distortion may be seen in the spectra of the substituted PAHs. Fig. 8.11 shows a comparison of the spectrum of pyrene on a dry surface with the spectrum of protonated aminopyrene on a wet surface. These two spectra are almost identical, indicating that the pyrene molecules bonded on the type 2 sites approximately as in a surface complex. A similar argument has been used by Lianos [118] to suggest the existence of the complexes between pyrene molecules and some polar

solvent molecules.

(B) Another common feature seen in these results is that all the fluorescence and absorption spectra observed on a dry surface, whether the Ham effect is expected or not, are much more diffuse and are broadened in comparison with those obtained on a wet surface. This is another indication of a stronger specific interaction on the type 2 sites. Because of this broadening, the emission and absorption spectra of most of these PAHs, except for pyrene and coronene, are more overlapped. This broadening apparently results in evident self-absorption, even at the low surface concentrations used in these experiments. The changes in the perylene fluorescence spectrum, for which a Ham effect is not expected, may be interpreted in terms of self-absorption.

8.4 A QUALITATIVE OBSERVATION OF TEMPERATURE DEPENDENCE OF THE LUMINESCENCE QUANTUM YIELDS

Lowering the temperature normally affects the luminescence quantum yield in two ways. First, since lowering the temperature will depopulate the distribution of higher vibronic energy levels of the lowest excited singlet state, and hence suppress the probability of intersystem crossing to the triplet excited state, an increase of the fluorescence quantum yield may then occur. Equation

(8.2) $$k_{IM} = k_{IM}^{\circ} + k_{IM}'\exp(-W_{IM}/kT)$$

describes the temperature dependence of a non-radiative decay rate constant [130]. Lowering the temperature will reduce the second term, and therefore tend to increase the fluorescence quantum yield. Second, lowering the temperature increases the effective "viscosity" of the system, and can slow down diffusion and bimolecular processes. Thus phosphorescence, which is otherwise quenched by traces of oxygen or other impurities, is more easily seen at a low temperature.

The low temperature luminescence spectra of these aromatic hydrocarbons were examined with a cryostat attached to the fluorescence spectrophotometer. The results are shown in Figs. 8.12-17. A number of interesting features can be observed.

(A) For all these aromatic hydrocarbons except coronene, fluorescence, and in some cases phosphorescence, quantum yields increase with decreasing temperature. This phenomenon can be interpreted by the decreasing of quenching and non-radiative decay rates at low temperatures.

(B) Phosphorescence can be seen in the spectra of phenanthrene, chrysene, and coronene on both wet and dry surfaces. However, the dry surface favours the occurrence of

phosphorescence; for instance, the phosphorescence of phenanthrene appeared at 10K on a wet surface but at 150K on a dry surface; the phosphorescence of coronene appeared at 240K on the wet surface but at room temperature on the dry surface. The difference seen on the dry and the wet surfaces can be interpreted by one or both of the following two mechanisms. The strong specific interaction on the dry surface broadened the energy levels of both excited singlet and triplet states of the fluorophors, thus the intersystem crossing might occur with a lower activation energy. On the other hand, the prolonged heating in vacuum removed more thoroughly the adsorbed oxygen, thus the phosphorescence quenching was reduced.

(C) An interesting phenomenon is seen with coronene. On a wet surface the fluorescence quantum yield decreases with decreasing temperature, while the phosphorescence yield does not change very much below 240K. On a dry surface, on the contrary, the fluorescence quantum yield does not change with temperature, but the phosphorescence yield increases with decreasing temperature. The reason for this behaviour is not clear at this moment.

8.5 ARE THERE EXCIMERS INVOLVED?

In section 6.2 of Chapter 6, we have mentioned that with the surface concentrations of pyrene used in this work (< 0.1

mg, and mostly <0.01 mg pyrene per gram of SiO_2), no excimer or excimer-like species is significantly present on the surface. This can be seen in Fig. 8.18, where the excimer or excimer-like emission, supposedly a broad band from 420-560 nm, is not seen until the pyrene concentration reaches 0.5 mg/g on both wet and dry surfaces. It should also be noted that the ground state dimer of pyrene [10,11,25,145] absorbs at above 350 nm, but all our lifetime measurements for pyrene have been conducted at an excitation wavelength of 331 nm and an emission wavelength of 394 nm, therefore in our decay data the excimer or excimer-like emission should be negligible.

These data also show that on increasing the pyrene concentration on a dry surface, the fine structure (normally a feature of a wet surface) appears at a concentration of 0.5 mg/g or above. This phenomenon seems to be an indication that the type 2 sites are preferably occupied by the pyrene molecules, and there is still a considerable number of type 1 sites on the dry silica gel surface, but they can be occupied only at a relatively high pyrene concentration. These data, therefore, imply that type 2 sites are stronger adsorption sites. Another observation relevant to the occupation preference for the two types of sites is shown in Fig. 8.19. Here the silica gel (K-60) was soaked in concentrated HNO_3 for 24 hours, then rinsed with distilled water until neutral effluent was obtained. This treatment

was presumably to generate more hydrogen bonded hydroxyl groups on the silica gel surface [146]. The silica gel was then heated in vacuum at 800°C for 8 hours. Pyrene was loaded to 0.05 mg/g. Three emission spectra were taken at different time delays after the sample was sealed. It is interesting to note that the first spectrum, taken immediately after the sample preparation, shows the typical wet surface feature! These results suggest that, (a) after a long time of dehydroxylation, type 1 sites still exist on the surface; (b) the pyrene molecules, kinetically, find type 1 sites first, then gradually migrate to type 2 sites and reach equilibrium.

8.6 SUMMARY

The study of absorption and luminescence spectra has produced more evidence for the model suggested by the lifetime distribution analysis described in the last two chapters:

(A) The luminescence spectra show that the wet surface, as an environment for adsorbed aromatic hydrocarbons, is similar to a strong polar solvent.

(B) Spectroscopic evidence suggests that the dry surface provides stronger adsorption and more specific interaction with aromatic molecules.

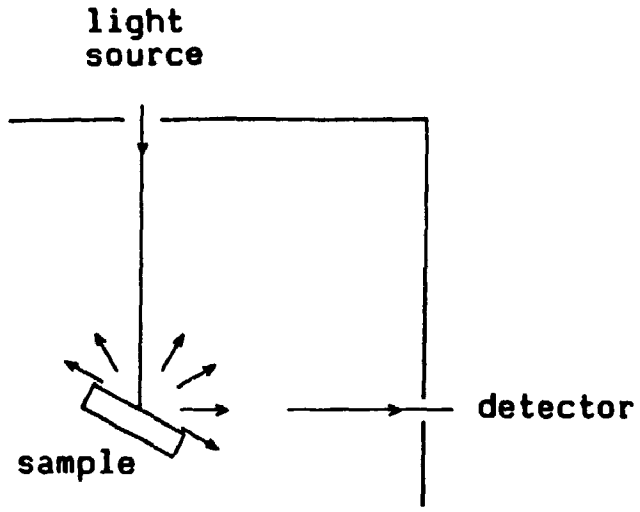

Fig. 8.1 A schematic diagram showing the sample cuvette set-up for the emission spectrum measurements.

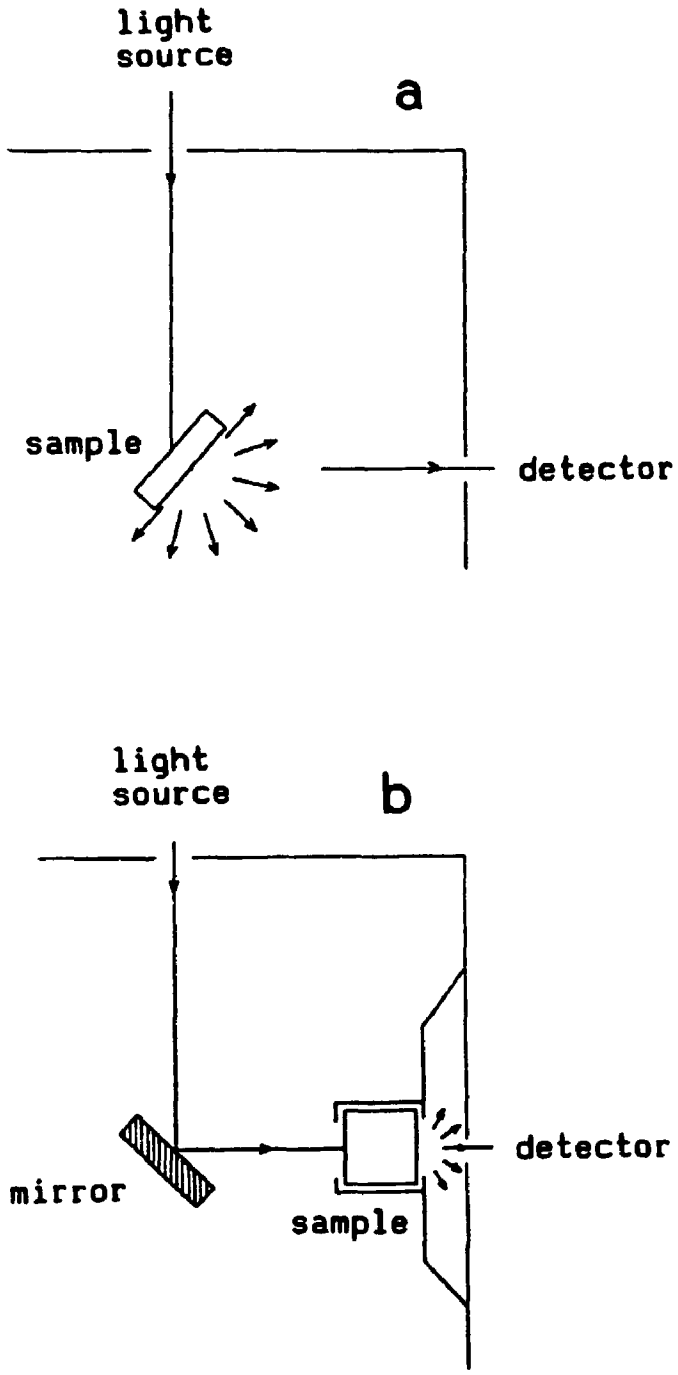

Fig. 8.2 A schematic diagram showing the sample cuvette set-up for the absorption spectrum measurement, (a) using 1 mm flat cuvette; (b) using 10 mm cube cuvette.

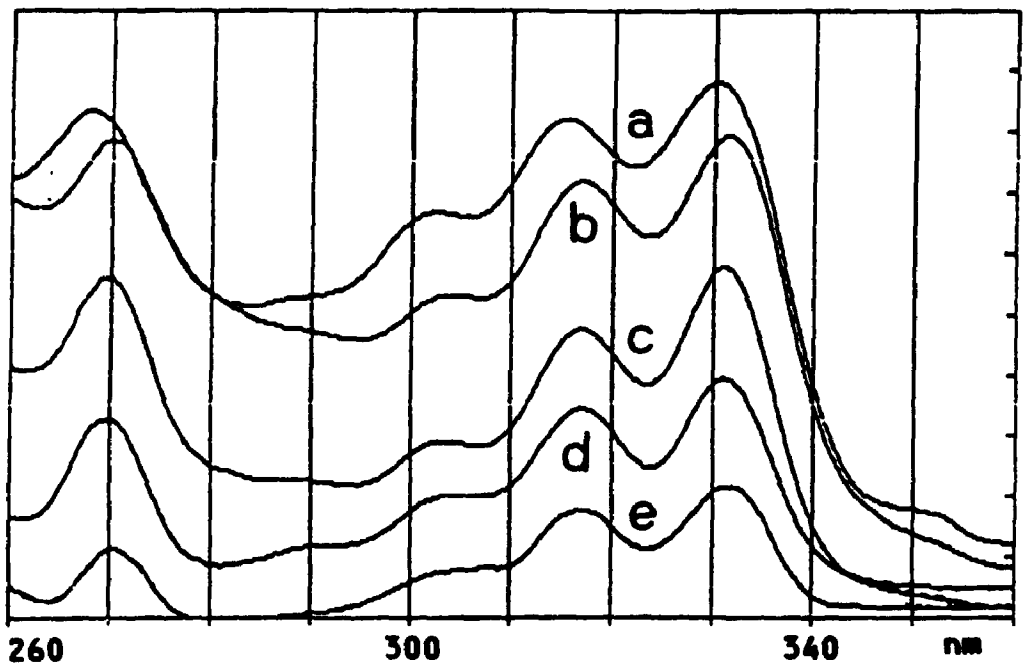

Fig. 8.3 The absorption spectra of pyrene adsorbed on a wet surface, obtained at various surface concentrations. (a) 0.1 mg/g; (b) 0.05 mg/g; (c) 0.02 mg/g; (d) 0.01 mg/g; (e) 0.005 mg/g. The experimental set-up is the one shown in Fig.8.2 (a).

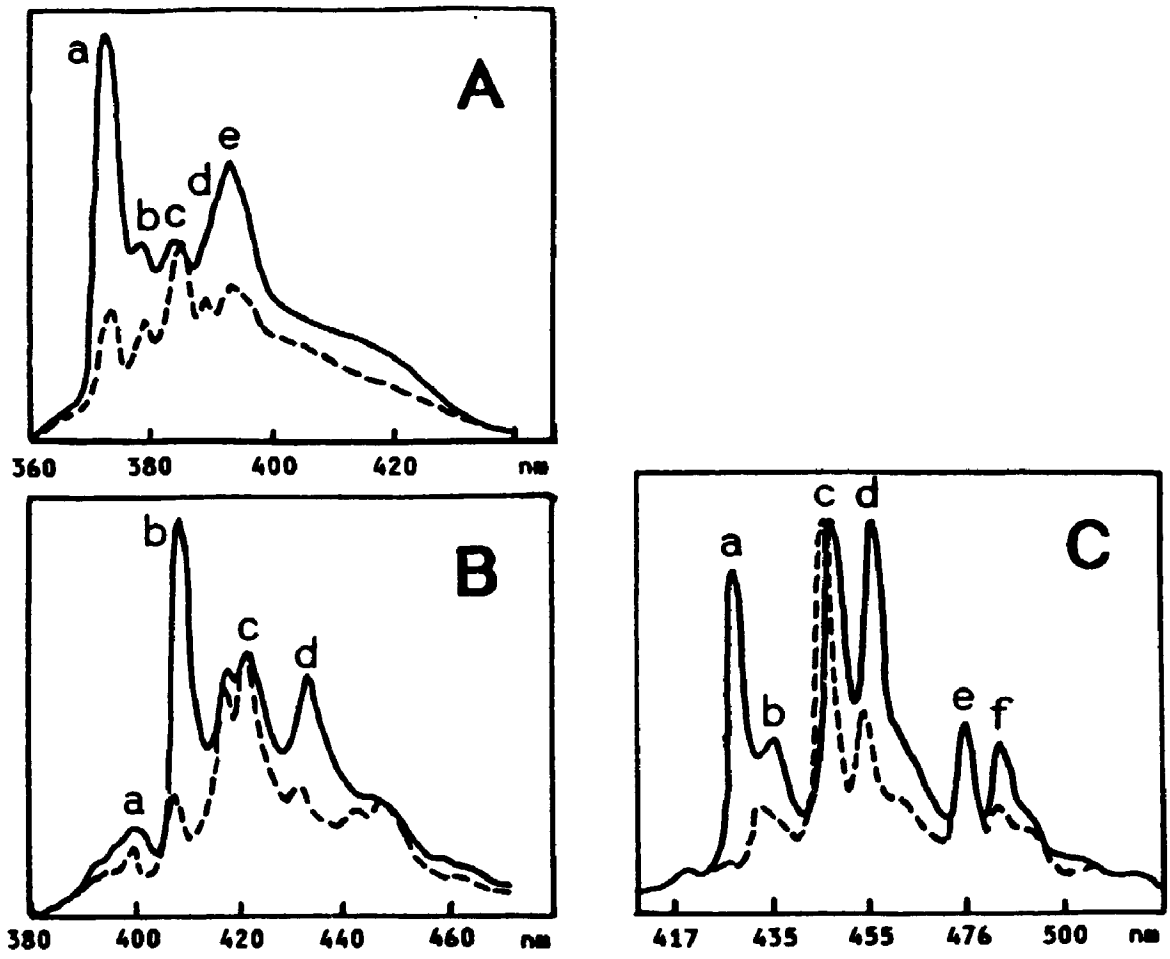

Fig. 8.4 The fluorescence spectra of pyrene, benzoperylene and coronene in typical non-polar and polar solvents: (A) pyrene in heptane(-----), and in dichloromethane(——)[117]; (B) benzoperylene in heptane(- ---), and in N,N-dimethylformamide (——)[141]; (C) coronene in n-heptane(-----), and dimethylsulfoxide (——)[138].

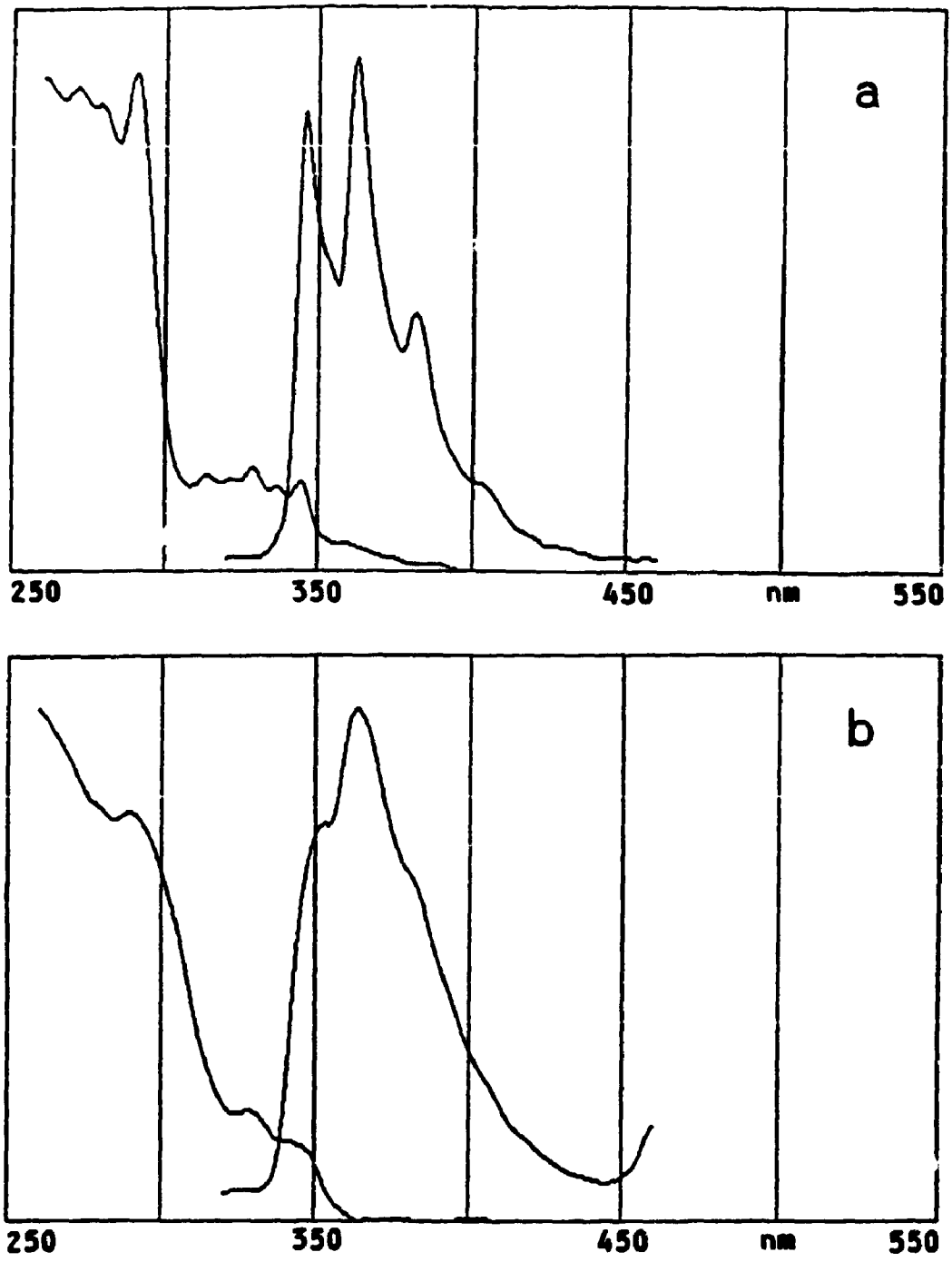

Fig. 8.5 The emission and absorption spectra of phenanthrene, adsorbed on a wet surface(a), and on a dry surface(b).

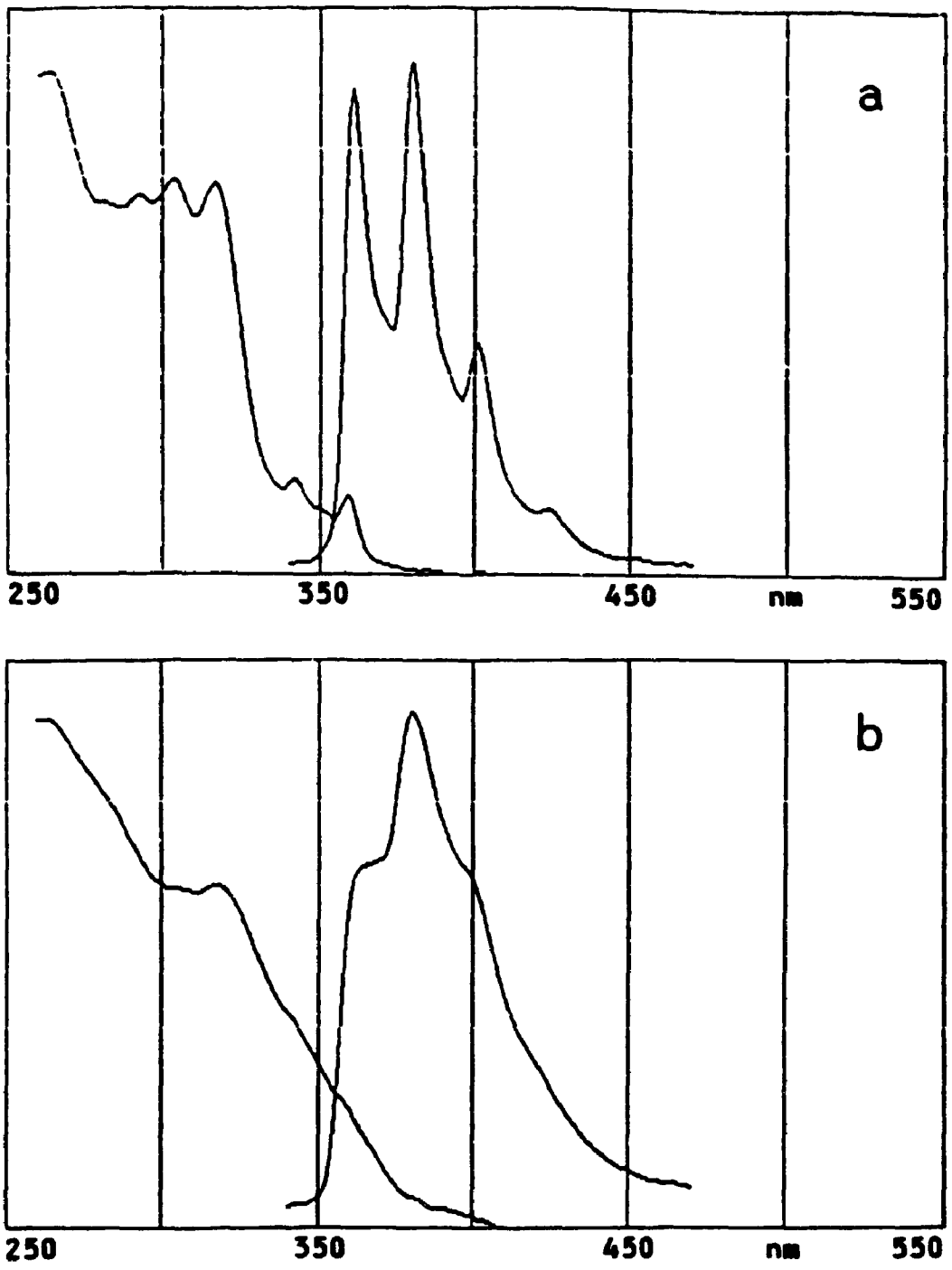

Fig. 8.6 The emission and absorption spectra of chrysene adsorbed on a wet surface(a), and on a dry surface(b).

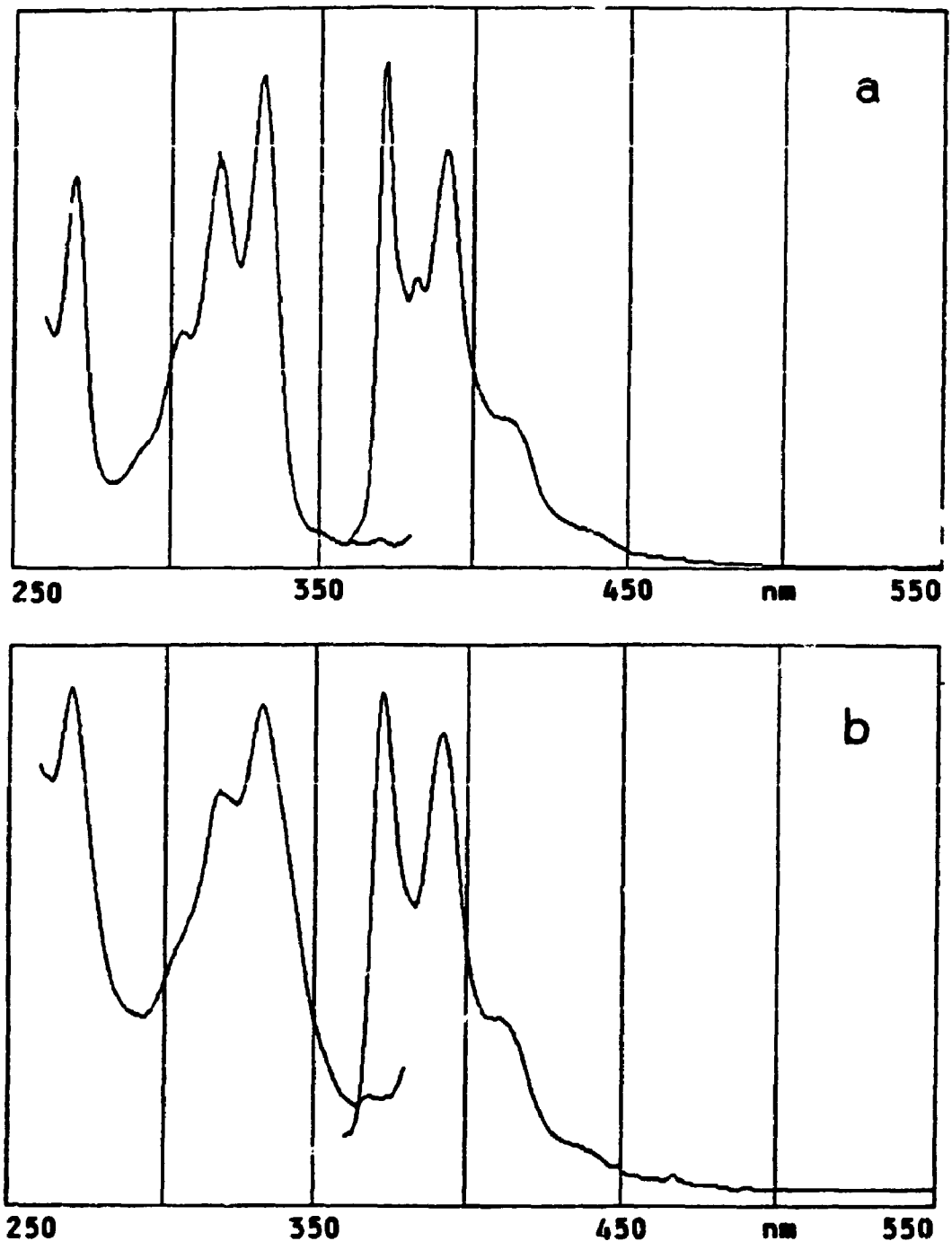

Fig. 8.7 The emission and absorption spectra of pyrene, adsorbed on a wet surface(a), on a dry surface(b).

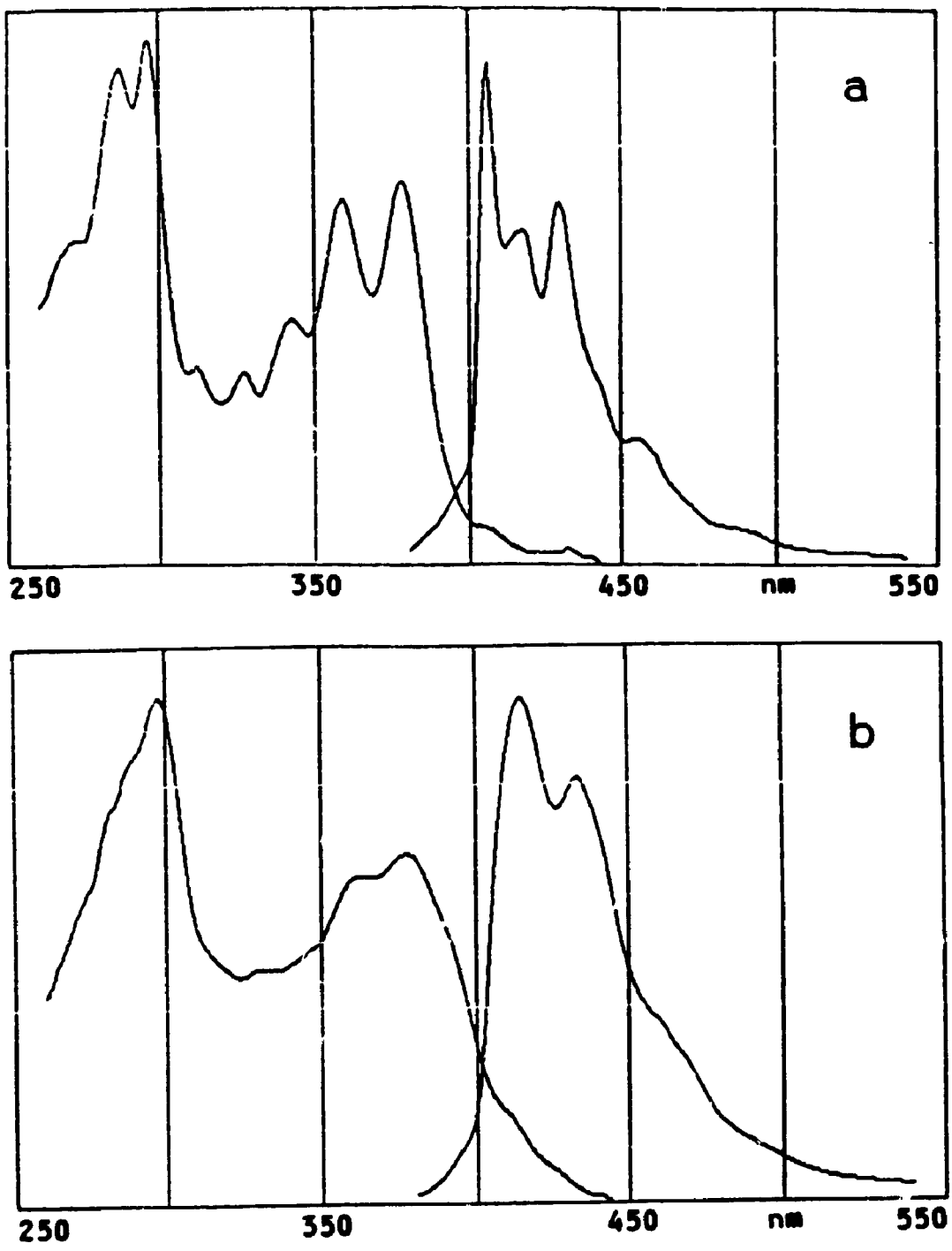

Fig. 8.C The emission and absorption spectra of benzoperylene, adsorbed on a wet surface(a), and on a dry surface(b).

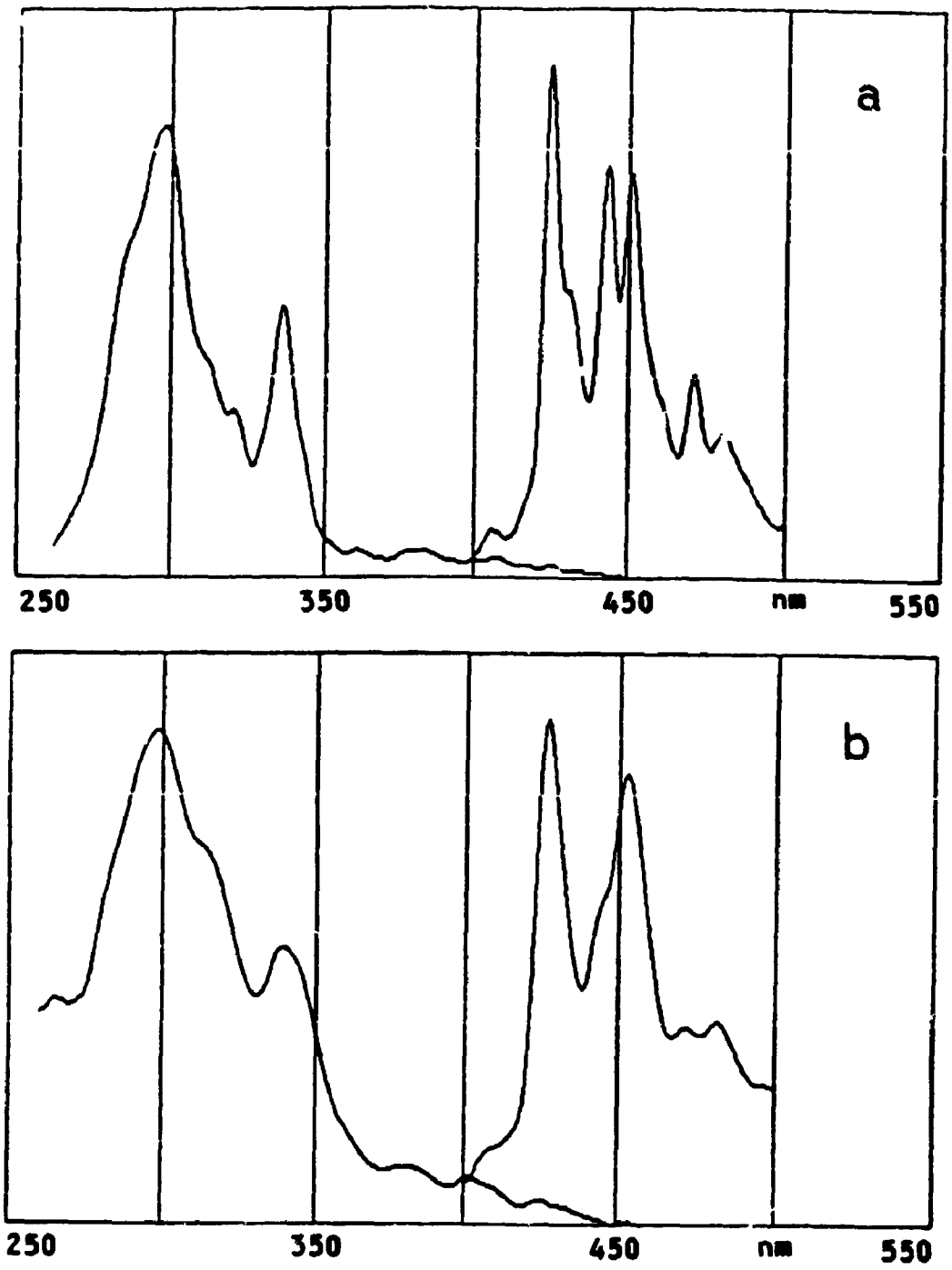

Fig. 8.9 The emission and absorption spectra of coronene, adsorbed on a wet surface(a), on a dry surface(b).

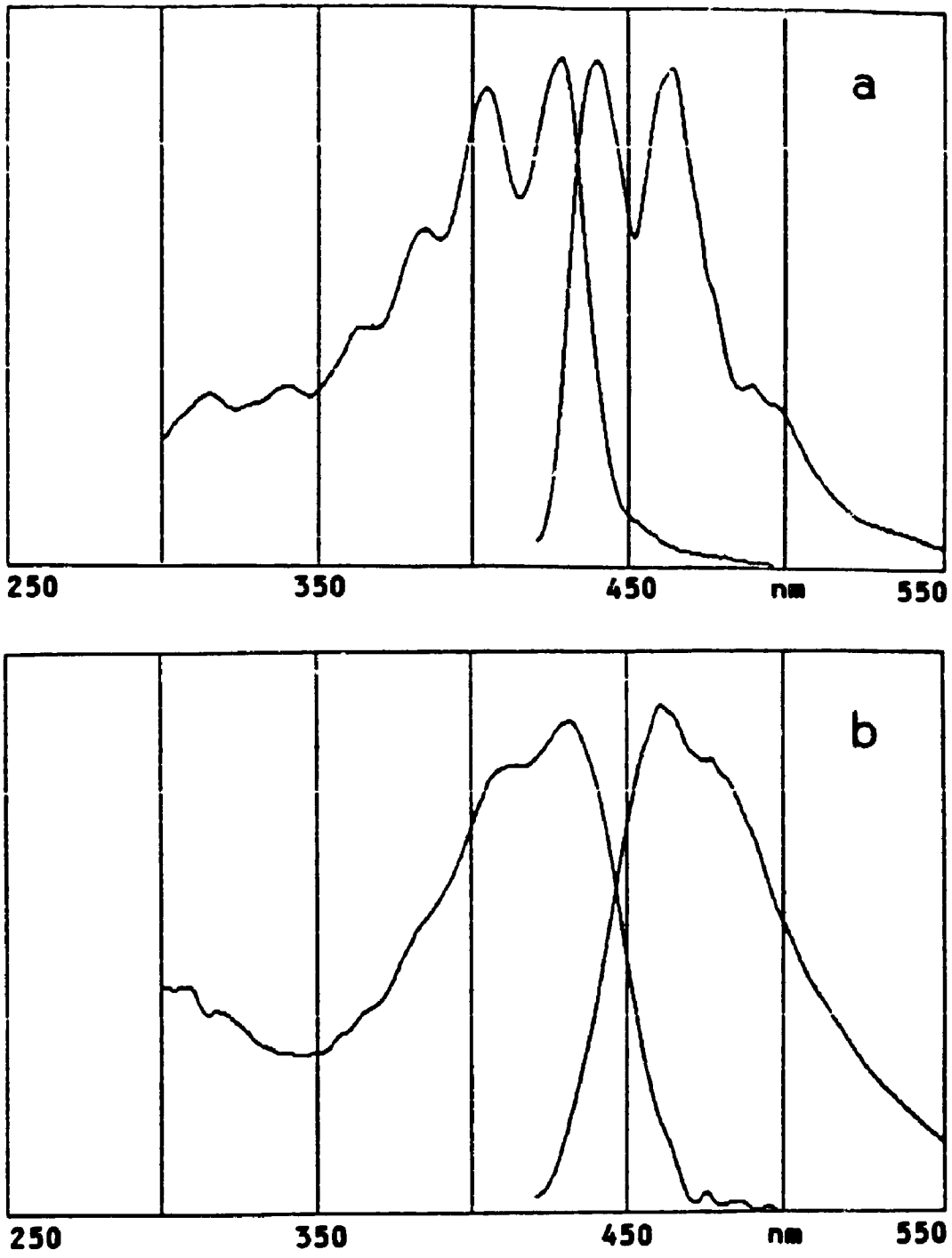

Fig. 8.10 The emission and absorption spectra of perylene, adsorbed on a wet surface(a), and on a dry surface(b).

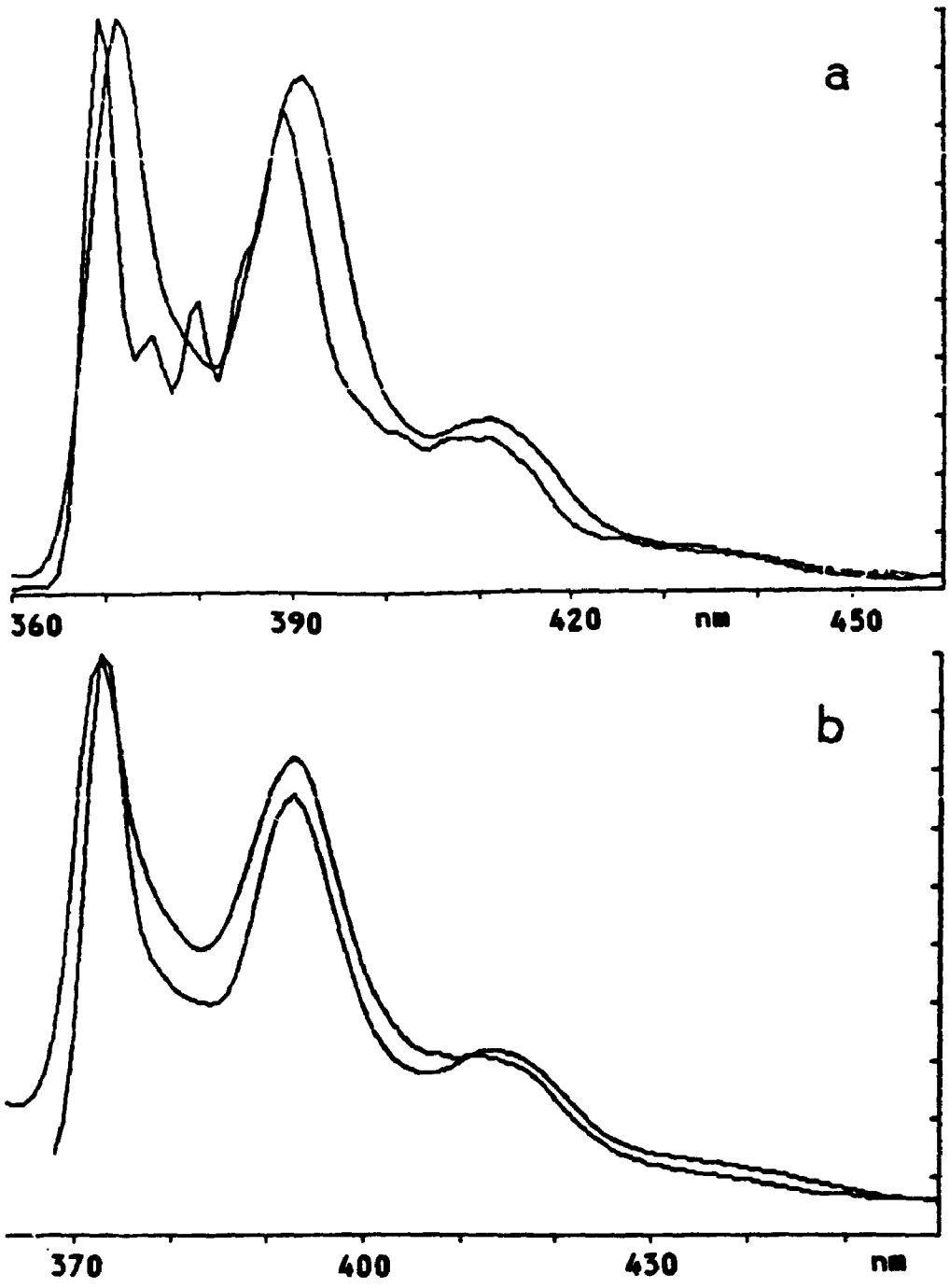

Fig. 8.11 A comparison of the emission spectra of pyrene on a wet and on a dry silica gel surface (a), and a comparison of the emission spectra of pyrene adsorbed on a dry surface and of protonated aminopyrene adsorbed on a wet surface (b).

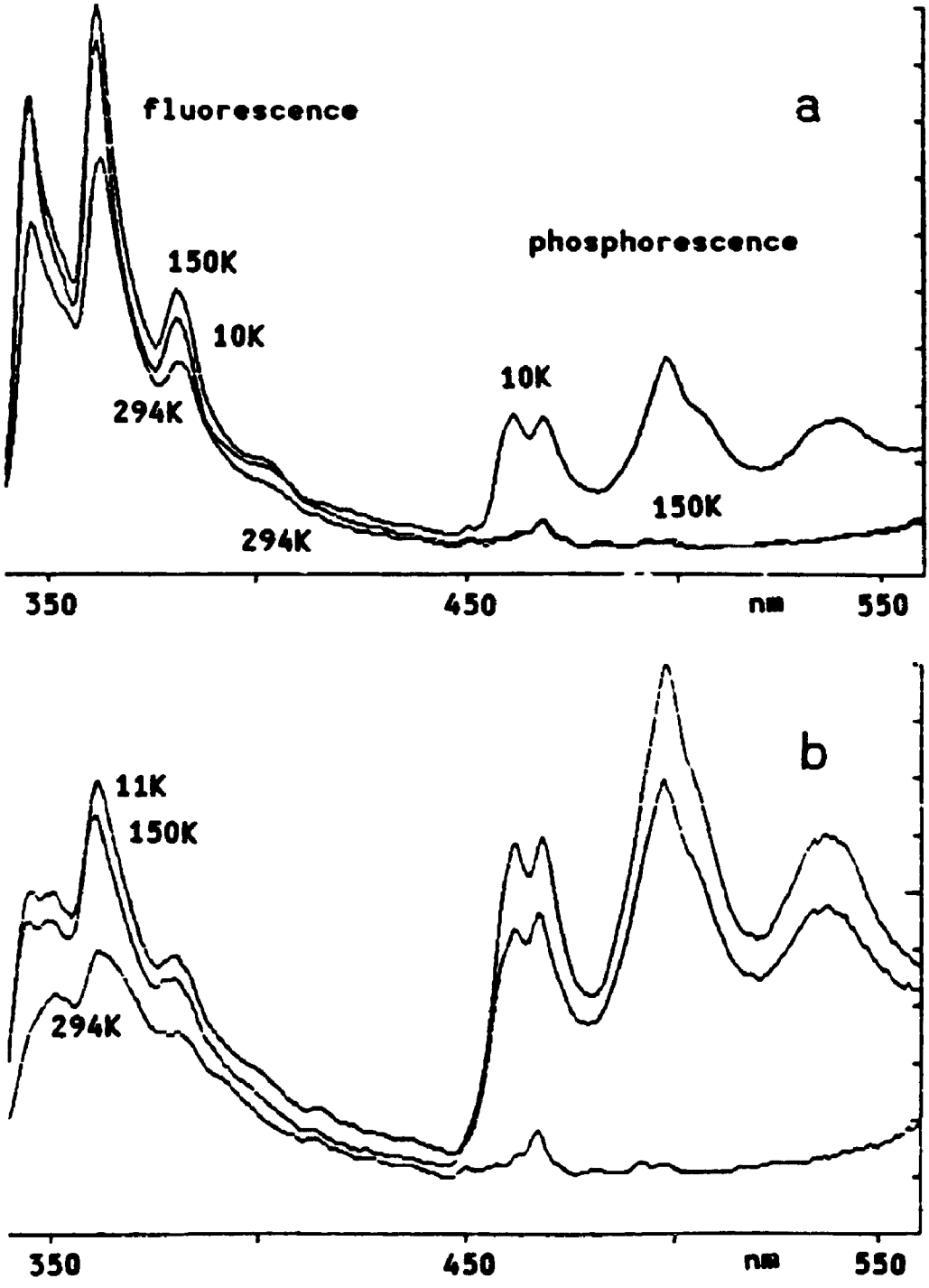

Fig. 8.12 Low temperature luminescence spectra of phenanthrene adsorbed on (a) a wet surface, (b) a dry surface.

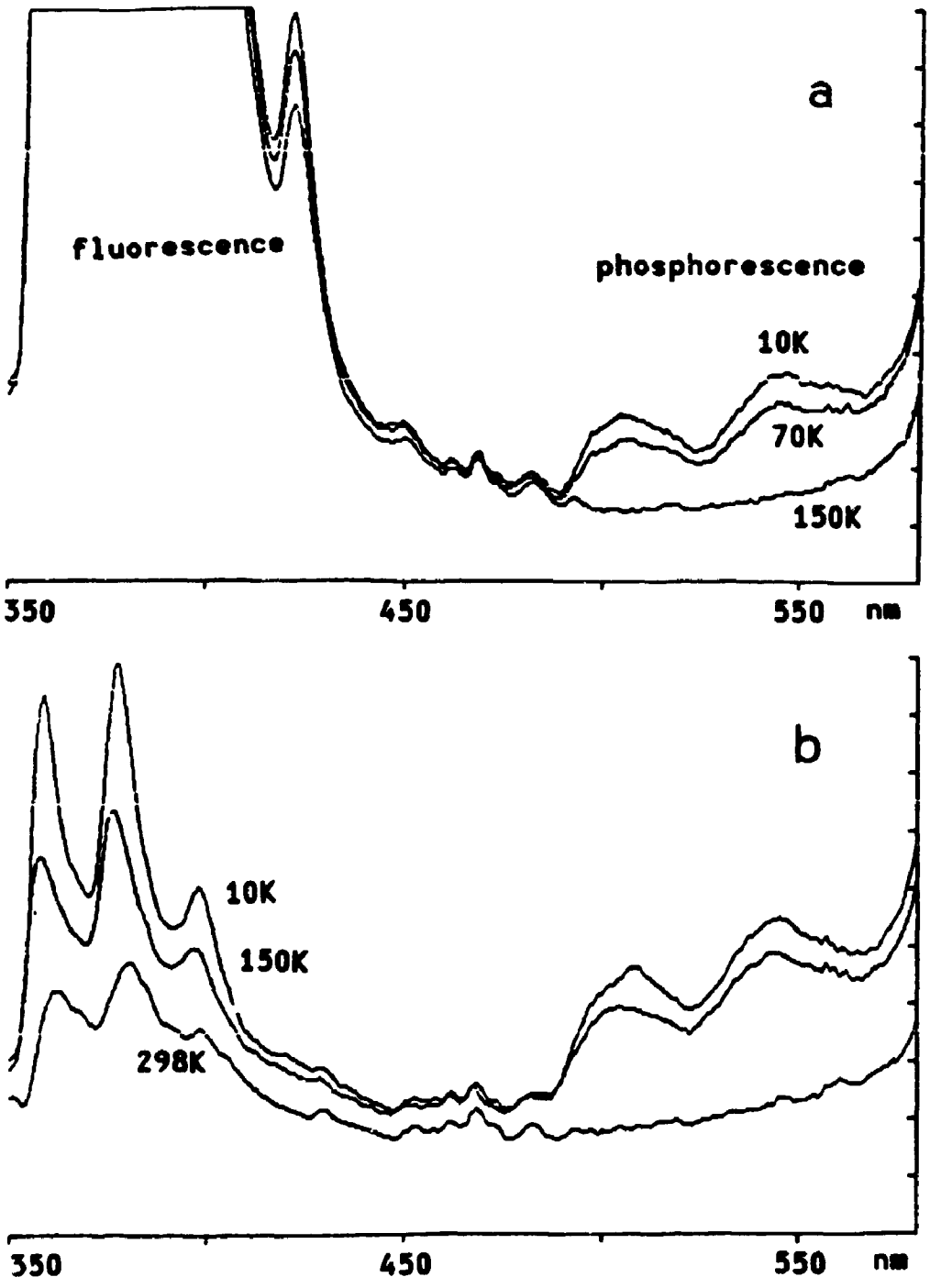

Fig. 8.13 Low temperature luminescence spectra of chrysene adsorbed on (a) a wet surface, (b) a dry surface.

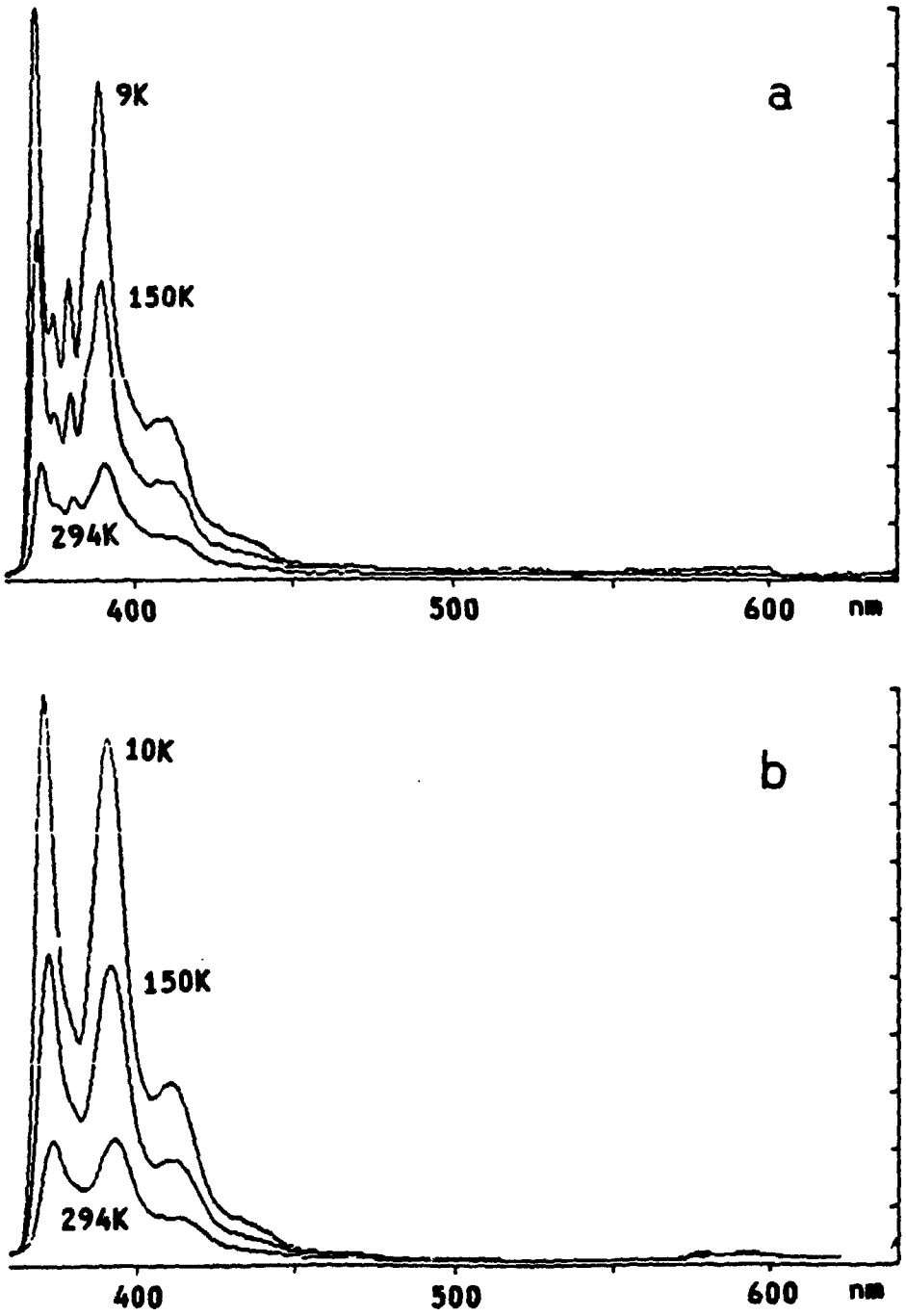

Fig. 8.14 Low temperature luminescence spectra of pyrene adsorbed on (a) a wet surface, (b) a dry surface.

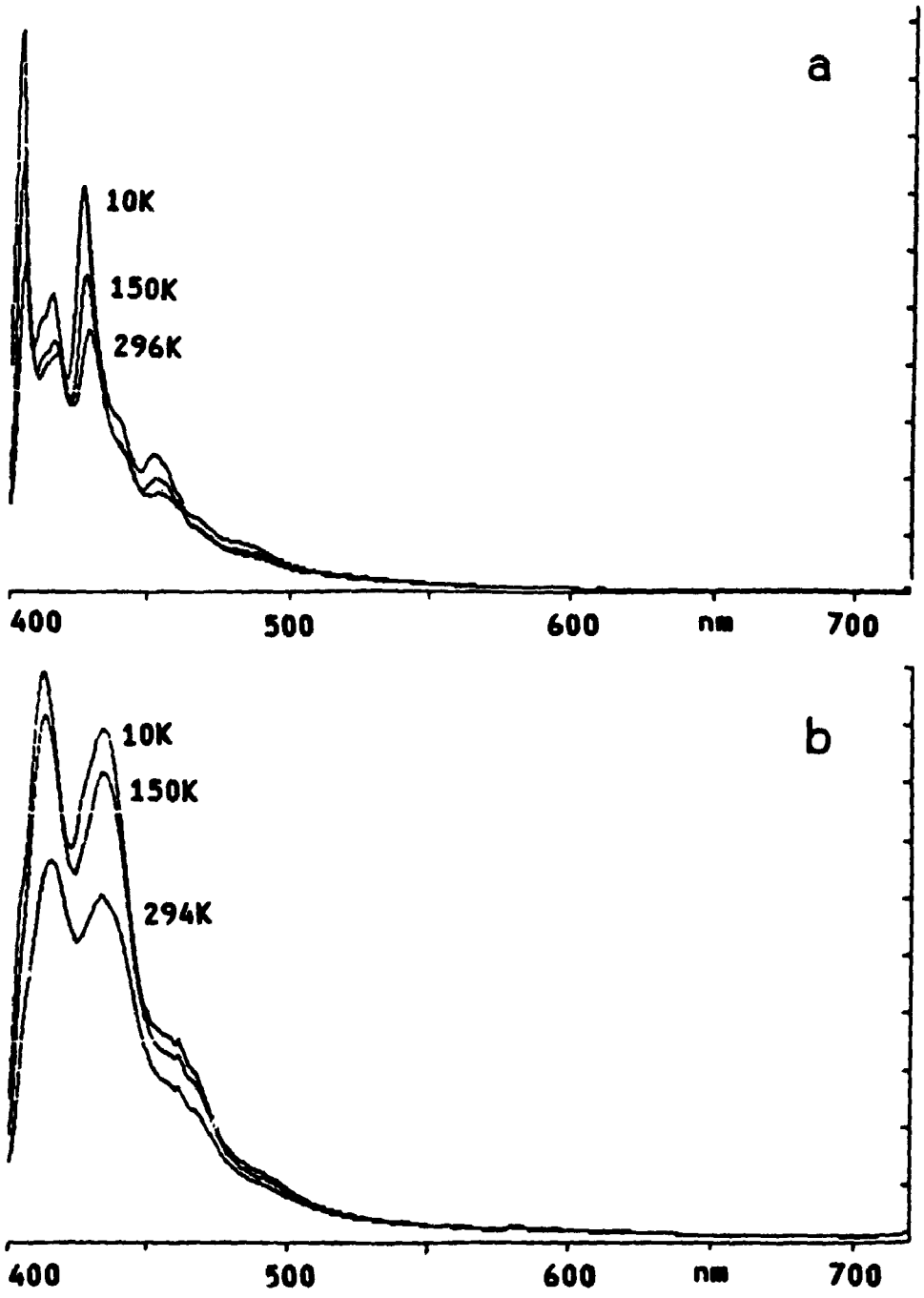

Fig. 8.15 Low temperature luminescence spectra of benzoperylene adsorbed on (a) a wet surface, (b) a dry surface.

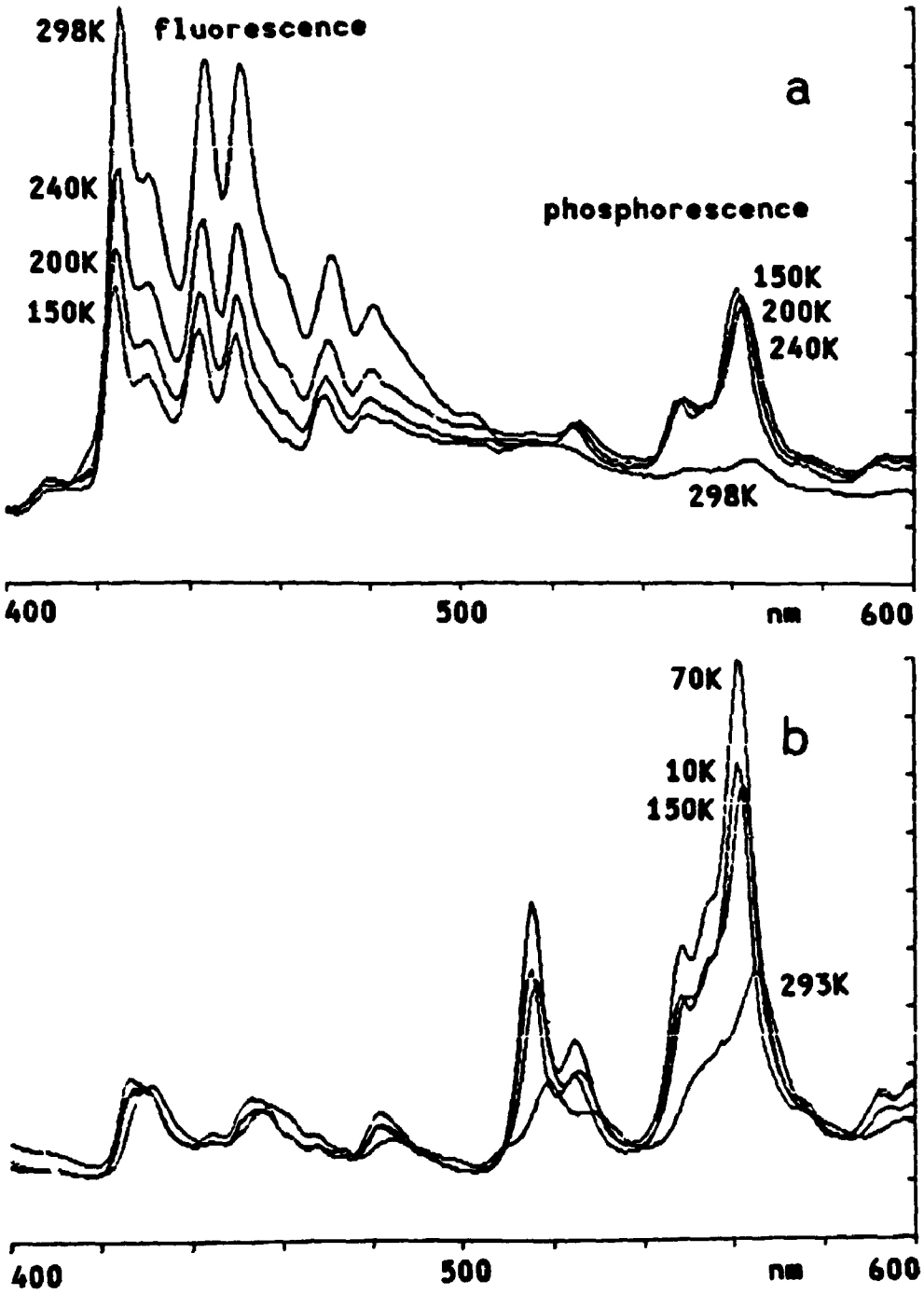

Fig. 8.16 Low temperature luminescence spectra of coronene adsorbed on (a) a wet surface, (b) a dry surface.

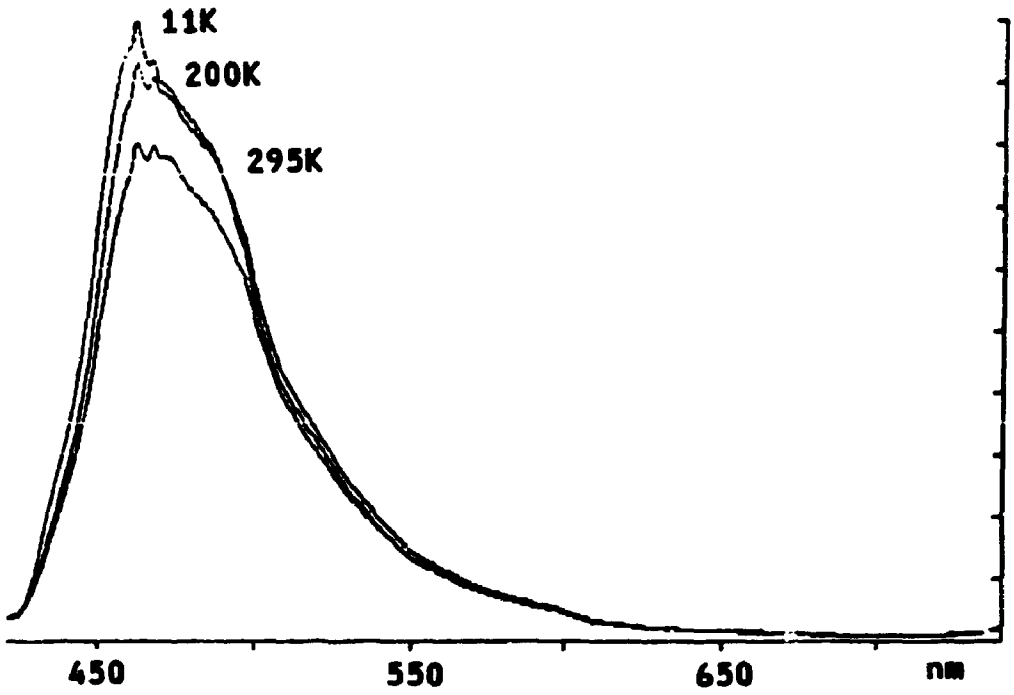

Fig. 8.17 Low temperature luminescence spectra of perylene adsorbed on a dry surface.

Fig. 8.18 Emission spectra of pyrene as a function of the surface concentration. The silica gel was K-60. The excitation wavelength was 331 nm.

(a) on a wet surface: (1) 0.025 mg/g, (2) 0.10 mg/g, (3) 0.25 mg/g, (4) 0.50 mg/g, (5) 2.5 mg/g, (6) 10 mg/g

(b) on a dry surface: (1) 0.05 mg/g, (2) 0.25 mg/g, (3) 0.50 mg/g, (4) 1.25 mg/g, (5) 2.5 mg/g

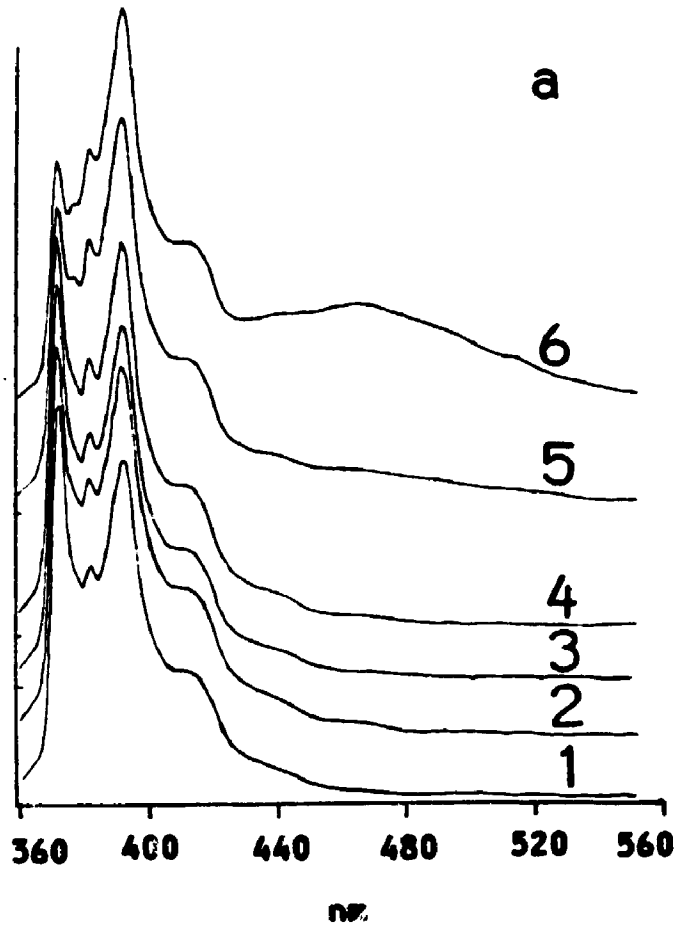
a
6
5
4
3
2
1
360
400
440
480
520
560
nm

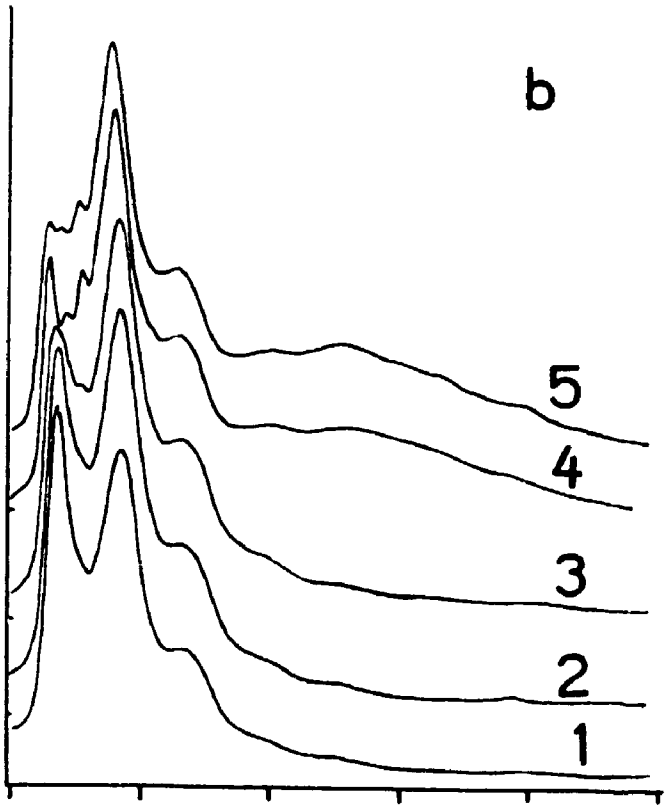
b
5
4
3
2
1

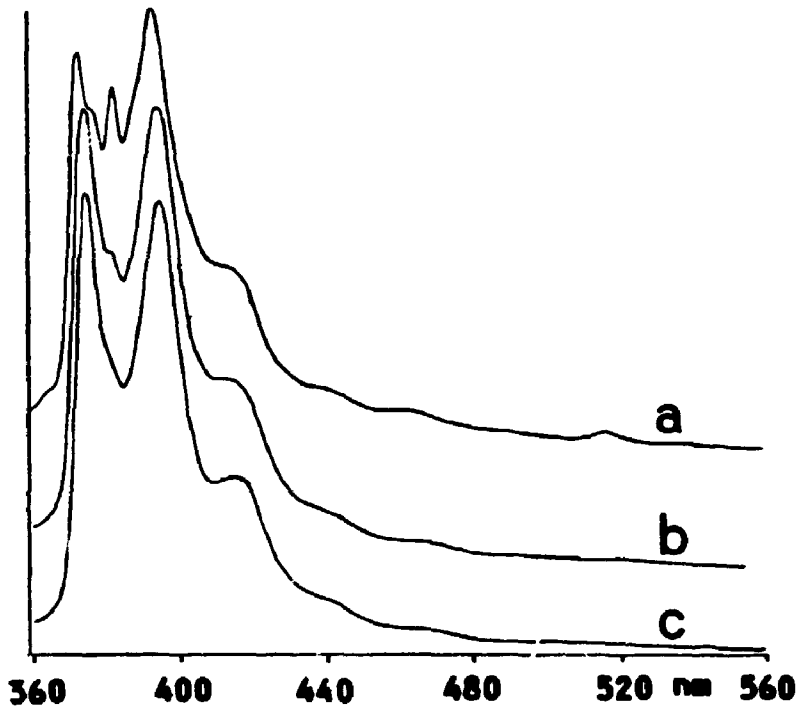

Fig. 8.19 Emission spectra of pyrene, adsorbed on a dry surface, as a function of age of the sample. The silica gel was previously treated with concentrated acid before dehydroxylation. The spectra were measured (a) immediately, (b) 1.5 hours, (c) 48 hours, after the sample was prepared and sealed.

CHAPTER 9 FLUORESCENCE QUANTUM YIELD ESTIMATION FOR PAHS ADSORBED ON SILICA GEL SURFACES

9.1 INTRODUCTION

A fluorescence quantum yield is defined as the fraction of excited molecules, which emit a photon following excitation. Two methods, known as the primary method and the secondary method, are commonly used for its determination [147]. Excellent reviews on this subject are available elsewhere [148-150]. The primary method determines the ratio of (a fraction of) the total fluorescence photons, to (an equal fraction of) the total absorbed photons. In order to ensure that equal fractions of emitted and absorbed photons are detected, careful optical design is essential. The more popular method is the secondary method. A secondary method compares the fluorescence photons from an unknown sample, with that from a standard sample, under the condition that both samples absorb an equal number or a known ratio of excitation photons.

Although numerous photophysical studies have been conducted on fluorescent molecules adsorbed on powdered solid materials such as silica gel, only a small number of these studies has been devoted to the determination of fluorescence quantum yields of such adsorbed molecules.

Oelkrug and coworkers have studied this problem since the late 1970s [151-153]. They measured the luminescence quantum yields of a number of aromatic molecules adsorbed on "wet" and preheated alumina surfaces, and derived the corresponding radiative and non-radiative decay rate constants. Originally, in these studies, a primary method was used [151,152]; but in a later paper [153], it was for some reason decided to estimate a quantum yield relative to the value of phenanthrene physisorbed on an alumina surface; the latter was assumed to be equal to the value of that in solution. Margins of error up to 100% were observed. The fluorescence lifetime was assumed to be a single exponential to permit the calculation of the radiative decay rate, although such a calculation was not in fact valid.

Nevertheless, most photophysical studies on surfaces are restricted to direct observations of emission and excitation spectra, or determinations of fluorescence lifetimes. Consequently, the detailed decay mechanism in these heterogeneous systems is, compared with that in homogeneous system, still very poorly understood. For adsorbed molecules, an accurate measurement of their extinction coefficient as a function of wavelength is extremely difficult, if not impossible. For those compounds whose transitions to the lowest excited singlet states are weak, a fluorescence quantum yield measurement, in conjunction with a lifetime measurement, is the only way to obtain the

radiative and non-radiative decay rate constants. We present in this chapter the results of our attack on this problem, in the hope of achieving a "complete" study of the photophysics of the adsorbed PAHs.

9.2 THEORETICAL CONSIDERATIONS ABOUT THE QUANTUM YIELD MEASUREMENT IN TURBID MATERIALS

In an ideal case, when the medium can be assumed to possess an infinite scattering power, the problem of determining the fluorescence quantum yield is conceptually easier. In this case, all the incident excitation light, except a portion that is absorbed by the fluorescent molecules on the surface of the medium, must be back-scattered from the front surface; and all the fluorescence light is diffusely emitted from the front surface also. The fluorescence quantum yield can thus be measured, in principle, by monitoring the diffusely reflected excitation light and the diffusely emitted fluorescence light. For example, Wrighton, Ginley and Morse [154] have determined the absolute emission quantum yield of powdered samples, using a conventional scanning emission spectrophotometer. They assumed that, for their powdered sample in a cuvette, the angular distributions of diffusely reflected light and of emitted light were the same, and that Lambert's cosine law was obeyed. Hence the same fraction of emitted light, and of

reflected light, was collected by the detection system. The fluorescence quantum yield could thus be determined, by measuring the ratio of fluorescence intensity to the difference between the back scattered intensities of excitation light from a blank, and from a loaded sample (see equation 9.2).

The most difficult case is that in which a semi-transparent medium of finite scattering power, such as silica gel powders, is involved. In this case, neither the well established techniques used for transparent solutions, nor the relatively simple method for white and opaque solid powders, are suitable, because the medium is neither a transparent nor a perfect scattering material. In such a medium, the incident light and the emitted fluorescence light are "leaking" in all possible directions, and the distribution of the leaking light along the surface of the bulk sample is a complicated function of the optical properties of the sample. Special measures must, therefore, be taken for such cases.

Recently, a remarkable effort to estimate fluorescence quantum yields in a turbid system has been made by G.R.Seely [155-157]. He discussed a sophisticated approach that involved measuring a so-called "apparent quantum yield", similar to what Wrighton and coworkers did, then calculating a correction factor, based on the optical properties of the

medium, in order to deduce the true quantum yield. Since this is a recent and serious effort to deal with this problem, a brief description of Seely's approach is given as follows.

Seely's treatment is based on the Kubelka and Munk (K & M) theory of light transport in scattering media [158-160]. The mathematical details can be found in the cited references. Here we only describe Seely's basic idea. According to Seely, we may assume that the medium is an infinitely broad plate with a finite thickness, and is evenly illuminated from the left side with ideally diffused light of intensity I_0, as illustrated in Fig. 9.1. If, for simplicity we further assume that the medium itself does not absorb any incident light, then the total input light intensity can be consumed only in the following two ways. The incident light is partly back-reflected from the left surface, designated $j(L)$, and partly passes through the plate and escapes from the right side surface, designated $i(0)$. The rest of the incident light is absorbed by the fluorescent molecules, and a portion of the absorbed light is reemitted as fluorescence. If the medium does not absorb the fluorescence light, then it will escape partly through the left surface, $j_f(L)$, and partly through the right surface, $i_f(0)$. The fluorescence quantum yield is calculated by equation (9.1),

$$\phi = \frac{j_f(L) + i_f(0)}{I_0 - i(0) - j(L)} \tag{9.1}$$

The so called "apparent quantum yield", observed by Seely and Wrighton, is defined by (9.2),

$$\phi_{ap} = \frac{j_f(L)}{j_0(L) - j(L)} \tag{9.2}$$

where $j_0(L)$ is the back-scattered incident light when there are no fluorescent molecules present in the medium. Obviously, when the scattering power of the medium is infinite, which implies $I_0 = j_0(L)$ and $i(0) = i_f(0) = 0$, the apparent quantum yield is just the true quantum yield, i.e. $\phi = \phi_{ap}$. When the medium is semi-transparent, the discrepancy between ϕ and ϕ_{ap} is a complicated function of the optical properties of the medium, and the distribution and concentration of the fluorescent molecules in the medium. This discrepancy may be calculated, in the ideal case, from the K & M theory. Seely's approach is to measure the ϕ_{ap}, and to calculate the theoretical discrepancy between ϕ and ϕ_{ap}, and then to correct the ϕ_{ap} to find the true ϕ.

Seely's treatment, when applied to real fluorescence instrumentation and real samples, is still questionable. The

optical conditions assumed by the K & M theory, such as a uniform medium, even illumination on the infinite large surface, cannot actually be obtained. Therefore, Seely's treatment corrects, in fact, the error of the theoretical apparent quantum yield against an ideal case, the K & M model, but the discrepancy between the experimentally observed "apparent quantum yield" and the theoretical apparent quantum yield is still unknown [161].

9.3 A PRIMARY METHOD BASED ON DIFFUSE REFLECTANCE: EXPERIMENTAL AND RESULTS

Stimulated by the methodologies of Seely and Wrighton, an attractive idea arose during the course of this work: that is whether we can experimentally compensate for, instead of theoretically "correcting", the discrepancy between a real silica gel sample and an ideal scattering material.

Silica gel powders are turbid materials and do not absorb light of wavelength longer than 260 nm. Suppose, as shown in Fig. 9.2, the sample cuvette is backed up with mirrors from the back and edges, and is illuminated evenly on the front surface. In principle, this should be experimentally achievable. Under this condition, the front surface of the cuvette is artificially made the only opening for light input and output; and the majority of incident photons would

travel into the medium for a distance, be scattered, reflected and refracted many times, until they eventually escape from the front surface. These escaped photons may, therefore, be assumed to have been completely randomized in their directions. This implies that the bulk of silica gel powders, under the above designated conditions, can be considered as an ideal diffuser which transfers the collimated excitation light into diffused light, except for the portion absorbed by the fluorescent molecules in the medium. A part of the absorbed light will be emitted as fluorescence, which, ideally, is alsc diffused. Based on the same arguments as Wrighton's, the measured apparent fluorescence quantum yield should approximate the true one.

The experimental set-up for testing this idea is shown in Fig. 9.3 a. A Perkin-Elmer 650-40 fluorescence spectrophotometer was again employed. The sample compartment was equipped with a device that held a sample cuvette in a fixed orientation, and which was adjustable if so desired. The 1 x 10 mm cuvette was backed with a U shaped mirror made of polished aluminum. In front of the detection monochromator, there was an attenuator to adjust the light intensity to be measured, so that both the scattered and emitted light would be in the proper range of the detector sensitivity.

For most of the measurements, the excitation light beam was

aimed at the lower part of the sample cuvette at an incident angle of 30 degree from the normal. The directly illuminated area was about 16 mm^2 or larger. Two matching cuvettes, one filled with a blank silica gel sample and the other with a PAH loaded silica gel sample, were prepared. The spectrophotometer was run in the correction mode. Five measurements were needed for the calculation, as described in the following.

(A) Integrated scattered light from the blank. The excitation monochromator was fixed at the selected excitation wavelength λ while the detection monochromator scanned over a range of $\lambda \pm 20$ nm. J_0 represents the area under this curve.

(B) Scattered light intensity, I_0 , obtained from the blank at a long wavelength, usually 580 nm, where the adsorbed molecules did not absorb at all.

(C) Integrated scattered light from the sample, J, obtained at the excitation wavelength in the same way as J_0.

(D) Scattered light intensity, I, from the sample at the same wavelength as I_0 .

(E) Integrated area under the emission spectrum from the sample, J_f.

The apparent quantum yield was then calculated according the following equation, which was based on equation (9.2):

$$\phi_{ap} = \frac{J_f}{J_0(I/I_0) - J} \qquad (9.3)$$

here the factor I/I_0 was introduced to correct the error due to the discrepancy of sizes or positions of the two cuvettes.

The influence of powder sizes and a back mirror on the results was tested with 9-aminoacridine hydrochloride at a surface concentration of 0.15 mg/g. Two different Kieselgel-60 silica gel powders, 230-400 mesh and 35-70 mesh respectively, were used. The results are listed in Table 9.1. These results suggest that for the 230-400 mesh powders, which possess better scattering power, the employment of mirror back-up is not essential; but for the larger sized powders (35-70 mesh), which look more transparent, measurements, with and without mirror back-up, result in a big difference. Based on the discussion given in Section 9.2, which indicates that the apparent quantum yield approximates the true quantum yield when the scattering power of the medium approaches infinity, the result from the 230-400 mesh silica gel is presumably better than that from the 35-70 mesh silica gel. For the present we may tentatively consider the value of 0.73 to be closer to the

true value than 0.98. If this is the case, these data suggest that the use of back mirror is indeed a valid technique in the determination of fluorescence quantum yields for turbid materials, and this cuvette-mirror system can be considered as a "compact integrating sphere".

Table 9.1 Effect of mirror back-up on the measured apparent quantum yield of 9-aminoacridine hydrochloride at 0.25 mg/g.

back	Kieselgel-60 (200-400 mesh)	Kieselgel-60 (35-70 mesh)
mirror backed	0.74	0.76
not backed	0.73	0.98

Unfortunately, at present, neither a well established quantum yield determination method, nor any commonly accepted "true" fluorescence quantum yield data, are available for fluorescent compounds adsorbed on silica gel surfaces. We are, therefore, unable to compare these results with any "standard". To assess the reliability of these results is as difficult as it is to measure them. What has been done in this work is, (a) to compare the results from a variety of measurements under reasonable conditions to test the stability of the results, and (b) to appraise the reasonableness of these results, in conjunction with information from other sources.

Table 9.2 presents results of repeated measurements of a pyrene sample. The silica gel was not heated in vacuum (so called "wet") and was loaded with pyrene at 0.16 mg/g. The measurements were done with the cuvette in four different orientations. The angles represent the incident light with respect to the normal direction of the cuvette surface. We avoided using 45° as the incident angle, because in such a case the specular reflection light from the cuvette surface would severely interfere with the measurement.

Table 9.2 Cuvette orientation dependence of measured apparent quantum yield of pyrene on Kieselgel-60 (35-70 mesh), 0.16 mg/g.

angle	blank calibrated	self calibrated	diffuser used
20°	0.36	0.30	0.465
30°	0.34	0.335	0.45
60°	0.25	0.29	0.39
70°	0.23	0.26	0.40
average	0.295±0.065	0.296±0.031	0.426±0.037

The three columns contain three groups of data taken under varied conditions of measurement. The data in the first column were obtained by the normal method described above. In comparison, the data in the second column were obtained from a single sample cuvette. The integrated scattered

light, J_0, was measured in the same way as in step (1), but with the sample itself rather than a blank, and at a wavelength where the adsorbed molecules did not absorb light at all, normally 580 nm. Since there was only one cuvette and it was not touched throughout the measurement, the factor I/I_0 in equation (9.10) was equal to unity. In this way the possible errors due to cuvette position and size were eliminated, but a pre-calibration then became critical. The data in the third column were obtained with a quartz diffuser placed in front of the sample so that the incident light was partially diffused and the sample cuvette was illuminated more evenly. From a theoretical point of view this type of incident light was preferred.

These data suggest the following: (a) a lower incident angle gives a higher yield; (b) a single sample measurement without a blank gives the same result as sample-blank measurement, therefore the blank seems not really necessary; (c) the use of a front diffuser, which presumably can give better results, gives a higher yield. If, for the moment, we give all these numbers an equal weight, then the average fluorescence quantum yield and the deviation are 0.34 ± 0.08, which corresponds to a percent deviation of 24%, for pyrene adsorbed on the wet surface. This is considered a reasonable error estimate for the results obtained in this work. The same level of error was reported by Wrighton [154] in their studies. Considering even in the simplest case, the

quantum yield measurements in solutions, the experimental uncertainties from laboratory to laboratory run 10-20%, it seems pointless at the present time to expect better results for such a complicated system.

Table 9.3 presents the data obtained from repeated measurements for another four aromatic hydrocarbons adsorbed on wet surfaces, using the standard method. 9-aminoacridine was included because we originally intended to use this compound as a standard. The 9-aminoacridine used here was in the form of the hydrochloride. In water it has a fluorescence quantum yield close to unity. For a time it was assumed that its quantum yield did not change significantly on a silica gel surface, but this turned out not to be the case. A similar situation was found with perylene: its lifetime did not change significantly on either wet surface or dry surface, compared with that in solution, but the quantum yield measured on a silica gel surface was about 30% lower than that observed in solution. There are two possible interpretations for such an "unpredicted" result: it may simply be considered as an optical artifact, a systematic error in our measurements; or it may be caused by a real photophysical effect of the silica gel surface. On the basis of the observations in this work, we believe, at least partly, that this "reduced" quantum yield should be attributed to a photophysical effect of the surface. Evidence is seen in the low temperature fluorescence spectra

(see Fig. 8.17 in Chapter 8), the perylene fluorescence quantum yield on the dry silica gel surface increases by about 19% at 11K, compared with that at 295K. If this set of data is accepted, then the "true" fluorescence quantum yield of perylene at room temperature should not exceed 0.84. Otherwise Fig. 8.17 would imply a quantum yield of more than 100%, for perylene at 11K. This reasoning shows that 0.75 is, at least, not an unreasonable value for perylene on the surface.

Table 9.3 Fluorescence quantum yield measured with diffuse reflectance method

compound	quantum yield
chrysene	0.11
perylene	0.75
benzoperylene	0.28
coronene	0.13
9-aminoacridine	0.76

9.4 A PRIMARY METHOD BASED ON THE INTEGRATING SPHERE: EXPERIMENTAL AND RESULTS

The main advantage of using an integrating sphere is that the irregularities in the angular distribution of the

intensity of the scattered and the fluorescence light, can presumably be averaged out. Hence the error due to this source may be suppressed. In practice, however, the preparation and the use of an integrating sphere is a delicate and difficult technique, and to get reliable results with such a sphere is as difficult as other methods.

An integrating sphere technique was also employed in this work for comparison. These measurements were again conducted on the Perkn-Elmer fluorescence spectrophotometer, equipped with an integrating sphere. Fig. 9.3 b shows the experimental set-up for this method. The integrating sphere was made from a flask approximately 80 mm in diameter. The fluorescence viewing window was about 6 mm in diameter and was off-centre so that it viewed a portion of the internal wall of the sphere. The sphere was coated with MgO by burning magnesium ribbon in an O_2 stream at the openings. The sample was sealed in a quartz or pyrex glass tube and was installed on the short arm attached to the stopper. The excitation light came into the sphere through another window, also 6 mm in diameter, directly illuminating the sample tube. The orientation of the sample tube was such that no light could be directly reflected from the sample tube to the viewing window.

The detection system of the fluorescence spectrophotometer was calibrated with the integrating sphere, with a blank

silica gel sample installed. The instrument was run in the correction mode. Five measurements, similar to those described in the previous section, but with samples in the integrating sphere, were needed for the calculations. The formula was the same as equation (9.3). Some samples have been measured with this method, and the average results are listed in Table 9.4.

Table 9.4 Fluorescence quantum yield measured with integrating sphere method

compound	silica gel treatment	quantum yield
perylene	wet	0.74
pyrene	wet	0.37
pyrene	200°c heated	0.25
pyrene	400°c heated	0.17
pyrene	600°c heated	0.096
pyrene	800°c heated	0.08

For all the PAHs measured with this method, the results are similar to those from the diffuse reflectance method. This suggests that the possible error from an irregular spatial distribution of scattered light in the diffuse reflectance method is not serious.

9.5 A SECONDARY METHOD BASED ON DIFFUSE REFLECTANCE: EXPERIMENTAL AND RESULTS

What is absolutely needed from a primary method is to establish a standard fluorescence quantum yield for silica gel samples. If a standard can be established, then all other samples may be more conveniently determined, by using a secondary method.

In the present work, a secondary method was also used to measure the relative quantum yields of the six PAHs adsorbed on the wet and the dry surface. At the outset, the quantum yield of pyrene on the wet surface was intuitively taken to be 0.37. This value was obtained from the integrating sphere method, listed in Table 4. Compared with the overall average of the results from the diffuse reflectance method (0.34 ± 0.08), to assume the "true" value to be 0.37 was considered feasible.

The order of these measurements was as follows:

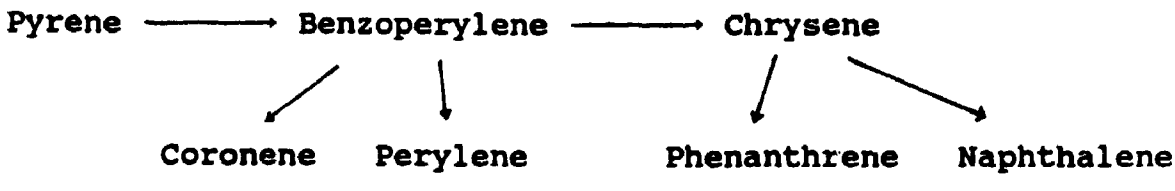

This arrangement was based on considerations of a proper overlapping of the absorption and emission spectra involved. The experimental set-up was essentially the same as illustrated in Fig. 8.2 a.

The calculation was based on the following equation, which was derived from equation (9.3):

$$\phi_x = \phi_s \frac{J_x I_s}{J_s I_x} \qquad (9.4)$$

where J_s and J_x were the areas under the corrected fluorescence spectra of the standard and unknown samples, respectively. I_s and I_x were the fractions of absorbed intensities at the common excitation wavelength. ϕ_s and ϕ_x were the quantum yields.

Fig. 9.4 shows the procedures for measuring the relative quantum yield of chrysene (as an unknown) against benzoperylene (as a standard), as a representative example. The absorption spectra of the two samples were repeatedly measured, then an appropriate excitation wavelength, 292 nm in this case, was selected, as shown in Fig. 9.4 a. I_x and I_s were the averages of the absorptions of the unknown and the standard respectively, at the selected excitation wavelength. At this excitation wavelength the corrected emission spectra were measured, as shown in Fig. 9.4 b. J_x

and J_s were the average areas under these emission spectra. The relative quantum yield was then calculated from equation (9.4). The results from these measurements are presented in Table 9.5. Some literature data for the fluorescence yields of these PAHs in ethanol are collected in Table 9.6. These results, even if we assume a possible 25% error in each value, indicate that the fluorescence quantum yields of pyrene, coronene, chrysene, and phenanthrene decrease in the order of; solvent, wet surface, dry surface. Only those of perylene and benzoperylene do not change significantly from a wet to a dry surface. These data will be further discussed in the next chapter.

Table 9.5 Fluorescence quantum yields determined by secondary method

compound	on wet silica gel	on dry silica gel
pyrene	(0.37)	0.11
benzoperylene	0.26	0.24
perylene	0.66	0.72
coronene	0.13	0.047
chrysene	0.095	0.061
phenanthrene	0.098	0.048
naphthalene	0.090	0.036

Table 9.6 Fluorescence quantum yields of PAHs in ethanol reported in the literature

compound	fluorescence yield [source]		
pyrene	0.65 [162]	0.72 [163-165]	0.53 [166]
benzoperylene			
perylene	0.89 [167]	0.94 [166]	
coronene	0.23 [165]		
chrysene	0.17 [164-166]		
phenanthrene	0.10 [168]	0.13 [164-166]	0.13 [164]
naphthalene	0.21 [164-166,169]	0.12 [168]	0.19 [170]

9.6 DISCUSSION

The fluorescence quantum yield determination is a very difficult problem in surface photophysics. Since there is very little work reported in this field, we are not able to compare our results with corresponding literature data. Further investigations would certainly be desirable.

Based on the available information, however, there is one conclusion that can be made for certain: the fluorescence quantum yields of most of the PAHs studied are remarkably different from that of these PAHs in solution. As discussed in section 9.3 for perylene, the measured quantum yield of 0.75 for perylene on a wet surface, seemingly "too low", can be understood when the low temperature fluorescence

observation (Fig. 8.17) is taken into account. The changes of the quantum yields of the other PAHs are more easily understood, because, in the first place, their lifetimes are greatly changed on going from solutions to the surface.

A low temperature fluorescence observation appears to be a useful technique to check the reasonableness of some results of the surface fluorescence quantum yield measurements. This technique cannot be used for solutions, because on changing the temperature, say from 295K to 10K, there is always some phase change, accompanied by a change of optical properties, on the sample involved. Since the surface sample, presumably, does not change its optical properties on going from a room temperature to a low temperature, the low temperature quantum yield, relative to the value at a room temperature, may indicate an "upper limit" to the room temperature value. This technique is considered more reliable for the dry silica gel, because in this kind of sample, possible trace amounts of water have been removed. Otherwise the freezing of this residual water may affect the optical properties of silica gel at low temperatures. Further studies with this technique will be helpful in establishing a standard for surface fluorescence quantum yield measurements.

A reasonable level of confidence in the results reported in this work is also based on the fact that almost all quantum

yields obtained with the two primary methods studied are consistent with each other within a reasonable error; and their magnitudes are also reasonable compared with the literature data for the same compound in solution (see Table 9.5). A general trend is that, from solutions to wet silica gel surfaces, the fluorescence quantum yields of these PAHs tend to drop by 25-50%. This trend may be understood as a result of increased non-radiative decay rates, promoted by the strong interaction between these PAH molecules and the surface. More discussion will be given in the next two chapters.

The existing errors are considered to come mainly from the following sources:

(A) The assumed identity of spatial distributions of scattered and emitted light is but a rough approximation. For this approximation to be valid, either an even illumination of the front surface of the sample cuvette, or a very small fraction of absorbtion, is required. But these conditions are not readily achieved with the present instrumentation. For example, the relative absorption was determined by two measurements, using diffusely reflected light: one with a blank, another with a loaded silica gel sample. The instability of the light source and the scanning system would impose about ±2% of error on each measurement. If we require the fraction of absorbed light to be lower

than ±9%, then the calculated percentage absorption will contain an error of ±40%. This situation has forced us to conduct the quantum yield measurements at an absorption level above 30%, at the cost of a larger discrepancy in the spatial distributions of scattered and emitted light.

More uniform illumination of the cuvette surface could be achieved by dispersing the excitation beam with lenses or by placing a diffuser in front of the sample. This technique will, presumably, suppress the discrepancy between the spatial distributions of scattered and emitted light. More experiments are needed to control fully these factors.

(B) The imperfect reflection of the aluminum mirror is another source of systematic errors. Presumably, the sign of the error from this source can be determined by comparing the results of measurements with and without the back mirror. A quantitative study of the reflection properties of the polished aluminum surface would be significant.

(C) Because of multiple scattering of the emitted light in the medium, reabsorption of the fluorescence light is expected to be severe in silica gel powders. For perylene the error due to reabsorption was estimated to be -7%. This correction was not made in the present study. This problem, as well as some other experimental pitfalls such as polarization effects, needs further investigation.

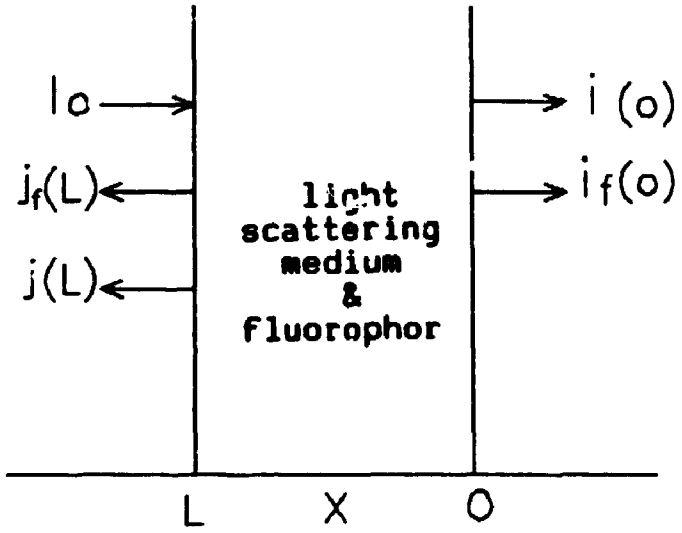

Fig. 9.1 A schematic diagram showing the basic idea of Seely's approach. L and 0 represent the left and right surfaces of the medium respectively. I_0, the incident light intensity on the left surface; j(L), back-scattered light intensity on the left surface; i(0), transmitted light intensity on the right surface; $j_f(L)$, fluorescence light intensity toward the left; $i_f(0)$, fluorescence light intensity toward the right.

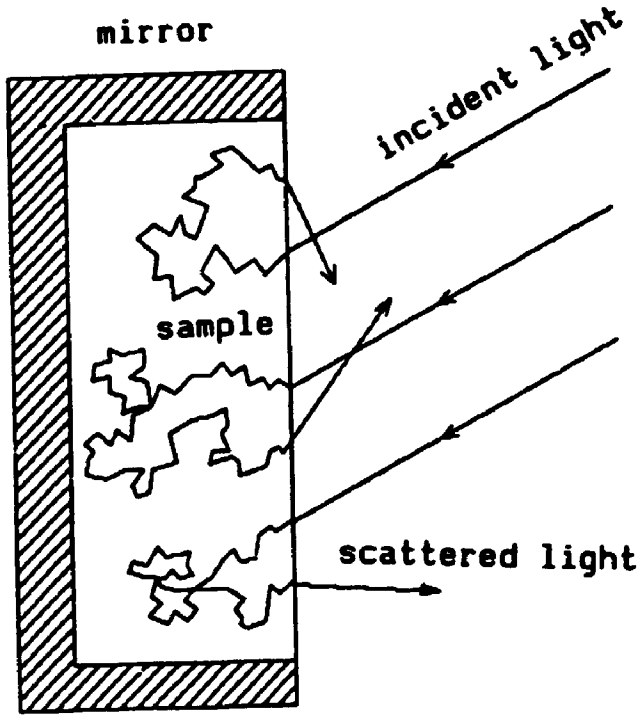

Fig. 9.2 A schematic diagram of a sample cuvette with a back-up mirror, showing the diffuse reflectance of incident light from the sample.

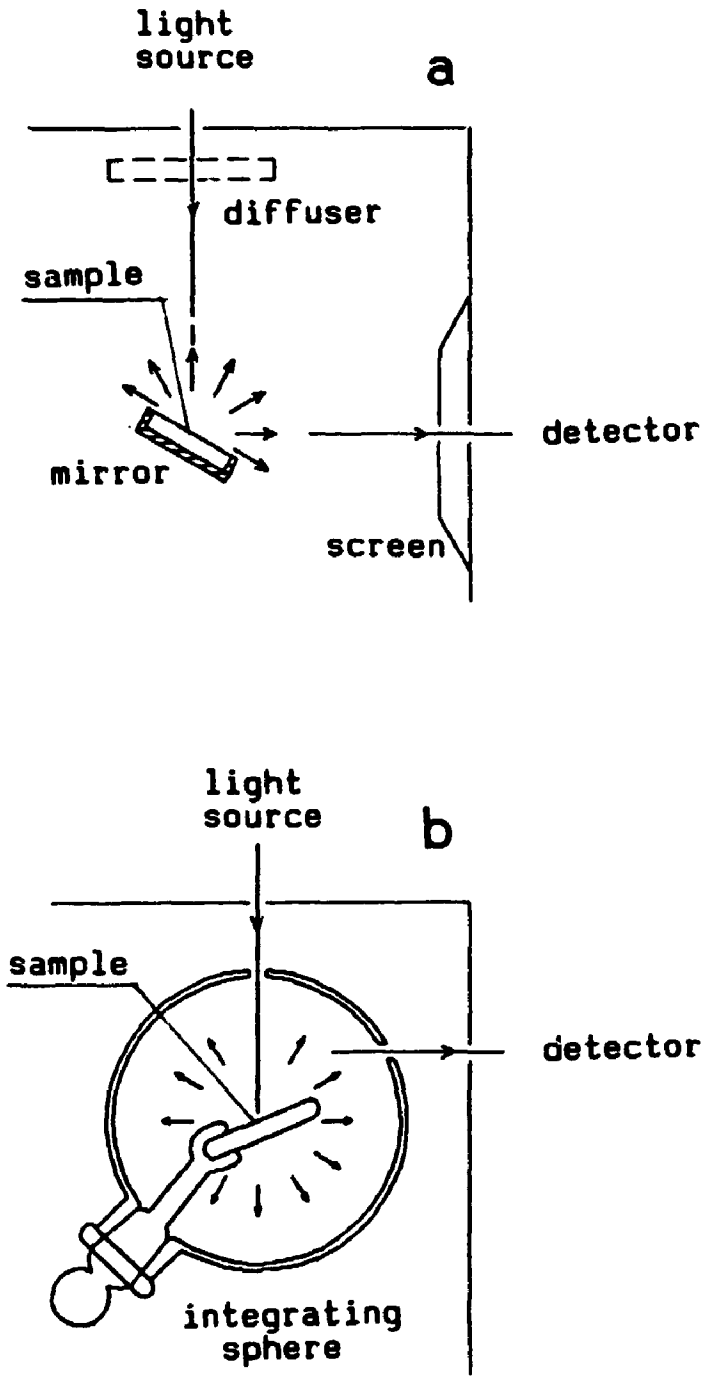

Fig. 9.3 A schematic diagram showing the experimental set-up for fluorescence quantum yield measurements with the primary methods: (a) the method based on diffuse reflectance, using a mirror-backed sample cuvette; (b) the method based on an integrating sphere.

Fig. 9.4 The procedure for fluorescence quantum yield measurements with a secondary method: (a) the absorption spectra of a chrysene sample and a benzoperylene sample (292 nm is selected as the excitation wavelength because at this wavelength the two samples are very close in their absorption); (b) the corrected emission spectra from these two samples, at 292 nm excitation.

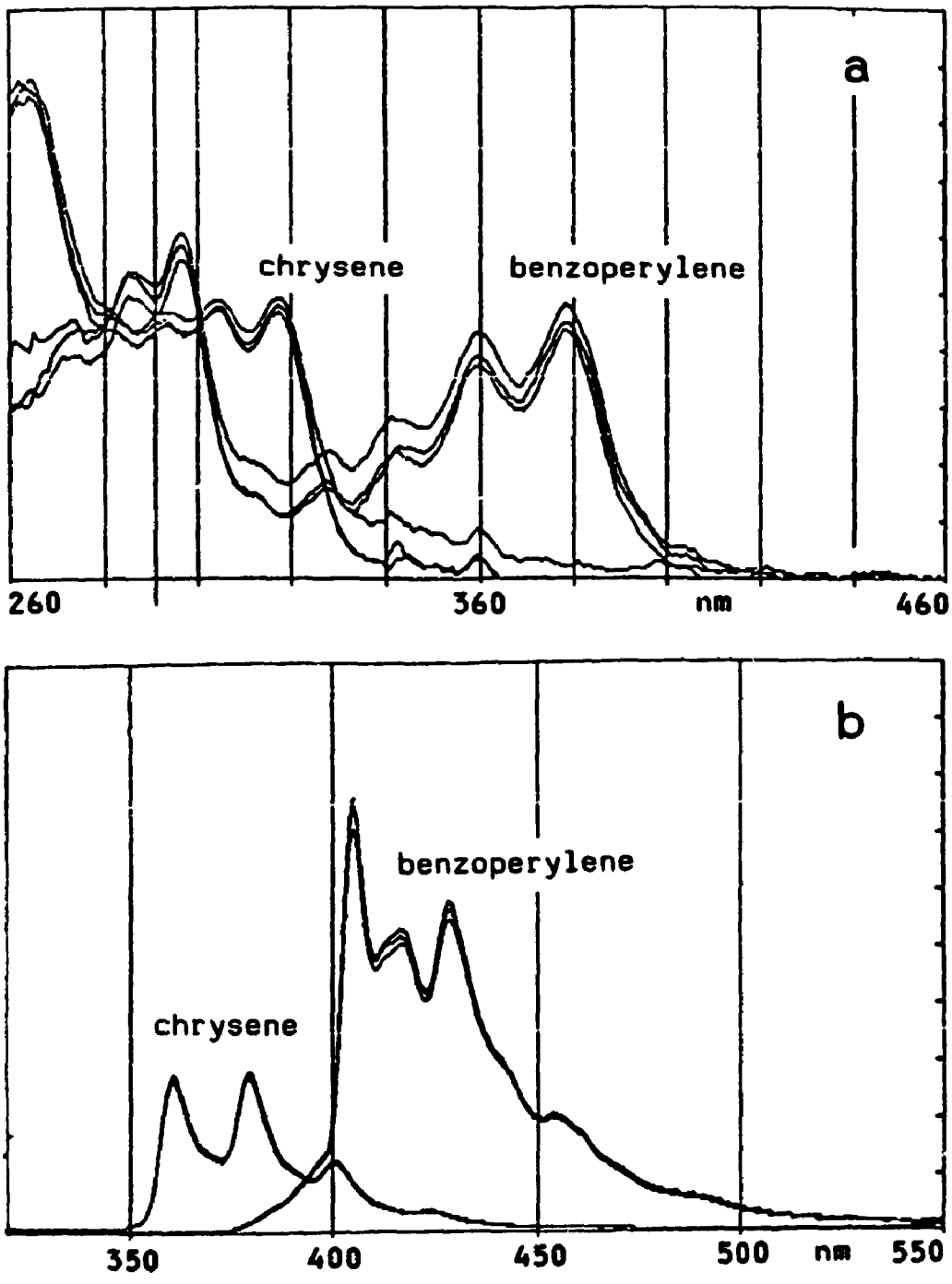
a
chrysene
benzoperylene
260
360
nm
460
b
benzoperylene
chrysene
350
400
450
500
nm
550

CHAPTER 10 ESTIMATION OF RADIATIVE DECAY RATES FROM QUANTUM YIELDS AND LIFETIME DISTRIBUTIONS

10.1 INTRODUCTION

In a homogeneous system, the decay mechanism of excited molecules is studied by measuring the fluorescence lifetimes and the quantum yields. Then, by using the equation

$$\phi = \frac{k_{FM}}{k} \tag{10.1}$$

where the ϕ is the fluorescence quantum yield, k is the total decay rate constant, and k_{FM} is the radiative decay rate constant, both the radiative and non-radiative decay rate constants may be obtained. This equation is implied in the definition of the fluorescence quantum yield, that is, the ratio of the number of fluorescence photons emitted after the excitation, to the total number of photons absorbed. Because the decay of a population of excited molecules follows first order kinetics, the rate of emission of fluorescence photons is $k_{FM}m^*$, and the rate of photon absorption, in the steady state, is km^*, where m^* is a steady state population of excited molecules. This definition may, thus, be expressed as equation (10.2):

$$\phi = \frac{k_{FM}\, m^*}{k\, m^*} \qquad (10.2)$$

Here the m^* can be cancelled, hence equation (10.1) is obtained.

When the molecules under investigation are adsorbed on a surface, however, this type of fundamental study becomes much more complicated. The problem lies not only in the difficulties in the experimental measurement of the quantum yield, but also in the dispersed feature of the decay kinetics. Both the decay rate and the excited molecule population become distribution functions of μ, the molecular state. In these circumstances, the fluorescence quantum yield may then be expressed, in the discrete case, as equation (10.3):

$$\phi = \frac{\sum_{\mu} k_{FM}(\mu)\; m^*(\mu)}{\sum_{\mu} k(\mu)\; m^*(\mu)} \qquad (10.3)$$

Here the excited molecule population distribution $m^*(\mu)$ cannot be eliminated from the equation, as has been possible in equation (10.2). What is required, then, is to derive an expression for $m^*(\mu)$, in terms of some measurable function. Then $k_{FM}(\mu)$ can be derived.

10.2 DERIVATION OF THE BASIC EQUATION

For a dispersed photophysical system, we introduce the following assumptions. (a) The total fluorescence intensity is a function of the available molecular states, and the elapsed time t after the excitation. (b) The molecular states can be described [171] by a variable μ, so that we can write the total fluorescence intensity as $j'(\mu,t)$. (c) We restrict our interest to systems in which the time dependent part, in the fluorescence intensity function $j'(\mu,t)$, has the form e^{-kt}. That is

$$j'(\mu,t) = j(\mu)\ e^{-kt} \tag{10.4}$$

where k is the total decay rate constant. (d) For each molecular state, μ, the corresponding molecular population, radiative decay rate constant and non-radiative decay rate constant are $m^*(\mu)$, $k_{FM}(\mu)$ and $k_{IM}(\mu)$ respectively.

On physical grounds, the molecular state, μ, is a "natural" independent variable, because the photophysical behaviour of the system under investigation is ultimately determined by the distribution of the molecular populations in different states. In practice, however, the fundamental and measurable variable is the total decay rate, $k(\mu)$, defined by equation (10.5)

$$\kappa(\mu) = k_{FM}(\mu) + k_{IM}(\mu) \tag{10.5}$$

We are forced, therefore, to make an unfavourable variable change of $\mu = \mu(k)$. Equation (10.4) becomes equation (10.6)

$$i'(k,t) = i(k)\ e^{-kt} \tag{10.6}$$

Integration over all possible k, $k \in (a,b)$, yields

$$I(t) = \int_a^b i(k)\ e^{-kt}\ dk \tag{10.7}$$

where $a > 0$, $b < \infty$. I(t) is a measurable function, the total fluorescence intensity as a function of the time elapsed after the excitation impulse. This equation is normally employed as the definition [31] of "decay rate distribution".

Substituting $t = 0$ into equation (10.6), we get

$$i(k) = i'(k,0) \tag{10.8}$$

This states that i(k) is the fluorescence intensity as a function of k at $t = 0$, the moment when the impulse excitation is applied. This function is sometimes called the "decay rate distribution", but the more exact term is, perhaps, the rather cumbersome "initial fluorescence

intensity distribution in k domain".

On the other hand, integration of equation (10.6) over t yields the total fluorescence photon flux in the steady state as a function of k, designated as P(k). That is, the photon population emitted at a decay rate k in steady-state:

$$(10.9) \qquad P(k) = \int_a^b i(k)\ e^{-kt}\ dt = \frac{i(k)}{k}$$

Therefore, the steady state molecular population distribution may be expressed by equation

$$(10.10) \qquad m^*(k) = \frac{P(k)}{k_{FM}(k)} = \frac{i(k)}{k_{FM}(k)\ k}$$

As discussed before, the overall quantum yield, which is normally measured under steady state conditions, may be represented in terms of continuous functions by equation

$$(10.11) \qquad \phi = \frac{\int_a^b k_{FM}(k)\ m^*(k)\ dk}{\int_a^b k\ m^*(k)\ dk}$$

In case the molecular state is unique, this equation reduces to equation (10.1).

Substituting the expression for $m^*(k)$, given in equation (10.10), into (10.11), we obtain equation (10.12) that relates the unknown function $k_{FM}(k)$ to the measurable variables or distributions:

$$(10.12) \qquad \phi = \frac{\int_a^b \frac{i(k)}{k}\,dk}{\int_a^b \frac{i(k)}{k_{FM}(k)}\,dk} = \frac{\bar{\tau}(k)}{\bar{\tau}^o(k)}$$

where $\tau(k) = 1/k$, $\tau^o(k) = 1/k_{FM}(k)$, and the bar means average over $i(k)$. This can be considered as the basic equation for dispersed photophysics corresponding to equation (10.1) for non-dispersed systems. The physical interpretation of this equation is that, when the "initial intensity distribution in k domain" (decay rate distribution) is available, the quantum yield is expressed as the ratio of the average $\tau(k)$ and average $\tau^o(k)$, both weighted by the k distribution.

Equation (10.12) may be rearranged to

$$(10.13) \qquad \int_a^b \frac{i(k)}{k_{FM}(k)}\,dk = \frac{\int_a^b \frac{i(k)}{k}\,dk}{\phi}$$

In a simple case when $k_{FM}(k)$ can be assumed to be a constant, we have

$$(10.14) \qquad \phi = k_{FM} \frac{\int_a^b \frac{i(k)}{k}\, dk}{\int_a^b i(k)\, dk} = k_{FM}\, \bar{\tau}$$

This equation implies that in the case when the dispersion is determined by the non-radiative decay rate only, then the average lifetime, τ (= 1/k), weighted by the initial intensity distribution in k domain (decay rate distribution), should replace the τ (or 1/k) in equation (10.1).

If $k_{FM}(k)$ is not a constant, it is still possible, in principle, to obtain a numerical solution for the only unknown function $k_{FM}(k)$ in (10.13). Thus we may modify the environment of the fluorescent molecules to produce different molecular population distributions, which should lead to different (overall) quantum yields, ϕ, and different decay rate distributions, i(k). Suppose we do so and get a set of n ϕ and n i(k)'s for n different molecular population distributions, designated by j = 1, 2, ····· n. We now have n equations like (10.13). To seek a numerical solution, the integrals in these equations are made discrete (into n components) and the system of these equations is then replaced by an n x n finite linear system. That is

$$(10.15)\qquad \sum_{i=1}^{n} I_j(k_i)\left[\frac{1}{k_{FM}(k_i)}\right] = \frac{\sum_{i=1}^{n} \frac{I_j(k_i)}{k_i}}{\phi_j}$$

where j takes 1, 2, ..., n. In principle, this system of equations can be solved for the k_{FM}'s.

In practice, however, the fluorescence quantum yield is generally very difficult to determine, and this is especially so for turbid materials such as silica gel. It is difficult, therefore, to recover $k_{FM}(k)$ with the n large.

10.3 RADIATIVE AND NON-RADIATIVE DECAY RATES OF PYRENE ADSORBED ON THE TWO TYPES OF SURFACE SITES

In Chapter 6 and Chapter 7, we have shown that the lifetimes of the PAHs studied in this work may be described by bimodal distributions. As a first approximation, we assume the $k_{FM}(k)$'s within each model (peak) are constant, designated as $k_{FM}(1)$ and $k_{FM}(2)$ respectively. Under these conditions, equation (10.13) may be rewritten as equation

$$(10.16)\qquad \frac{\text{Integral}(1)}{k_{FM}(1)} + \frac{\text{Integral}(2)}{k_{FM}(2)} = \frac{\text{Integral}(3)}{\phi}$$

where, $\text{Integral}(1) = \int_a^c i(k)\,dk,$

$$\text{Integral}(2) = \int_c^b i(k)\, dk,$$

$$\text{Integral}(3) = \int_a^b \frac{i(k)}{k}\, dk,$$

where c is the point on the k axis at which the two models or peaks are separated, or the k value where the distribution function is the minimum between the two peaks. An example of the selection of a, b, and c is shown in Fig. 10.3 b.

In order to test this approach, the lifetime distribution and fluorescence quantum yield data, obtained in the dehydroxylation experiments discussed previously, were reviewed. These results were substituted into equation (10.16), so that several equations in two unknowns were obtained. Solving any pair taken out of these equations would yield a set of $k_{FM}(1)$ and $k_{FM}(2)$. It should be mentioned that to determine a set of solutions for $k_{FM}(1)$ and $k_{FM}(2)$, only two samples, prepared under two different conditions, were necessary. The data derived from additional samples were calculated and compared, however, to test for possible deviations.

These tests, if they can lead to reasonable and self-consistent radiative decay rates, may also enhance our

confidence in the measured quantum yields. As already discussed in Chapter 9, because of the absence of standard quantum yield data for PAHs adsorbed on silica gel surfaces in the literature, we are not able to justify these results on a very solid basis. Use of these results to deduce some otherwise unknown properties of the system is, therefore, an acceptable way to check the "compatibility" of these results with other information from other sources.

For this purpose, the required initial intensity distribution in k domain (decay rate distribution) may be directly recovered, or may be obtained by converting the corresponding lifetime distribution into the k domain. In the following calculations, the latter method has been used. In Figs.10.1 (a) - (e), are shown the results of the five dehydroxylation experiments discussed in Chapter 6. These decay rate distributions are converted from the lifetime distributions shown in Fig. 6.3. In these experiments the silica gel was preheated in vacuum at 25, 200, 400, 600, and 800°C (see Chapter 6). The fluorescence quantum yields were measured using the integrating sphere method (see Sec.9.4 in Chapter 9). The quantum yields, obtained from the samples preheated at 25, 200, 400, 600, and 800°C, are 0.37, 0.25, 0.17, 0.096, and 0.084 respectively. The calculated three integrals and the corresponding quantum yields are substituted into equation (10.16). This yields the following five equations:

$$(25^{\circ}C) \quad 0.0074566\ \tau^{\circ}(1) + 0.0002413\ \tau^{\circ}(2) = \frac{1.45832}{0.37}$$

$$(200^{\circ}C) \quad 0.0027726\ \tau^{\circ}(1) + 0.0030539\ \tau^{\circ}(2) = \frac{0.61202}{0.25}$$

$$(400^{\circ}C) \quad 0.0017652\ \tau^{\circ}(1) + 0.0048571\ \tau^{\circ}(2) = \frac{0.45749}{0.17}$$

$$(600^{\circ}C) \quad 0.0015227\ \tau^{\circ}(1) + 0.0077351\ \tau^{\circ}(2) = \frac{0.45717}{0.096}$$

$$(800^{\circ}C) \quad 0.0006133\ \tau^{\circ}(1) + 0.0089830\ \tau^{\circ}(2) = \frac{0.29316}{0.084}$$

where the $\tau^{\circ}(1) = 1/k_{FM}(1)$ and $\tau^{\circ}(2) = 1/k_{FM}(2)$ are the natural lifetimes of pyrene on the wet (long lifetime peak) and the dry (short lifetime peak) silica gel. The results of solving the different combinations of two of the above equations are listed in Table 10.1.

In Table 10.1, it can be seen that most of the results are self-consistent, except those marked with * in which the 600°C preheated sample is involved. The discrepancy of the results derived from the 600°C sample is probably caused by a big error in the estimated quantum yield. The averages marked with *, given at the bottom of the table, were calculated with the 600°C preheated sample disregarded; and they were believed more reliable than the overall averages.

If the poor precision of the estimated quantum yields is taken into account, these results should be considered surprisingly good, in the sense that four out of five experiments are consistent.

Table 10.1 Calculated natural lifetimes of pyrene on the wet and dry silica gel

Combinations	$\tau^{\circ}(1)$ ns	$\tau^{\circ}(2)$ ns
25 & 200	518	332
25 & 400	517	366
25 & 600*	512	515
25 & 800	517	353
200 & 400	455	389
200 & 600*	262	564
200 & 800	492	355
400 & 600*	-370	689
400 & 800	561	350
600 & 800*	1766	267
average	523 ± 518	418 ± 129
average*	503 ± 42	357 ± 19

It should be mentioned that, in the course of this work, the fluorescence decay data and the quantum yield data treated here were obtained long before the SMM program and the mathematical manipulation used in this chapter were developed. These calculations should be considered as a bias-free test of the validity of all the techniques involved in this work. We do not intend to claim these measured and derived data as established, standard data; instead, we suggest that there is a consistent approach, based on lifetime distribution analysis, by which one may

carry out a systematic photophysical study of PAHs adsorbed on silica gel surfaces, and perhaps of many other heterogeneous systems. Needless to say, more extensive experimental studies are required.

The corresponding radiative decay rates of pyrene, derived from the averages, together with the calculated total decay rates as well as the non-radiative decay rates, are listed in Table 10.2. Included is a comparison with data from the literature for pyrene in various solvents [130].

Table 10.2 Comparison of radiative and non-radiative decay rates of pyrene obtained in this work and the literature data

Environment	Decay rate ($10^6 s^{-1}$) k	k_{FM}	k_{IM}	Ref.
cyclohexane	2.20	1.45	0.75	[130]
	2.33	1.51	0.82	[115]
2-propanol	2.59	1.68	0.91	[115]
ethanol	2.06	1.36	0.7	[130]
	2.68	1.93	0.75	[115]
acetonitrile	2.94	2.06	0.88	[115]
dimethylformamide	3.57	2.50	1.07	[115]
silica gel (wet)	5.1	1.99	3.11	
silica gel (dry)	46.1	2.80	43.3	

Ware and coworkers [115] have shown that the radiative decay rates of pyrene increase with the increase of solvent polarity. The above results are, therefore, quite reasonable, provided that we assume the functional groups on

silica gel surface are strongly polar. A remarkable feature of the photophysical behaviour of pyrene on silica gel surfaces is that the non-radiative decay rate drastically increases from solution to wet surface, and more so from wet surface to dry surface. In comparison, in solvents the non-radiative decay rate does not change very much from non-polar to polar solvents. This may be interpreted as an indication that, besides a polar micro-environment effect similar to that provided by a polar solvent, some kind of specific interaction between PAH molecules and some surface functional groups takes place as well.

These results show also that the dramatic change of total decay rate k is mostly caused by the non-radiative decay pathway. From wet surface to dry surface, the radiative decay rate k_{FM} increases by a factor of 1.5 while the total decay rate k increases by a factor of 9. This provides a reasonable level of justification for the original assumption, made for equation (10.16), where $k_{FM}(k)$ is approximated by a constant $k_{FM}(n)$, n = 1 or 2, within each peak.

10.4 RADIATIVE AND NON-RADIATIVE DECAY RATES OF THE OTHER PAHS ADSORBED ON THE TWO TYPES OF SURFACE SITES

To test this approach further, we calculated the radiative and non-radiative decay rates for the other five PAHs, using

the same bimodal approximation. The method of these calculations was the same as that for pyrene, but was based on two samples with silica gel preheated at 25°C (wet surface) and 800°C (dry surface) for each PAH. The decay rate distributions are shown in Figs. 10.2-6. The derived results are listed in Table 10.3 in comparison with corresponding data in various solvents.

Table 10.3 Comparison of radiative and non-radiative decay rates of PAHs

PAH	Environment	k	k_{FM}	k_{IM}	Ref.
phenanthrene	cyclohexane		3.9		[130]
	heptane	16.8	2.7	14.1	[130]
	isobutanol	15.8	3.3	12.5	[130]
	cyclohexanol	16.5	4.0	12.5	[130]
	silica gel(w)	24.9	2.63	22.3	
	silica gel(d)	145.1	6.53	138.6	
chrysene	cyclohexane	22.4	2.61	19.8	[130]
	silica gel(w)	34.4	3.47	30.9	
	silica gel(d)	147.5	8.77	138.7	
benzoperylene	polymethyl methacrylate	4.08	1.53	2.55	[172]
	silica gel(w)	9.57	2.62	6.95	
	silica gel(d)	49.0	12.7	36.3	
coronene	polymethyl methacrylate	3.12	0.84	2.28	[172]
	silica gel(w)	5.03	0.78	4.25	
	silica gel(d)	26.6	1.09	25.5	
perylene	ethanol	167	145	21.7	[130]
	benzene	202	180	22.4	[130]
	silica gel(w)	126	89	37	
	silica gel(d)	101	76.9	24.5	

The results in this Table may contain large errors, because both the lifetime distribution analysis and the quantum yield measurement suffer from the problem of instability. Some common trends, however, are still noticeable and they may be interpreted in terms of our existing knowledge. These trends are the following.

(A) The effect of the wet and the dry surface, on the radiative and non-radiative decay rates of the PAHs, may again be grouped in terms of the lowest excited singlet state of the PAH. This is similar to what has been noted in lifetime distribution analysis (see Chapter 7), but here we are able to discuss radiative and non-radiative decay rates separately.

(B) The radiative decay rates of ^1L_b type PAHs adsorbed on the wet surface are similar to the same compound in a strongly polar solvents. On the dry surface, the radiative decay rates of these PAHs become much higher, but are still of the same order of magnitude as those in polar solvents.

(C) The non-radiative decay rates of the ^1L_b type adsorbed PAHs are more sensitive to the state of the surface, compared with the corresponding radiative decay rates. It can be seen that, on the wet silica gel surface, the non-radiative decay rates of these PAHs are generally higher than those in polar solvents, and on the dry surface they

further increase by about one order of magnitude.

(D) Based on the calculations in this chapter, it is found that the observed modification of lifetime distributions derived from variously dehydroxylated silica gel surfaces (discussed in Chapter 6 and 7) is mainly contributed by non-radiative decay pathways.

Ware's data [115] have showed that the non-radiative decay rate of pyrene is only slightly affected by the solvent polarity. These decay rate data, therefore, suggest again that there should be a second reason, presumably a specific interaction, between some surface groups and the PAH molecules, which is responsible for the dramatic increase of the non-radiative decay rate of these PAHs on the surface, especially on the dry surface.

(E) The only exception is perylene. We have discussed earlier that its special behaviour may be related to its special lowest excited singlet state (compared with those of the other five PAHs), the ^1L_a state. Its radiative decay rate seems to decrease on silica gel surfaces, especially on dry surfaces. Its non-radiative decay rate on silica gel surfaces is higher than that in solvents. Because only one PAH of this type is studied in this work, we are not able to discuss any "trend". Evidently the behaviour of this type of PAH needs further investigation.

10.5 SUMMARY

In summary, the decay rate data obtained above suggest that, on both wet and dry silica gel surfaces, the adsorbed PAHs experience a strongly polar environment effect. This polar environment effect, however, is not sufficient to account for all the decay rate data, and especially for the non-radiative decay. We have to conclude, therefore, that there is another effect, and that this effect is specific to the silica gel surface in comparison with that found in solution, and is dominant on the dry silica gel surface. This effect causes a drastic increase of non-radiative decay rate in the ^1L_b type PAHs.

It is impressive, at this point, to review some emission spectra presented in Chapter 8. An interesting example is pyrene. We have seen in Fig. 8.11 and in Fig. 8.4 (a) that the fluorescence emission spectrum of pyrene on the wet silica gel is very similar to that of pyrene in water and methanol, but on the dry surface the pyrene fluorescence spectrum loses all detail and is very similar to that of the protonated aminopyrene on the wet silica gel surface. These spectra also suggest that the wet surface provides a polar environment to PAH molecules, but the dry surface is more likely to form surface complexes with these PAH molecules. We will further discuss this in the following chapter.

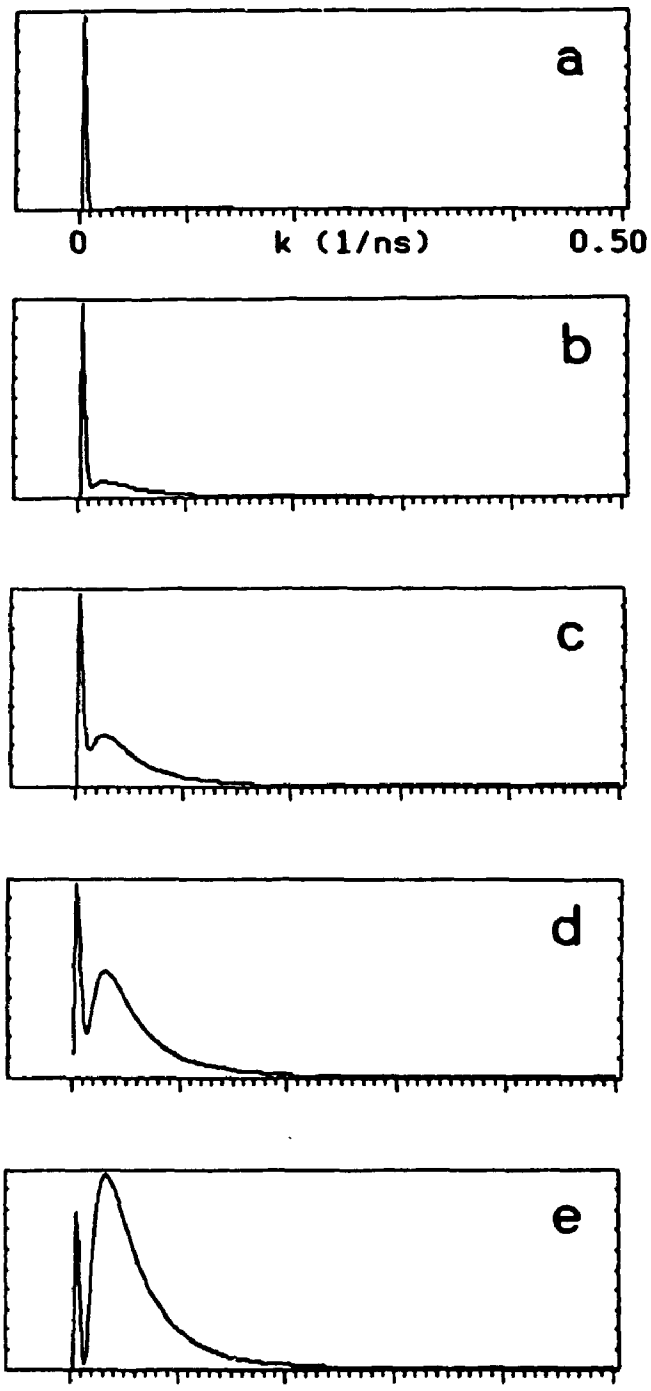

Fig. 10.1 The decay rate(k) distributions of pyrene adsorbed on variously dehydroxylated silica gel surfaces. These k-distributions were converted from the corresponding lifetime distributions shown in Fig.6.3 of Chapter 6.

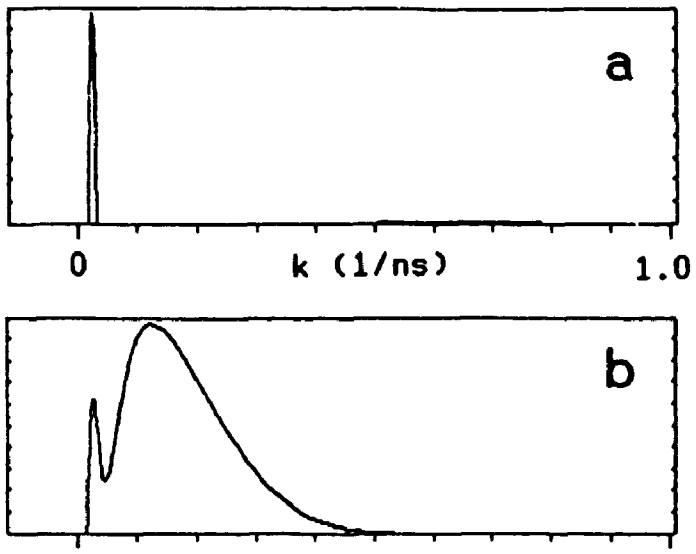

Fig. 10.2 The decay rate distributions of phenanthrene adsorbed on wet and dry silica gel surfaces. These k-distributions were converted from the lifetime distributions shown in Fig.7.2 of Chapter 7.

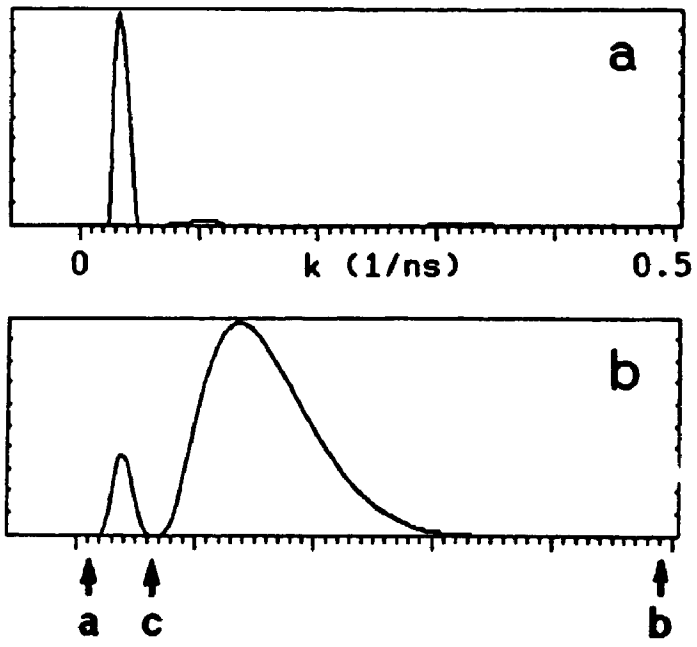

Fig. 10.3 The decay rate distributions of chrysene adsorbed on wet and dry silica gel surfaces. These k-distributions were converted from the lifetime distributions shown in Fig.7.3 of Chapter 7.

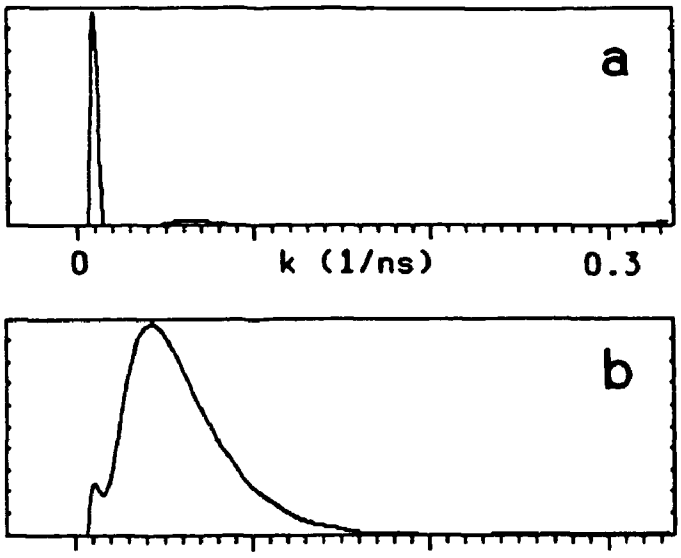

Fig. 10.4 The decay rate distributions of benzoperylene adsorbed on wet and dry silica gel surfaces. These k-distributions were converted from the lifetime distributions shown in Fig.7.4 of Chapter 7.

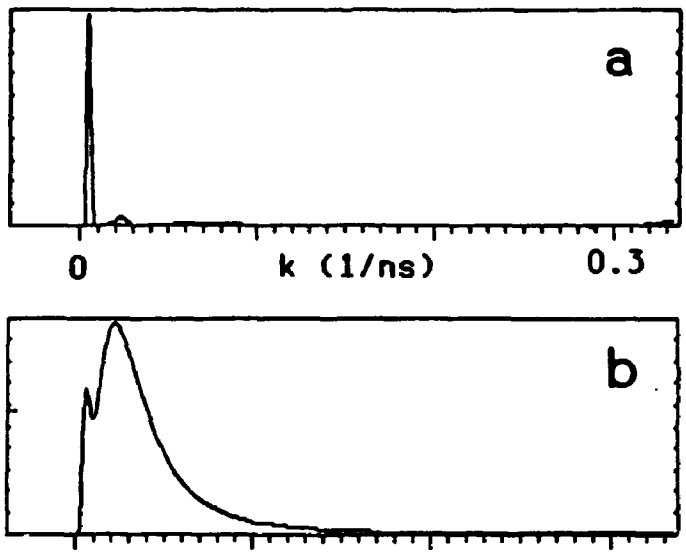

Fig. 10.5 The decay rate distributions of coronene adsorbed on wet and dry silica gel surfaces. These k-distributions were converted from the lifetime distributions shown in Fig.7.5 of Chapter 7.

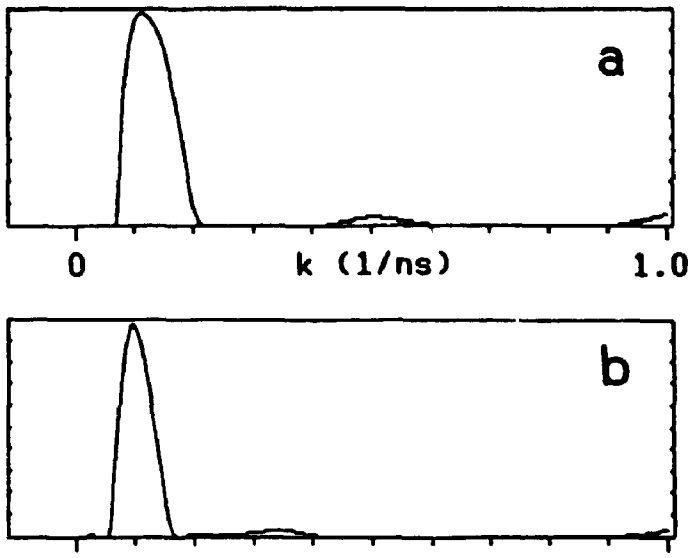

Fig. 10.6 The decay rate distributions of perylene adsorbed on wet and dry silica gel surfaces. These k-distributions were converted from the lifetime distributions shown in Fig.7.6 Chapter 7.

CHAPTER 11 PHOTOPHYSICS OF PAHS ADSORBED ON SILICA GEL SURFACES: CONCLUSION AND DISCUSSION

11.1 PHOTOPHYSICAL STUDIES OF FLUORESCENT MOLECULES ADSORBED ON SILICA GEL SURFACES: THE LIFETIME DISTRIBUTION APPROACH

(A) This thesis describes a systematic photophysical study of PAHs adsorbed on silica gel surfaces, using a novel approach in which lifetimes are treated as distributions. Such an approach, to the author's knowledge, is investigated and reported here for the first time.

(B) The theoretical basis of lifetime distribution analysis has been discussed in this thesis. The principles of this analysis are addressed in terms of the theory of the Fredholm integral equation of the first kind, and the theory of inverse problems.

(C) The ill conditioned nature of lifetime distribution analysis has been demonstrated and discussed, using extensive simulated and real surface fluorescence data. The conclusion is that a regularization technique must be employed to obtain stable solutions. Such regularized, stable solutions reveal the principal information content carried by the data, and are required by physical determinacy of the physical system studied.

(D) A lifetime distribution analysis program, based on the Marquardt algorithm and Phillips' smoothing technique, has been developed in this work, with fair success in dealing with the decay data obtained from the PAH-silica gel system.

(E) The techniques of fluorescence quantum yield determination for PAHs adsorbed on silica gel surfaces have been investigated. A novel technique, based on the diffuse reflectance of a mirror-backed sample cuvette, has been demonstrated. An integrating sphere technique, and a relative quantum yield measurement technique, were also studied. The results from all three of these approaches appear to be consistent with each other, and they seem to be reasonable, compared with the corresponding literature values for the PAHs in solution.

(F) The mathematics for the manipulation of the lifetime distribution data and the fluorescence quantum yield data, to deduce the radiative and non-radiative decay rates, has been developed.

(G) The lifetime distributions, absorption and emission spectra, and fluorescence quantum yields of six PAHs adsorbed on hydroxylated (wet) and highly dehydroxylated (dry) silica gel surfaces have been measured. Most of these data, to the author's knowledge, are reported for the first time.

(H) It has been found in this work that the photophysical behaviour of the PAHs may be correlated with the symmetry of the lowest excited singlet state of the adsorbed PAH. Remarkable photophysical effects have been observed for those PAHs whose lowest excited singlet states are of the ^1L_b type, or in other words, whose $S_1 - S_0$ transitions are forbidden; but not for the PAH whose lowest excited singlet state is of the ^1L_a type.

(I) The observed photophysical behaviour may be rationalized with a model as follows.

The (mutually) hydrogen bonded surface OH groups, dominant on the wet surface, provide to adsorbed PAH molecules a polar environment which is similar to that provided by a polar solvent. The interaction between an adsorbed PAH molecule and hydrogen bonded OH groups appears to be of a dipole-induced-dipole nature. The isolated surface OH groups, present in a large number on the dry surface, seem to form complexes with adsorbed PAH molecules. The interaction is considered to be a specific interaction, presumably of a hydrogen bonding (between the PAH molecule and the isolated OH groups) nature.

On a silica gel surface, there are normally both hydrogen-bonded hydroxyl groups and isolated hydroxyl groups. A small number of PAH molecules may be distributed on the two types

of surface sites, and reach an equilibrium represented by the following equation

(11.1) $$(-OH) + (-OH)_n \cdots PAH \rightleftharpoons (-OH) \cdot PAH + (-OH)_n$$

where (-OH) is an isolated hydroxyl group and $(-OH)_n$ are hydrogen bonded hydroxyl groups; "$\cdots$" denotes a dipole-induced-dipole interaction; and "$\cdot$" denotes a specific interaction. The dehydroxylation process modifies the relative populations of (-OH) and $(-OH)_n$, and therefore shifts the equilibrium.

A determination of the equilibrium constant for this reaction is possible, based on the techniques developed in this thesis. For this purpose, we have to derive the population distribution of $(-OH)_n \cdots PAH$ and $(-OH) \cdot PAH$. This is possible, because we know how to get the lifetime distributions, and how to get radiative decay rates related to these distributions. On the other hand, by using well-developed techniques, such as that used by Voort and coworkers [92] (see Chapter 5), we may determine the total population distributions of (-OH) and $(-OH)_n$ for blank silica gel samples. Therefore, in principle, the surface concentrations of all four species involved in equation (11.1) may be determined. The equilibrium constant is then calculated by equation 11.2.

$$(11.2) \qquad K = \frac{[(-OH)_n]\ [(-OH)\cdot PAH]}{[(-OH)_n\cdots PAH]\ [(-OH)]}$$

11.2 THE PHOTOPHYSICS OF PAHS ADSORBED ON SILICA GEL SURFACES

The proposed model in (I) of the last section is based on the following observations.

(J) Lifetime distribution analysis gives a bimodal distribution for all studied PAHs of the ^1L_b type, adsorbed on silica gel surfaces. Two types of surface sites and two types of interaction are, therefore, assumed.

The bimodal lifetime distribution is in good accord with the IR spectra of silica gel surfaces, in which two peaks can also be distinguished (see section 5.1 in Chapter 5). The parallel behaviour of the two peaks in the lifetime distribution (see Chapters 6, 7, 10) and the two bands in the IR spectra of silica gel (see Chapter 5), in dehydroxylation experiments, suggests that the bimodal lifetime distribution and the two bands in IR spectra may have a common origin. If this is the case, we can then assign the short lifetime peak to the PAH molecules adsorbed on isolated silanol groups, because on 800°C preheated silica gel, the majority of hydroxyl groups become isolated, as indicated by the IR studies. If this short lifetime peak

is so assigned, then the long lifetime peak should be correspondingly assigned to the PAH molecules adsorbed on hydrogen bonded OH groups.

(K) The emission spectra of these PAHs on the wet surface show the typical Ham effect, and resemble those of the same PAH in polar solvents. Also the calculated radiative and non-radiative decay rates for these PAHs on the wet surface is of the same order of magnitude as those of the same PAH in polar solvents. The similarity of the wet surface to polar solvents is, therefore, assumed.

(L) The emission spectra of these PAHs on the dry surface show a dramatic change compared with that of the same PAH on the wet surface and in polar solvents. This change (loss of fine structure in the spectra of pyrene, benzoperylene, and coronene) seems not interpretable simply on the basis of a polar environment effect.

(M) On the other hand, the calculated non-radiative decay rates for the PAHs adsorbed on the dry surface are too high to be simply accounted for in terms of a polar environment effect. In conjunction with the observation (L), the formation of a surface complex is, therefore, considered to be a possible interpretation.

Evidence is available in the literature that an isolated OH

group can, indeed, complex with aromatic hydrocarbons through their π system. Nakajima [143,173], when observing the Ham effect of pyrene as a function of solvent polarity, noted that the intensity of the forbidden 0-0 band showed a relatively rapid increase on addition of a small amount of a polar solvent such as an alcohol to a non-polar solution, suggesting the importance of some specific interaction. Lianos and Georghiou [118,119] observed, using IR spectroscopy, 1:1 complex formation between alcohols and pyrene and 1-methylpyrene, in a 0.02M solution of alcohol in CCl_4. They found a much shortened lifetime component which was then assigned to the complex. In the last decade, the formation of complexes of aromatics with molecules that have hydrogen-bonding capabilities has been the subject of numerous experimental and theoretical studies. The existence of such complexes has been confirmed by X-ray diffraction [92], microwave spectroscopy [175,176], matrix-isolation IR spectroscopy [177], and ab initio quantum-chemical calculations [178-180].

(N) The remarkable difference between the PAHs whose lowest excited singlet states are of the ^1L_b type and of the ^1L_a type can be interpreted as follows. The $S_1 - S_0$ transition of ^1L_b type PAHs is forbidden. The interaction of the surface functional groups with the PAH molecules, whether by a dipole-induced-dipole interaction or a specific interaction, modifies the symmetry of the molecules, thus,

increasing the allowableness of this transition. This results in an increased radiative decay rate. However, the drastic increase of non-radiative decay rate has to be interpreted in terms of a specific interaction, presumably the formation of a surface complex.

REFERENCES AND FOOT NOTES

[1] J.H. deBoer, Z.Physik.Chem., **B14**, 163(1931). See review by A.Terenin, Advan.Catal. **15**, 227(1964).

[2] N.G.Yaroslavskii and A.N.Terenin, Dokl.Akad.Nauk SSSR, **66**, 885(1949). See M.L.Hair, "Infrared Spectroscopy in Surface Chemistry", Marcel Dekker, Inc., New York, 1967.

[3] G.Kortum, Trans.Faraday Soc., **58**, 1624(1962).

[4] D.Oelkrug, W.Flemming, R.Füllemann, R.Günther, W.Honnen, G.Krabichler, M.Schäfer, S.Uhl., Pur.Appl.Chem., **58**, 1207(1986).

[5] J.K.Thomas, J.Phys.Chem. **91**, 267(1987).

[6] P.de Mayo and L.J.Johnston, in "Preparative Chemistry, Using Supprorted Reagents" Academic Press, Inc., New York, 1987.

[7] K.Kalyanasundaram, "Photochemistry in Microheterogeneous Systems", Academic Press, Inc., Orlando, 1987.

[8] K.A.Zachariasse, in "Photochemistry on Solid Surfaces", Ed. M.Anpo and T.Matsuura, Elsevier, Amsterdam, 1989.

[9] R.K.Bauer, P.de Mayo, L.V.Natarajan and W.R.Ware, Can.J.Chem., **62**, 1279(1984).

[10] R.K.Bauer, P.de Mayo, W.R.Ware and K.C.Wu, J.Phys.Chem., **86**, 3781(1982).

[11] C.Francis, J.Lin and L.A.Singer, Chem.Phys.Lett. **94**, 162(1983).

[12] K.Chandrasekaran and J.K.Thomas, J.Colloid and Interface Sci., **106**, 532(1985).

[13] G.Beck and J.K.Thomas, Chem.Phys.Lett., **94**, 553(1985)

[14] X.Liu, K.-K.Lu and J.K.Thomas, J.Phys.Chem. **93**, 4120(1989).

[15] R.K.Bauer, R.Borenstein, P.de Mayo, K.Okada, M.Rafalska, W.R.Ware and K.C.Wu, J.Am.Chem.Soc., **104**, 4635(1982).

[16] P.de Mayo, L.V.Natarajan and W.R.Ware, Chem.Phys.Lett., **107**, 187(1984).

[17] P.de Mayo, L.V.Natarajan and W.R.Ware, J.Phys.Chem., **89**, 3526(1985).

[18] J.Stahlberg, M.Almgren and J.Alsins, Anal.Chem., **60**, 2487(1988).

[19] U.Even, K.Rademann, J.Jortner, N.Manor and R.Reisfeld, Phys.Rev.Lett., **52**, 2164(1984).

[20] D.Rojanski, D.Huppert, H.D.Bale, X.Dacai, P.W.Schmidt, D.Farin, A.Seri-Levy and D.Avnir, Phys.Rev.Lett., **56**, 2505(1986).

[21] D.Pines-Rojanski, D.Huppert and D.Avnir, Chem.Phys.Lett., **139**, 109(1987).

[22] D.Pines, D.Huppert and D.Avnir, J.Chem.Phys., **89**, 1177(1988).

[23] R.W.Kessler, S.Uhl, W.Honnen and D.Oelkrug, J.Luminesc., **24/25**, 551(1981).

[24] D.R.James, Y.-S.Liu, P.de Mayo and W.R.Ware, Chem.Phys.Lett., **120**, 460(1985).

[25] D.Avnir, R.Busse, M.Ottolenghi, E.Wellner and K.A.Zachariasse, J.Phys.Chem., **89**, 3521(1985).

[26] S.Uhl, G.Krabichler, K.Rempfer and D.Oelkrug, J.Mol.Struct., **143**, 279(1986).

[27] K.Hara, P.de Mayo, W.R.Ware, A.C.Weedon, G.S.K.Wong and K.C.Wu, Chem.Phys.Lett., **69**, 105(1980).

[28] T.Fujii, E.Shimizu and S.Suzuki, J.Chem.Soc., Faraday Trans. 1, **84(12)**, 4387(1988).

[29] D.R.James and W.R.Ware, Chem.Phys.Lett., **120**, 455(1985).

[30] D.R.James and W.R.Ware, Chem.Phys.Lett., **126**, 7(1986).

[31] D.R.James, Y.-S.Liu, N.O.Peterson, A.Siemiarczuk, B.D.Wagner and W.R.Ware, SPIE - The International Society for Optical Engineering, **743**, 117(1987).

[32] A.K.Livesey and J.C.Brochon, Biophys.J., **52**, 693(1987).

[33] A.Siemiarczuk, B.D.Wagner and W.R.Ware, SPIE - The International Society for Optical Engineering, **1054**, 54(1989).

[34] A.Siemiarczuk, B.D.Wagner and W.R.Ware, J.Phys.Chem., **94**, 1661(1990).

[35] J.R.Alcala, E.Gratton, and F.G.Prendergast, Biophys.J., **51**, 587(1987).

[36] J.R.Alcala, E.Gratton, and F.G.Prendergast, Biophys.J., **51**, 597(1987).

[37] J.R.Lakowicz, H.Cherekn, I.Gryczynski, N.Joshi and M.L.Johnson, Biophys.Chem., **28**, 35(1987).

[38] M.R.Eftink and C.A.Ghiron, Biophys.J., **42**, 467(1987).

[39] T.Parasassi, F.Conti, E.Gratton and O.Sapora, Biochim.Biophys.Acta, **898**, 196(1987).

[40] R.Fiorini, M.Valentino, S.Wang, M.Glaser, and E.Gratton, Biochemistry, **26**, 3864(1987).

[41] D.R.James, J.R.Turnbull, B.D.Wagner, W.R.Ware and N.O.Peterson, Biochemistry, **26**, 6272(1987).

[42] R.M.Fiorini, M.Valentino, M.Glaser, E.Gratton, and G.Curatola, Biochim.Biophys.Acta, **939**, 485(1988).

[43] B.W.Williams and C.D.Stubbs, Biochemistry, **27**, 7994(1988).

[44] R.M.Fiorini, E.Gratton, and G.Curatola, Biochim. Biophys.Acta, **1006**, 198(1989).

[45] M.L.Wratten, E.Gratton, M.van de Ven, and A.Sevanian, Biochem.Biophys.Res.Commun., **164**, 169(1989).

[46] G.Zolese, E.Gratton, and G.Curatola, Chem.Phys.Lipids, **55**, 29(1990).

[47] A.Siemiarczuk and W.R.Ware, Chem.Phys.Lett., **160**, 285(1989).

[48] A.Siemiarczuk and W.R.Ware, Chem.Phys.Lett., **167**, 263(1990).

[49] J.Huang and F.V.Bright, J.Phys.Chem., **94**, 8457(1990).

[50] F.V.Bright, G.C.Catena, and J.Huang, J.Am.Chem.Soc., **112**, 1343(1990).

[51] B.D.Wagner and W.R.Ware, J.Phys.Chem., **94**, 3489(1990).

[52] J.C.Brochon, A.K.Livesey, T.Pouget, and B.Valeur, Chem.Phys.Lett., **174**, 517(1990).

[53] R.Krasnansky, K.Koike, and J.K.Thomas, J.Phys.Chem., **94**, 4521(1990).

[54] Y.-S.Liu and W.R.Ware, unpublished work. See also 1[30].

[55] J.G.McWhirter and E.R.Pike, J.Phys.A:Math.Gen., **11**, 1729(1978).

[56] J.N.I[illegible]mas, "Excited State Lifetime Measurements", Academic Press, New York, 1983.

[57] J.M.Easter, R.P.de Toma, L.Brand, Biophys.J., **16**, 571(1976).

[58] R.Dyson, I.Isenberg, Biochemistry, **17**, 3223(1971).

[59] I.Isenberg, R.Dyson, Biophys.J., **9**, 1337(1969).

[60] W.J.Albery, P.N.Bartlett, C.P.Wilde, and J.R.Darwent, J.Am.Chem.Soc., **107**, 1854(1985).

[61] W.J.Albery, P.N.Bartlett, J.Electrochem.Soc., **129**, 2254(1982).

[62] K.F.Scott, J.Chem.Soc.Faraday Trans. 1, **76**, 2056(1980).

[63] G.F.Miller, in "Numerical Solution of Integral Equations", Ed. L.M.Delves, and J.Walsh, Clarendon Press, Oxford, (1974), pp.175-188.

[64] P.C.Sabatier, in "Applied Inverse Problems", Ed. P.C.Sabatier, Springer-Verlag, New York, (1978), pp.1-26.

[65] R.L.Parker, Ann.Rev.Earth Planet.Sci., **5**, 35(1977).

[66] A.N.Tikhonov, and V.Y.Arsenin, "Solutions of Ill-Posed Problems", John Wiley & Sons, New York, 1977.

[67] B.W.Rust, and W.R.Burrus, "Mathematical Programming and the Numerical Solution of Linear Equations", American Elsevier Publishing Company, Inc., New York, 1972.

[68] R.Bellman, R.E.Kalaba, and J.A.Lockett, "Numerical Inversion of the Laplace Transform: Applications to Biology, Economics, Engineering, and Physics", American Elsevier Publishing Company, Inc., New York, 1966.

[69] K.B.Wolf, "Integral Transforms in Science and Engineering", Plenum Press, New York, (1979), Chapter 4.

[70] G.E.Backus and F.Gilbert, Geophys.J.R.Astron.Soc., **16**:169, 205(1968).

[71] M.Bertero, P.Boccacci, and E.R.Pike, Proc.R.Soc.Lond.A **383**, 15(1982).

[72] M.Bertero, P.Boccacci, and E.R.Pike, Proc.R.Soc.Lond.A 393, 51(1984).

[73] M.Bertero, P.Brianzi, and E.R.Pike, Proc.R.Soc.Lond.A 398, 23(1985).

[74] D.L.Phillips, J.Assoc.Comput.Mach., 9, 84(1962).

[75] A.N.Tichonov, Soviet Math.Dokl., 4, 1624(1963).

[76] S.Twomey, J.Assoc.Comput.Mach., 10, 97(1963).

[77] V.F.Turchin, V.P.Kozlov, and M.S.Malkevich, Soviet Phys.Uspekhi., 13, 681(1971).

[78] J.A.Scales, P.Docherty, and A.Gersztenkorn, Inverse Problems, 6, 115(1990).

[79] A.Tarantola, and B.Valette, J.Geophys., 50, 159(1982).

[80] A.Tarantola, and B.Valette, Rev.Geophys.Space Phys., 20, 219(1982).

[81] (a) D.W.Marquardt, J.Soc.Ind.Appl.Math., 11, 431(1963). (b) K.Levenberg, Quarterly of Appplied Mathematics, 2, 164(1944).

[82] L.R.Lines, and S.Treitel, Geophysical Prospecting, 32, 159(1984).

[83] P.R.Bevington, "Data Reduction and Error Analysis for the Physical Sciences", McGraw-Hill Book Company, New York, 1969.

[84] R.W.Hamming, "Introduction to Applied Numerical Analysis", McGraw-Hill Book Company, New York, 1971, p.238-239.

[85] S.L.S.Jacoby, J.S.Kowalik and J.T.Pizzo, "Iterative Methods for Nonlinear Optimization Problems", Prentice -Hall, Inc., Englewood Cliffs, New Jersey, 1972, p. 246-247.

[86] A.K.Livesey, P.Licinio, and M.Delaye, J.Chem.Phys., 84, 5102(1986).

[87] J.Claerbout and F.Muir, Geophysics, 38, 826(1973).

[88] R.K.Iler, "The Chemistry of Silica", John Wiley & Sons (1979).

[89] L.T.Zhuravlev, Langmuir, 3, 316(1987).

[90] L.H.Little, A.V.Kiselev, and V.I.Lygin, "Infrared Spectra of Adsorbed Species", Academic Press, London, 1966.
M.L.Hair, "Infrared Spectroscopy in Surface Chemistry", Marcel Dekker, New York, 1967.
A.V.Kiselev and V.I.Lygin, "Infrared Spectra of Surface Compounds", Wiely, New York, 1975.

[91] I.Tsuchlya, J.Phys.Chem. 86, 4107(1982).

[92] P.V.D.Voort, I.G.-D'Hamers and E.F.Vansant, J.Chem.Soc.Faraday Trans., 86, 3751(1990).

[93] J.B.Peri and A.L.Hensiey Jr., J.Phys.Chem., 72, 2926(1968).

[94] D.W.Sindorf and G.E.Maciel, J.Am.Chem.Soc., 105, 1487(1983).

[95] R.S.Mulliken, J.Am.Chem.Soc., 74, 811(1952).

[96] M.Basila, J.Chem.Phys., 35, 1151(1961).

[97] L.R.Snyder, J.Phys.Chem., 67, 2622(1963).

[98] P.Hobza, J.Sauer, C.Morgeneyer, J.Hurych and R.Zahradnik, J.Phys.Chem., 85, 4061(1981).

[99] W.Pohle, J.Chem.Soc.Faraday Trans., 1. 78, 2101(1982).

[100] L.M.Bollinger, and G.E.Thomas, Rev.Sci.Instrum., 32, 1044(1961).

[101] Y.Koechlin, Thesis, Uniersity of Paris, 1961.

[102] D.V.O'Connor, and D.Phillips, "Time-correlated Single Photon Counting", Acamemic Press, London, 1984.

[103] P.D.Coates, J.Phys.E., Ser.2, 1, 878(1968).

[104] J.Yguerabide, Methods Enzymol., 26, 498(1972).

[105] T.Fujii. A.Ishii, H.Satozono, S.Suzuki, M.Che, and M.Anpo, Bull.Chem.Soc.Japan., 63, 2475(1990).

[106] T.Fujii, A.Ishii, S.Suzuki, and M.Anpo, Chemistry Express, 4, 471(1989).

[107] V.N.Yankovich, V.V.Osipov, A.M.Eremenko, and A.A.Chuiko, Theor.Exp.Chem., 23, 1, 117(1987)

[108] R.K.Bauer, P.de Mayo, K.Okada, W.R.Ware, and K.C.Wu, J.Phys.Chem., 87, 460(1983).

[109] C.Francis, J.Lin, L.A.Singer, Chem.Phys.Lett., 96, 162(1982).

[110] D.J.S.Birch and R.E.Imhof, Analytical Instrumentation, 14(3&4), 293(1985).

[111] A.Siemiarczuk and W.R.Ware, J.Phys.Chem., 93, 7609(1989).

[112] S.C.Constable, R.L.Parker, C.G.Constable, Geophysics, 52, 289(1987).

[113] B.Russell, "History of Western philosophy", George Allen and Unwin, Ltd, 1946, ch.14.

[114] G.Nelson, G.Patonay, I.M.Warner, Anal.Chem., 60, 274(1988).

[115] K.Hara and W.R.Ware, Chem.Phys., 51, 61(1980).

[116] P.Lianos, A.K.Mukhopadhyay and S.Georghiou, Photochem.phtobiol., 32, 415(1980).

[117] P.Lianos, B.Lux, and D.Gerard, J.Chim.Phys.Phys-Chem.Biol., 77, 907(1980).

[118] P.Lianos, and S.Georghiou, Photochem.Photobiol., 30, 355(1979).

[119] P.Lianos, and S.Georghiou, Photochem.Photobiol., 29, 843(1979).

[120] A.Nakajima, Bull.Chem.Soc.Japan, 46, 2602(1973).

[121] I.B.Berlman, "Handbook of Fluorescence Spectra of Aromatic Molecules", Academic Press, New York, 1965.

[122] W.R.Ware, J.Phys.Chem., 66, 455(1962).

[123] J.B.Birks and D.J.Dyson, Proc.Roy.Soc.,A, 275, 135(1963).

[124] C.D.Amata, M.Burton, W.P.Helman, P.K.Ludwig and S.A.Rodemeyer, J.Chem.Phys., 48, 2374(1968).

[125] J.B.Birks and S.Georghiou, J.Phys., B, 1, 958(1968).

[126] S.Speiser, Appl.Phys., 19, 165(1979).

[127] A.Kearvell and F.Wilkinson, Chem.Phys.Lett., 11, 472(1971).

[128] J.R.Platt, J.Chem.Phys., 17, 484(1949).

[129] D.W.Bjarneson, Ph.D Thesis, University of Western Ontario, 1991.

[130] J.B.Birks, "Photophysics of Aromatic Molecules", Wiley-Interscience, London, 1970.

[131] K.Shibata, Methods Biochem.Anal., 7, 77(1959).

[132] W.L.Butler, J.Opt.Soc.Am., 52, 292(1962)

[133] R.W.Kessler and F.Wilkinson, J.Chem.Soc., Faraday Trans. 1, 77, 309(1981)

[134] J.S.Ham, J.Chem.Phys., 21, 756(1953)

[135] G.Durocher and C.Sandorfy, J.Mol.Spectrosc., 20, 410(1966)

[136] E.Clar, "Polycyclic Hydrocarbons", Academic Press, London, 1964.

[137] A.Nakajima, Bull.Chem.Soc.Japan, 44, 3272(1971).

[138] A.Nakajima, J.Luminesc., 8, 266(1974).

[139] A.Nakajima, J.Mol.Spectrosc., 61,467(1976).

[140] K.Kalyanasundaram and J.K.Thomas, J.Am.Chem.Soc., 99:7, 2039(1977).

[141] A.K.Mukhopadhyay and S.Georghiou, Photochem. Photobiol., 31, 407(1980).

[142] V.Glushko, M.S.R.Thaler and C.D.Karp, Arch.Biochem. Biophys., 210, 33(1981).

[143] A.Nakajima, Spectrochim.Acta, 38A, 693(1982).

[144] D.C.Dong and M.A.Winnik, Photochem.Photobiol., 35, 17(1982).

[145] K.Hara, P.de Mayo, W.R.Ware, A.C.Weedon, G.S.K.Wong and K.C.Wu., Chem.Phys.Lett., 69, 105(1980).

[146] J.H.Anderson, J.Lombardi, and M.L.Hair, J.Colloid and Interface Sci., 50, 519(1975).

[147] D.F.Eaton, EPA Newsl., 28, 21(1987).

[148] F.R.Lipsett, Prog.Dielectr., 7, 217(1967).

[149] J.N.Demas and G.A.Crosby, J.Phys.Chem., 75, 991(1971).

[150] J.N.Demas, "Optical Radiation Measurements", 3, 195(1982), Ed. K.D.Mielenz, Academic Press, New York.

[151] D.Oelkrug, M.Plauschinat and R.W.Kessler, J.Luminesc., **18/19**, 434(1979).

[152] W.Honnen, G.Krablchler, S.Uhl, and D.Oelkrug, J.Phys.Chem., **87**, 4872(1983).

[153] M.Plauschinat, W.Honnen, G.Krabichler, S.Uhl, and D.Oelkrug, J.Mol.Struct., **115**, 351(1984).

[154] M.S.Wrighton, D.S.Ginley and D.L.Morse, J.Phys.Chem., **78**, 2229(1974).

[155] G.R.Seely and G.A.Haggy. J.Phys.Chem., **91**, 440(1987).

[156] G.R.Seely, Biophys.J. **52**, 311(1987).

[157] G.R.Seely, J.Photochem.Photobiol. **A.45**, 325(1988).

[158] P.Kubelka J.Opt.Soc.Am., **38**, 448(1948).

[159] J.Goldman and R.R.Goodall, J.Chromatogr., **32**, 24(1968).

[160] J.Goldman J.Chromatogr., **78**, 7(1973).

[161] The K & M model, on which Seely's approach is based, is called a two-flux model. The use of a more sophisticated six-flux model has also been investigated, and is considered more precise in describing powdered samples. See R.Gade, U.Kaden, J.Chem.Soc.Faraday Trans., **86**, 3707(1990).

[162] C.A.Parker and C.G.Hatchard, Trans.Faraday Soc., **59**, 284(1963).

[163] B.Stevens and M.Thomaz, Chem.Phys.Lett., **1**, 535(1968).

[164] C.A.Parker and T.Joyce, Trans.Faraday Soc., **62**, 2785(1966).

[165] A.R.Horrocks and F.Wilkinson, Proc.Roy.Soc., **A.306**, 257(1968).

[166] W.R.Dawson and M.W.Windsor, J.Phys.Chem., **72**, 3251(1968).

[167] W.H.Melhuish, J.Phys.Chem., **65**, 229(1961).

[168] G.Weber and F.W.J.Teale, Trans. Faraday Soc., **53**, 646(1957).

[169] B.Stevens and M.Thomaz, Chem.Phys.Lett., **1**, 549(1968).

[170] C.A.Parker, Anal.Chem., **34**, 50(1962).

[171] The physical interpretation for μ could be, for example, the local polarity of environment, or the local density of quencher molecules.

[172] Derived from the data given by J.L.Kropp and W.R.Dawson, in "Molecular Luminescence", Ed. E.C.Lim, W.A.Benjamin, Inc., New York, 1969, p.39.

[173] A.Nakajima, Spectrochim.Acta, **30A**, 860(1974).

[174] J.L.Atwood, F.Hamada, K.D.Robinson, G.W.Orr and R.L.Vincent, Nature, **349**, 683(1991).

[175] W.G.Read, E.J.Campbell, G.Henderson, and W.H.Flygare, J.Am.Chem.Soc., **103**, 7670(1981).

[176] W.G.Read, E.J.Campbell. and G.Henderson, J.Chem.Phys., **78**, 3501(1983).

[177] A.Engdahl and B.Nelander, J.Phys.Chem., **89**, 2860(1985).

[178] B.V.Cheney, W.Schulz, J.Cheney, and W.G.Richards, J.Am.Chem.Soc., **110**, 4195(1988).

[179] J.L.Bredas, and G.B.Street, J.Am.Chem.Soc., **110**, 7001(1988).

[180] J.L.Bredas, and G.B.Street, J.Chem.Phys., **90**, 7291(1989).